CANADIAN JOURNAL OF RESEARCH

VOLUME 28 MAY, 1950 NUMBER 3

— SECTION A —

PHYSICAL SCIENCES

Contents

NATIONAL RESEARCH COUNCIL
OTTAWA, CANADA

CANADIAN JOURNAL OF RESEARCH

The *Canadian Journal of Research* is issued in six sections, as follows:

A. Physical Sciences	D. Zoological Sciences
B. Chemical Sciences	E. Medical Sciences
C. Botanical Sciences	F. Technology

For the present, Sections A, C, D, and E are to be issued six times annually, and Sections B and F, twelve times annually, each under separate cover, with separate pagination.

The *Canadian Journal of Research* is published by the National Research Council of Canada under authority of the Chairman of the Committee of the Privy Council on Scientific and Industrial Research. The *Canadian Journal of Research* is edited by a joint Editorial Board consisting of members of the National Research Council of Canada, the Royal Society of Canada, and the Chemical Institute of Canada.

Sections B and F of the *Canadian Journal of Research* have been chosen by the Chemical Institute of Canada as its medium of publication for scientific papers.

Canadian Journal of Research

Issued by THE NATIONAL RESEARCH COUNCIL OF CANADA

VOL. 28, SEC. A. MAY, 1950 NUMBER 3

MAGNETIC SUSCEPTIBILITIES OF IRON GROUP SALTS AT LOW TEMPERATURES[1]

BY A. F. JOHNSON[2] AND H. GRAYSON-SMITH[3]

Abstract

A magnetic balance of the Sucksmith ring type has been constructed. It is capable of a precision of 0.5 to 1% in measurements of displacement. The estimated maximum error in susceptibility measurements is 2%. This apparatus has been used to measure the temperature variation of the susceptibilities of chromium sulphate, hydrated and anhydrous, and of the nitrates of chromium, cobalt, and nickel. Measurements were made at several values of the magnetic field strength, so that a correction for small amounts of ferromagnetic impurity could be obtained. The reciprocals of the corrected specific susceptibilities were plotted against the absolute temperature. The intercepts on the temperature axis of the resulting straight lines gave the values of the Curie–Weiss constant. These values have been compared with those for other salts of the same ions. The effective Bohr magneton numbers were calculated and compared with theoretical values given by van Vleck.

Introduction

The salts of the transition metals, chromium to nickel, are all paramagnetic owing to the metallic ions, which have incomplete *d*-shells, and so have magnetic moments. According to the simple Langevin–Debye theory (1, 18), the susceptibility of a paramagnetic material should depend upon temperature according to Curie's law,

$$\chi = C/T. \tag{1}$$

However, for most paramagnetic solids, a better description of the experimental behavior is given by the Curie–Weiss law

$$\chi = C/(T - \Theta), \tag{2}$$

where Θ is an empirical constant, positive or negative.

The Curie constant, C in Equations (1) or (2), is determined by the magnetic moment of the ion. It is usual to define the effective magnetic moment per mole, μ_{eff}, and the effective magneton number, p_{eff}, by the relations

$$\mu_{eff} = \sqrt{3RC} = \sqrt{3R\chi_m(T - \Theta)} = p_{eff}\mu_B, \tag{3}$$

where χ_m is the molar susceptibility, and $\mu_B = 5565$ c.g.s. units per mole is the Bohr magneton. The effective magnetic moment is the value which would

[1] *Manuscript received October 15, 1949.*
Contribution from the Department of Physics, University of Toronto, Toronto, Ont.

[2] *Present address: U. S. Rubber Company, Detroit.*
[3] *Present address: Department of Physics, University of Alberta, Edmonton, Alta.*

be required according to classical theory in order to produce the observed susceptibility. It can be calculated by quantum methods (7, 18) for any free ion of known electronic configuration, but may be modified in various ways for bound ions in a crystal. These modifications will be discussed later in connection with the empirical values of μ_{eff} determined by the authors.

As far as the magnetic moment is concerned the theory gives a satisfactory explanation of the facts. Theoretical explanation of the Weiss constant, Θ in Equation (2), rests upon much less certain ground. Equation (2) also holds for ferromagnetic materials in the high temperature paramagnetic state, with Θ approximately equal to the Curie temperature. According to Heisenberg's theory of ferromagnetism (1, 6) the behavior in this case can be explained by assuming a strong exchange interaction between parallel aligned electron spins. A similar effect, involving interactions between neighboring ions, could also explain Equation (2) in cases where Θ is positive and of the order of 0 to 50°. This is almost certainly the case for certain of the transition group chlorides, which are known to become weakly ferromagnetic at very low temperatures (5, 12). On the other hand, some of the manganese compounds are known to become antiferromagnetic (2, 14), probably owing to stability of the antiparallel alignment of magnetic moments. The internal electric field of the crystal can also cause a tendency for the ions to align themselves, and so cause a temperature variation of χ which simulates the Weiss law over a fairly wide range of temperature (1).

In any case, one would expect a progressive change in the values of Θ for different salts of the same ion, with different inter-ion distances and different anions. It is therefore interesting to compare the paramagnetic constants of as many different salts of the transition group elements as possible. Such comparisons have been given by Van Vleck (18) and by Burton *et al.* (3), but the number of salts hitherto studied is not sufficient to make the evidence conclusive.

The principal purpose of the present investigation was to add to the experimental evidence on this point by studying several more simple salts of the ions in question. It was hoped that this might make it possible to decide whether or not the interactions between ions are the dominant factor. This hope has been only partially justified. However, the experiments have given further evidence, both on this point and on factors which modify the effective magnetic moment.

Apparatus

The magnetic balance constructed for this investigation was based upon the design of Sucksmith (16, 17) as adapted for low temperature measurements by Jackson (8). The essential components are shown in Fig. 1. The powdered sample was contained in a hard gelatin capsule C, which was sealed with glyptal laquer and then cemented to a quartz rod CF_1F_2, connected to a brass rod at F_2. The brass rod was attached by means of a coupling J to a phosphor-

bronze ring R, which carried two small mirrors M_1M_2. The ring was adjusted so as to be nearly circular under the weight of the suspension and sample. Then, when the magnetic field was applied, the force on the sample due to the field deformed the ring. The mirrors were attached at the points where

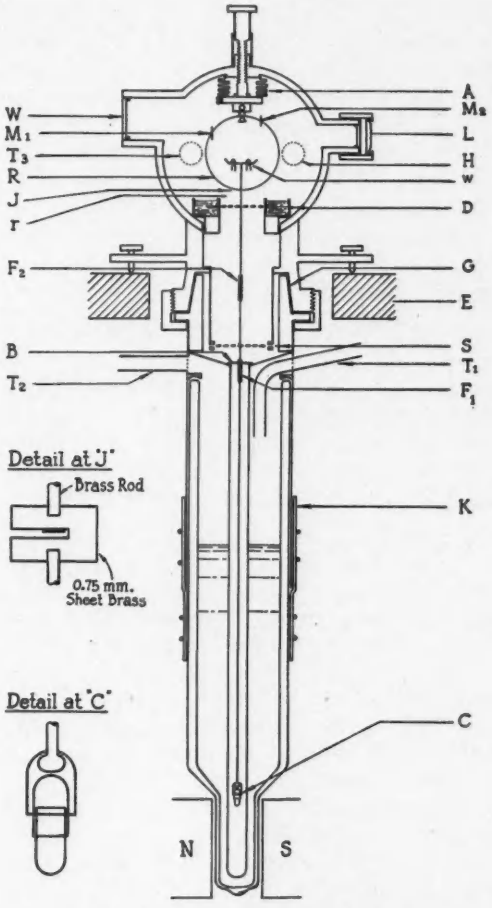

Fig. 1. Sucksmith type magnetic balance.

the angular deflection due to this deformation was a maximum. Light from a distant source passed through the lens L, was reflected by M_1 and M_2 and was focused by a microscope objective. By this device the displacement of the sample was magnified approximately 100 times.

The position of the suspended system could be adjusted by means of the screw adjustments and the sylphon bellows A. If necessary, the shape of the ring could be adjusted by adding small weights w, which could be manipulated by means of a hook passing through a sylphon bellows at the back of the case. The front of the case was sealed by means of a thick plate glass window.

The rings were made out of strips cut from phosphor-bronze sheet, bent into shape and soft-soldered together at the point of support. Several rings were made, with diameters 5 to 6 cm., width 2 to 3 mm., and thicknesses 0.05 to 0.125 mm. Each ring was shaped by trial to an ellipse of such eccentricity that it was pulled approximately circular by the load of the suspension and specimen. The ring finally selected had a sensitivity of 5.018 cm. per gm. at a scale distance of 65 cm. The deflection was linear for weights up to 500 mgm. By means of a vernier the vertical travel of the microscope could be read to 0.01 mm. Over the range of displacements observed in the experiment this gave a precision of 0.5 to 1% in the measured deflections, and an estimated maximum error in the susceptibility measurements of 2%.

The phosphor-bronze ring with its attached mirrors was very susceptible to vibration, and some form of damping was necessary. To isolate the system from external vibrations, the cryostat with the balance attached, the light source, and the microscope were all mounted on a marble slab E, resting on two strips of sponge rubber. To damp internal vibrations, the rod by which the specimen was suspended carried a hollow monel metal ring r which was immersed in an annular oil bath D. A flat spiral spring S of thin phosphor-bronze prevented the specimen support from swaying, or from being pulled sideways towards the pole-pieces of the magnet.

The specimen hung inside a long glass tube in a specially shaped Dewar flask. Various refrigerants were introduced into the Dewar flask through a double-walled glass tube at T_1, and the gas from the evaporating liquid was pumped off through T_2. The thin metal baffle B reduced radiation down the tube. By means of the ground bronze joint G, the surrounding tube and the Dewar flask could be removed to change the specimen. After the specimen was mounted, the tube in which it hung and the case containing the balance were filled with nitrogen at atmospheric pressure. Temperatures were indicated roughly by the vapor pressure of the cryostat liquid, but it was found necessary to measure them more accurately by means of a platinum resistance thermometer, which was wound around the lower part of the glass tube and cemented in place with glyptal.

For small specimens, where the magnetic field may be assumed constant over the volume of the specimen, the vertical component of the force is given by

$$F_x = m\chi H_y \partial H_y / \partial x, \tag{4}$$

where m is the mass of the specimen, χ is the specific susceptibility, and the pole-pieces of the magnet lie in the y-direction. The pole-pieces were 9 cm.

in diameter with a gap of 3.9 cm. The field between these poles was explored carefully, and the specimen was placed in the position where $H\partial H/\partial x$ was a maximum, and was changing least rapidly. This quantity was then very nearly constant over the volume of the specimen, and did not vary appreciably over the small displacement which occured during a measurement. It was therefore unnecesary to use a restoring force to bring the specimen back into the original position in the field.

In order to calibrate the magnet and to find the absolute values of $H\partial H/\partial x$ for different current strengths, a series of measurements was made with manganous sulphate. The susceptibility of this material has been well established over the temperature range concerned by Onnes and Oosterhuis (11). It was found that the calibration factor varied slightly with the temperature of the cryostat. The appropriate factor was therefore used for each of the four temperatures at which measurements were subsequently made.

Correction for Ferromagnetic Impurities

A serious source of error in the measurement of small susceptibilities is the presence of ferromagnetic impurities, either in the suspension system or in the sample. To test the suspension system a series of measurements was made with an empty gelatine capsule. Using the largest magnetic field which could be obtained from the magnet, the deflection was too small to observe, either at room temperature or at the temperature of liquid nitrogen. Therefore no correction was necessary for the suspension system.

In order to eliminate ferromagnetism in the samples, measurements were made at several different field strengths at each temperature. It can be assumed that any ferromagnetic material present would be magnetized to saturation at the field strengths used, and would have a constant magnetic moment M. The total force on the specimen is then

$$F = M\partial H/\partial x + m\chi H\partial H/\partial x = a|H| + b|H|^2, \tag{5}$$

since $\partial H/\partial x$ is everywhere proportional to the absolute value $|H|$ of the field at the center of the magnet. Therefore, if there is a small amount of ferromagnetic impurity, graphs of F against either $|H|^2$ or $H\partial H/\partial x$ will deviate slightly from the ideal straight line through the origin (Equation (4)). For large field strengths the slope of the curve of F against $H\partial H/\partial x$ should approach the value $m\chi$.

For the manganous sulphate standard a graph of balance displacement against $|H|^2$ was linear within experimental error, and no correction was necessary in using this standard to calibrate the magnet. In other cases a small deviation from linearity was observed. This is illustrated in Fig. 2 for the case of cobalt nitrate, which is typical of the various salts measured. In this figure, balance displacement is plotted against $H\partial H/\partial x$ for measurements taken at four different temperatures, and the small but distinct deviation can

be easily seen. In all cases the curves were very nearly linear for the larger field strengths, and corrected values of $m\chi$ could be readily determined from the slopes.

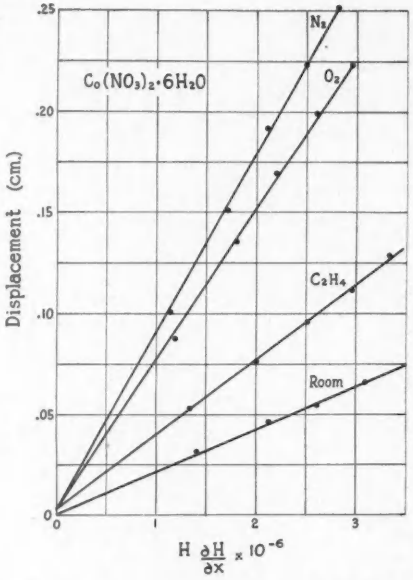

Fig. 2. Balance displacement vs. $H\partial H/\partial x$ for cobalt nitrate, at four different temperatures, to illustrate the small deviation from proportionality due to ferromagnetic impurity.

Experimental Results

New measurements were made on the salts listed in Table I, at room temperature, in liquid ethylene, liquid oxygen, and liquid nitrogen. The materials were obtained from British Drug Houses (Canada) Ltd., and were specified as having amounts of impurity less than those given in the list. The anhydrous chromium sulphate was prepared from the hydrate by heating it at 400°C. until the weight was constant. The loss of weight was 1 to 2% greater than that which would be accounted for by the removal of 18 H_2O per molecule.

The susceptibilities of these salts were derived from graphs of F against $H\partial H/\partial x$, as described above. They were then corrected for the small diamagnetism of the water of crystallization and of the anions, using values given by van Vleck (18). The final results are collected in Table II. For each specimen the corrected values of $1/\chi$ were plotted against the absolute temperature (Figs. 3 to 7). In all cases the resulting graphs were linear, showing that the Curie–Weiss law (Equation (2)) is accurately obeyed down to 77°K.

TABLE I

SPECIFICATIONS OF MATERIALS USED

Chromium sulphate, $Cr_2(SO_4)_3.18\ H_2O$

Chloride (Cl)	0.003%
Iron (Fe)	0.01%
Alkalis	0.5%

Chromium sulphate anhydrous, $Cr_2(SO_4)_3$

Chromium nitrate, $Cr(NO_3)_3.9\ H_2O$

Chloride (Cl)	0.003%
Sulphate (SO_4)	0.01%
Iron (Fe)	0.01%
Alkalis	0.5%

Cobalt nitrate, $Co(NO_3)_2.6\ H_2O$

Chloride (Cl)	0.001%
Sulphate (SO)	0.01%
Iron (Fe)	0.003%
Nickel (Ni)	0.002%
Alkalis and alkaline earths (Na)	0.03%
Ammonia	No reaction

Nickel nitrate, $Ni(NO_3)_2.6\ H_2O$

Chloride (Cl)	0.002%
Sulphate (SO_4)	0.01%
Cobalt (Co)	0.0005%
Iron (Fe)	0.001%
Alkalis and alkaline earths (Na)	0.03%

TABLE II

CORRECTED PARAMAGNETIC SUSCEPTIBILITIES

Salt	Mass of sample, gm.	Diamagnetic correction (per gm.)	Temperature, °K.	Corrected susceptibility (per gm.)
$Cr_2(SO_4)_3 18\ H_2O$	0.1171	0.50×10^{-6}	293.8	14.8×10^{-6}
			168.9	26.7
			90.5	53.9
			77.3	67.9
$Cr_2(SO_4)_3$	0.1529	0.31×10^{-6}	293.0	26.8×10^{-6}
			168.9	46.6
			90.3	98.1
			77.1	108.0
$Cr(NO_3)_3.9\ H_2O$	0.2075	0.43×10^{-6}	294.5	13.3×10^{-6}
			168.9	23.1
			90.4	50.3
			77.2	59.1
$Co(NO_3)_2.6\ H_2O$	0.1393	0.40×10^{-6}	294.8	31.1×10^{-6}
			168.8	54.5
			90.4	109.2
			77.0	127.6
$Ni(NO_3)_2.6H_2O$	0.1268	0.40×10^{-6}	295.8	12.7×10^{-6}
			169.1	23.7
			90.3	49.2
			77.2	61.2

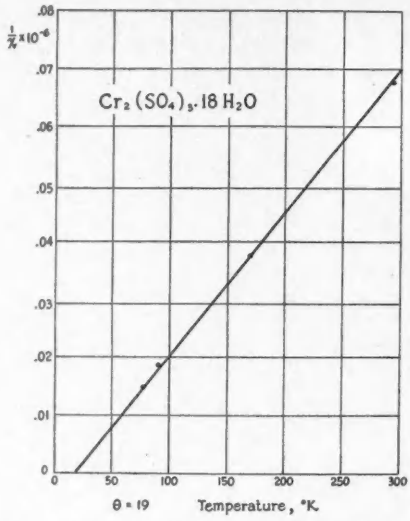

Fig. 3. Reciprocal susceptibility, $1/\chi$, for chromium sulphate hydrate, showing determination of the Weiss constant, Θ.

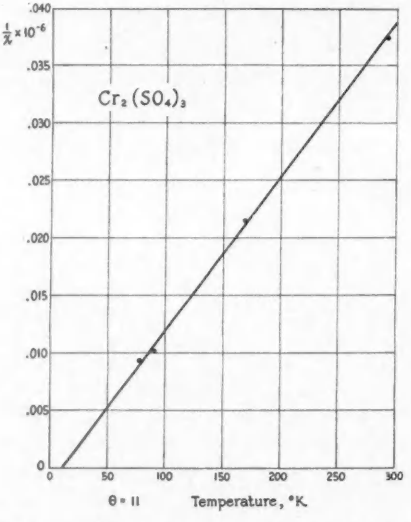

Fig. 4. Reciprocal susceptibility, $1/\chi$, for anhydrous chromium sulphate, showing determination of the Weiss constant, Θ.

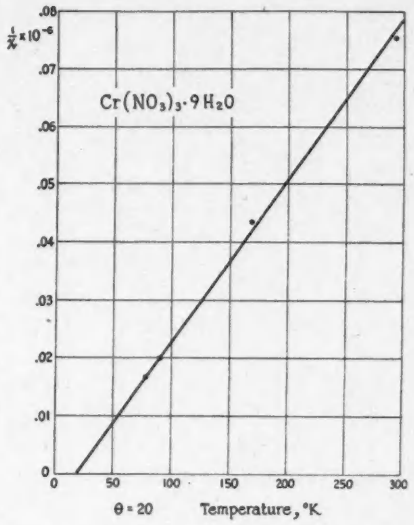

Fig. 5. Reciprocal susceptibility, $1/\chi$, for chromium nitrate, showing determination of the Weiss constant, θ.

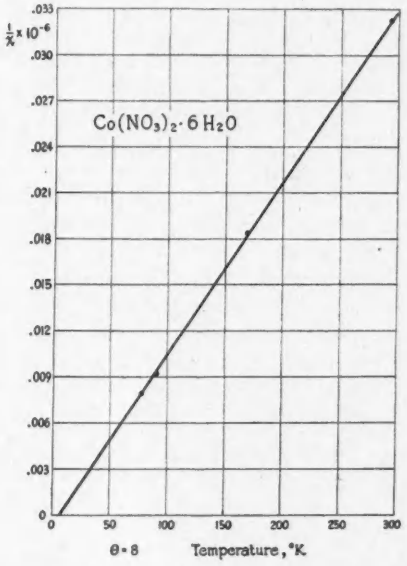

Fig. 6. Reciprocal susceptibility, $1/\chi$, for cobalt nitrate, showing determination of the Weiss constant, θ.

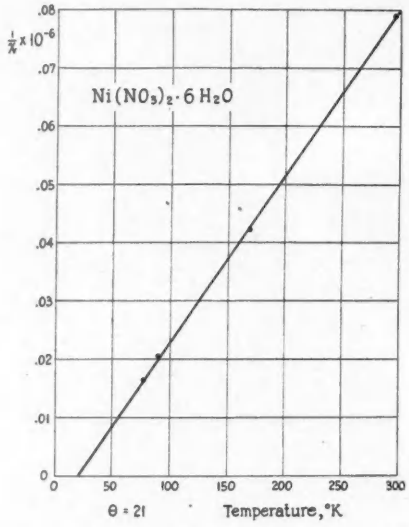

Fig. 7. Reciprocal susceptibility, $1/\chi$, for nickel nitrate, showing determination of the Weiss constant, θ.

Effective Magnetic Numbers

Experimental values of the effective magneton number, p_{eff}, were calculated for each salt, by means of Equation (3), and are given in the last column of Table III. The only previous measurements below room temperature on any of these salts are those of Serres (13) on chromium sulphate hydrate, and those of Janes (9) on nickel nitrate. In each case, measurements were made at only one value of the field strength, and no correction was made for ferromagnetic impurity. Serres gave a value of $p_{eff} = 3.85$ for Cr^{+++}, which is so much smaller than the present value as to suggest some radical difference in the materials measured. Janes used a different method of comparing experiment with theory, and did not quote values of p_{eff}. His values for the susceptibilities are somewhat higher than those found by the present authors. Chatillon (4) has shown that the values of p_{eff} for Co^{++} depend on the mode of preparation and history of the material. It is possible that variations can occur in the arrangement of the water of crystallization molecules, and that these can cause variations in the internal field.

According to the Langevin–Debye theory of paramagnetism (1) the molar susceptibility is given by

$$\chi_m = N^2 g^2 J(J+1)\,\mu_B^2/3RT, \tag{6}$$

which gives

$$p_{eff} = g\sqrt{J(J+1)}, \tag{7}$$

where J is the resultant angular momentum quantum number of the magnetic

ion, and g is the corresponding Landé factor. This theory is based upon the assumption that every ion is in the same quantum state, and it is expected to be a good approximation when the energy separation in the low-lying multiplet is large ($h\nu >> kT$). In the case of narrow multiplets and Russell–Saunders coupling van Vleck (18) has shown that

$$p_{eff} = \sqrt{L(L+1) + 4S(S+1)}. \tag{8}$$

The complicated case of intermediate multiplet widths has also been discussed by Laporte (10) and van Vleck (18). In this case the effective magneton number may vary with the temperature.

In the case of the salts of the iron group neither formula fits the experimental results very well. Stoner (15) first suggested that the internal electric field due to neighboring atoms in the crystal might quench the contribution of the orbital angular momentum to the magnetization. The expression for the magneton number then becomes

$$p_{eff} = \sqrt{4S(S+1)}. \tag{9}$$

In general where quenching is incomplete the value of p_{eff} should lie between those given by Formulas (8) and (9), as is the case for most of the salts of the iron group.

Table III shows the experimental values obtained in this work, compared with the different theoretical values. Column 7 gives the theoretical value for multiplet width comparable with kT, as calculated by van Vleck (18). The experimental values obtained for the Cr^{+++} ion in both the hydrated and anhydrous sulphates are somewhat higher than those previously obtained for chromium salts. These values are only slightly less than the theoretical value for narrow multiplets, and indicate very little quenching of the orbital moment. In the nitrate the value for the chromium ion indicates complete quenching of the orbital moment and partial quenching of the spin moment. The result for Co^{++} indicates partial quenching of the orbital moment, while that for Ni^{++} corresponds to almost complete quenching of the orbital angular momentum.

TABLE III

EFFECTIVE BOHR MAGNETON NUMBERS

Ion	Salt	Lowest state	Expt'l p_{eff}	Theoretical p_{eff}			
				$h\nu >> kT$	$h\nu << kT$	$h\nu \sim kT$	Spin only
Cr^{+++}	$Cr_2(SO_4)_3.18\ H_2O$	$^4F_{3/2}$	4.85	5.20	0.77	2.97	3.87
	$Cr_2(SO_4)_3$		4.89				
	$Cr(NO_3)_3.9\ H_2O$		3.43				
Co^{++}	$Co(NO_3)_2.6\ H_2O$	$^4F_{9/2}$	4.58	5.20	6.64	6.56	3.87
Ni^{++}	$Ni(NO_3)_2.6\ H_2O$	$^3F_4$	2.86	4.47	5.59	5.56	2.83

The Weiss Constant for Different Salts

In Table IV, values of the Weiss constant Θ have been collected for as many as possible of the simple salts of the iron group. Values marked with an asterisk are from the present investigation, and the remainder are from a comparison table given by Burton *et al.* (3).

TABLE IV

CURIE–WEISS CONSTANT FOR IRON GROUP SALTS

Ion	Salt	Θ	Salt	Θ	Salt	Θ	Salt	Θ
Cr^{+++}	$CrCl_3$	32	$Cr_2(SO_4)_3$*	11	$Cr_2(SO_4)_3.18\ H_2O$*	19	$Cr(NO_3)_3.9\ H_2O$*	20
Mn^{++}	$MnCl_2$	0	$MnSO_4$	−24	$MnSO_4.4\ H_2O$	0		
Fe^{++}	$FeCl_2$	20	$FeSO_4$	−31	$FeSO_4.7\ H_2O$	−1		
Co^{++}	$CoCl_2$	20	$CoSO_4$	−45	$CoSO_4.7\ H_2O$	−14	$Co(NO_3)_2.6\ H_2O$*	8
Ni^{++}	$NiCl_2$	67	$NiSO_4$	−79	$NiSO_4.7\ H_2O$	59	$Ni(NO_3)_2.6\ H_2O$*	21

Conclusion

As indicated in the introduction, it was hoped that comparison between different simple salts would show at least a qualitative correlation between the complexity of the salt and the value of the Weiss constant, Θ. This hope has been only partially realized.

The cases of hydrated and anhydrous chromium sulphate may be significant. These salts were found to have nearly the same effective magneton numbers, showing nearly the same degree of quenching of orbital momentum by the crystalline field. Then, if the necessity for using the Curie–Weiss law (Equation (2)) is due to interaction between ions, one would expect the value of Θ for the hydrated salt to be less than that for the anhydrous. On the other hand the presence of the polar H_2O groups in the hydrated salt makes the internal electric field larger than in the anhydrous salt. The fact that the observed value of Θ was larger for the hydrate suggests that the crystal field is the predominating factor in chromium sulphate. Measurements on these two salts in particular should be extended to still lower temperatures, where deviations from the Curie–Weiss must appear.

The only other correlation noticeable in Table IV is that the large values of Θ for nickel salts, considerably larger than the corresponding cobalt salts, extend to the newly measured nitrates.

Acknowledgments

The authors wish to express their thanks to Professors A. D. Misener and J. Reekie and to Mr. J. C. Findlay for many helpful suggestions and criticisms, and to Mr. Albert Owen for frequent assistance and practical advice. One

of the authors (A.F.J.) wishes also to acknowledge the assistance of the Research Council of Ontario, in the form of two scholarships which enabled him to undertake the work. Thanks are also due to the National Research Council for a grant-in-aid which provided technical assistance for this and other projects.

References

1. BATES, L. F. Modern magnetism. Cambridge: The University Press. 1948.
2. BIZETTE, H., SQUIRE, C. F., and TSAI. Compt rend. 207:449. 1938.
3. BURTON, E. F., GRAYSON-SMITH, H., and WILHELM, J. O. Phenomena at the temperature of liquid helium. Reinhold Publishing Corporation, New York. 1940.
4. CHATILLON, A. Ann. phys. 9:187. 1928.
5. DE HAAS, W. J. and SCHULTZ, B. H. J. phys. radium, 10:7. 1939.
6. HEISENBERG, W. Z. Physik, 49: 619. 1928.
7. HUND, F. Z. Physik, 33:855. 1925.
8. JACKSON, L. C. Proc. Roy. Soc. (London), 140A: 695. 1933.
9. JANES, R. B. Phys. Rev. 48:78. 1935.
10. LAPORTE, O. Z. Physik, 47:761. 1928.
11. ONNES, H. K. and OOSTERHUIS, E. Commun. Kammerlingh Onnes Lab. Leiden. No. 132e. 1912.
12. SCHUBNIKOW, L. W. and SCHALYT, S. S. Physik Z. Sowjetunion, 11:566. 1937.
13. SERRES, A. Ann. Phys. 17:5. 1932.
14. SQUIRE, C. F. Phys. Rev. 56:922. 1939.
15. STONER, E. C. Phil. Mag. 8:250. 1929.
16. SUCKSMITH, W. Phil. Mag. 8:158. 1929.
17. SUCKSMITH, W. Phil. Mag. 14:1115. 1932.
18. VAN VLECK, J. H. Theory of electric and magnetic susceptibilities. Clarendon Press, Oxford. 1932.

THE NEUTRON DENSITY NEAR A PLANE SURFACE IN A CAPTURING MEDIUM[1]

By Jeanne LeCaine[2]

Abstract

The variational method is applied to the Milne problem with capture, to obtain, for the density and for the angular distribution, expressions which give quite accurate values and which have a relatively simple analytical form. Tables of the density and angular distribution are included. The extrapolation distances determined by the Variational Method agree to high accuracy with the exact values. The angular distribution determined by the Variational Method is shown to be accurate within 0.05% in all cases where exact results are available. Tables are also given for the density and angular distribution in the Milne problem with capture and constant production.

Introduction

The formal solution of the Milne problem with capture has been obtained by Adler and Mark (1) using the Wiener–Hopf technique. Starting from the integral equation

$$f(z) = \frac{1-a}{2}\int_0^\infty f(z')\,E_1(|z-z'|)\,dz' \tag{1}$$

they have shown that the asymptotic solution for the density, expressed as a function of distance from the boundary, is

$$f_{as}(z) = j(o)\sqrt{\frac{2\nu^2(1-\nu^2)}{a(\nu^2-a)}}\sinh \nu\,(z + z_0(a)), \tag{2}$$

where $\nu(a)$ is the real root of the transcendental equation

$$(1-a)\frac{\operatorname{arth}\,\nu}{\nu} = 1 \tag{3}$$

and $z_0(a)$ is given by

$$z_0(a) = \frac{1-a}{2\nu}\int_0^1 \frac{1-a\mu^2}{1-\mu^2}\cdot\frac{\operatorname{arth}\,(\nu\mu)}{\left[1-(1-a)\,\mu\operatorname{arth}\mu\right]^2+\left[\frac{\pi(1-a)}{2}\right]^2}\,d\mu. \tag{4}$$

This integral has been evaluated by numerical integration for $a = 0, 0.1, 0.2, 0.3, 0.4, 0.5, 0.6, 0.7, 0.8, 0.9$. The values of $z_0(a)$ and $\nu(a)$ for these values of a are tabulated in the paper by Adler and Mark. As $a \to 1$, $z_0(a)$ becomes infinite, and, for a near 1, $z_0(a)$ is given by

$$z_0(a) = \frac{1}{1-a} + \frac{1}{2}\log(1-a) - \frac{1}{2}\log 2 + \frac{1-a}{2}\log 2 + \ldots\ldots \tag{5}$$

[1] *Manuscript received October 27, 1949.*
Contribution of the Chalk River Laboratories of the National Research Council of Canada. Issued as N.R.C. No. 2130. This work was completed April 17, 1945.
[2] *Now at Oklahoma Agricultural & Mechanical College, Stillwater, Oklahoma.*

Adler and Mark and Davison (2) have also shown that the density at the boundary is

$$f(o) = \sqrt{\frac{\nu^2}{a}} \cdot j(o). \tag{6}$$

They have obtained the angular distribution at the boundary, and the deviation of the true density from the asymptotic density, as rather complicated integrals. A few isolated values of the angular distribution have been obtained by numerical integration.

In the present paper the application of the Variational Method to this problem is discussed. It is intended to complement the rigorous work done and to give a simpler way of obtaining quite accurate values of the density and angular distribution.

The application of variational technique to the Milne problem without capture has already been discussed (5). It has been shown that a good approximation to z_0 can be obtained with a crude trial function, and that by choosing a trial function the behavior of which is similar to that of the true function it is possible to obtain an expression for the density which has a much simpler analytical form than that of the true density and which is a very good approximation to the true density over the whole range.*

In the following, a similar discussion is carried out for the Milne problem with capture. The trial function used is the logical generalization of that used in the case $a = 0$. For $a > 0$ the true density has not been calculated but from physical considerations the accuracy of the approximation would be expected to improve as a increases, since, as a increases, the distinction between the two semi-infinite media becomes less marked. In Section 6, Tables VII, VIII, some figures are given indicating the accuracy of approximation to the angular distribution, for $a = 0.1, 0.2, 0.4, 0.6$. In every case where the true value was determined it was found to be within 0.05% of the approximate value.

Notation

The variational technique used is based on the fact that (3, 8) for the non-homogeneous integral equation

$$q(z) = \int q(z')K(z, z')dz' + h(z), \tag{7}$$

$q(z)$ being the unknown function, and $K(z, z')$ a symmetric kernel, the functional

$$F(q) = \frac{\int q(z)\,[q(z) - \int q(z')K(z, z')\,dz']dz}{[\int h(z)q(z)dz]^2} \tag{8}$$

is a minimum when $q(z)$ is the solution of (7). $F(q)$ is then equal to

$$\frac{1}{\int h(z)q(z)dz}.$$

* *A comparison of the true density and the approximation to it obtained by Variational Technique has been given by C. Mark (7).*

We introduce the notation,

$$G_3(\nu, z) = \frac{1-a}{2\nu}\{e^{\nu z}E_1[(1+\nu)z] + e^{-\nu z}E_1[(1-\nu)z] - 2E_1(z)\} \tag{9}$$

$$= (1-a)\nu\int_1^\infty \frac{e^{-zu}}{u(u^2-\nu^2)}du$$

$$G_2(\nu, z) = \frac{1-a}{2\nu}\{e^{\nu z}E_1[(1+\nu)z] - e^{-\nu z}E_1[(1-\nu)z]\} \tag{10}$$

$$= -(1-a)\int_1^\infty \frac{e^{-zu}}{u^2-\nu^2}du.$$

The function $G_3(\nu, z)$ is finite, positive and monotone decreasing in z;

$$G_3(\nu, o) = -\frac{(1-a)\log(1-\nu^2)}{2\nu}$$

and as $z \to \infty$,

$$G_3(\nu, z) \sim \frac{(1-a)\nu}{1-\nu^2}\frac{e^{-z}}{z}.$$

The function $G_2(\nu, z)$ is finite, negative and monotone increasing in z; $G_2(\nu, o) = -1$ and as $z \to \infty$, $G_2(\nu, z) \sim \frac{-(1-a)e^{-z}}{(1-\nu^2)z}$. The slope of $G_2(\nu, z)$, as $z \to 0$, becomes infinite logarithmically. Also,

$$\lim_{\nu \to 0}\frac{1}{\nu}G_3(\nu, z) = E_3(z)$$

$$\lim_{\nu \to 0} G_2(\nu, z) = E_2(z). \tag{11}$$

We note also that

$$\frac{1-a}{2}\int_0^\infty e^{\nu z}E_1(|z-z'|)dz' = e^{\nu z} + \frac{G_3(\nu z) + G_2(\nu, z)}{2} \tag{12}$$

and

$$\frac{1-a}{2}\int_0^\infty e^{-\nu z}E_1(|z-z'|)dz' = e^{-\nu z} - \frac{G_3(\nu, z) - G_2(\nu, z)}{2}. \tag{13}$$

To obtain an approximation to $f(z)$ we can proceed by two slightly different methods. We can write

$$f(z) = K_1[\sinh \nu(z + z_0) + q_1(z)], \tag{14}$$

where $q_1(z)$ is $0(e^{-kz})$ as $z \to \infty$, $k > \nu$ and $K_1 = \sqrt{\frac{2\nu^2(1-\nu^2)}{a(\nu^2-a)}}$ if $j(o) = 1$. Substituting this in (1) and using (12) and (13) we obtain for $q_1(z)$ the nonhomogeneous equation

$$q_1(z) = \frac{1-a}{2}\int_0^\infty q_1(z')E_1(|z-z'|)dz' + \frac{\cosh \nu z_0}{2}G_3(\nu, z) + \frac{\sinh \nu z_0}{2}G_2(\nu, z), \tag{15}$$

from which we can obtain by variational technique an approximation to z_0 and $q_1(z)$.

Or we can write
$$f(z) = K_2 \left[e^{\nu z} + q_2(z)\right], \tag{16}$$

where
$$K_2 = K_1 \frac{e^{\nu z_0}}{2}, \text{ and } q_2(z) = e^{-2\nu z_0} e^{-\nu z} + 2e^{-\nu z_0} q_1(z). \tag{17}$$

Substituting (16) in (1) and using (12), we obtain the equation
$$q_2(z) = \frac{1-\alpha}{2} \int_0^\infty q_2(z') E_1(|z-z'|) dz' + \frac{G_3(\nu, z) + G_2(\nu, z)}{2}, \tag{18}$$

from which an approximation to z_0 and $q_2(z)$ can be obtained.

Method I

Let us consider first Equation (15). Here the nonhomogeneous term is
$$h(z) = \frac{\cosh \nu z_0}{2} G_3(\nu, z) + \frac{\sinh \nu z_0}{2} G_2(\nu, z). \tag{19}$$

$\int_0^\infty h(z) q_1(z) dz$ has been evaluated by Marshak as follows. Multiply (15) by $\sinh \nu(z + z_0)$, and integrate with respect to z, over the range $(0, \infty)$.

$$\int_0^\infty \sinh \nu(z+z_0) q_1(z) dz = \frac{1-\alpha}{2} \int_0^\infty \sinh \nu(z+z_0) \int_0^\infty q_1(z') E_1(|z-z'|) dz' dz$$
$$+ \int_0^\infty \sinh \nu(z+z_0) \left[\frac{\cosh \nu z_0}{2} G_3(\nu, z) + \frac{\sinh \nu z_0}{2} G_2(\nu, z)\right] dz.$$

By interchanging the order of integration and using (12) and (13), this becomes

$$\int_0^\infty q_1(z) \left[\frac{\cosh \nu z_0}{2} G_3(\nu, z) + \frac{\sinh \nu z_0}{2} G_2(\nu, z)\right] dz$$
$$= -\int_0^\infty \sinh \nu(z+z_0) \left[\frac{\cosh \nu z_0}{2} G_3(\nu, z) + \frac{\sinh \nu z_0}{2} G_2(\nu, z)\right] dz$$
$$= -\frac{1-\alpha}{8\nu^2} \left[(\cosh 2\nu z_0) \log(1-\nu^2) + \log(1-\nu^2) + \frac{2\nu^2}{1-\nu^2}\right]. \tag{20}$$

An appropriate choice of trial function for $q_1(z)$ is
$$\bar{q}_1(z) = AG_3(\nu, z) + BG_2(\nu, z) \tag{21}$$

The function (21) is suitable since it has the correct asymptotic behavior as $z \to \infty$, and since its slope becomes infinite logarithmically as $z \to 0$, which is easily seen to be true of the true function $q_1(z)$.

With $\bar{q}_1(z)$ given by (21) the functional (8) becomes
$$F(\bar{q}_1) = \frac{K_1 + K_2 \frac{B}{A} + K_3 \left(\frac{B}{A}\right)^2}{\left(L_1 + L_2 \frac{B}{A}\right)^2}, \tag{22}$$

where K_1, K_2, K_3, L_1, L_2 are integrals involving G_2, G_3, E_1 which can be evaluated analytically.* Only the ratio $\frac{B}{A}$ can be determined from the extremum property of $F(\bar{q}_1)$. We have $\frac{dF}{d\left(\frac{B}{A}\right)} = 0$

so that
$$\frac{B}{A} = \frac{2L_2K_1 - L_1K_2}{2L_1K_3 - L_2K_2}. \tag{23}$$

A good approximation to z_0 can be obtained by setting $F(q_1) = \frac{1}{\int h(z)q(z)dz}$, where $\frac{B}{A}$ for $F(q_1)$ is given by (23) and $\int h(z)q(z)dz$ is given by (20), so that we have the transcendental equation for z_0:

$$\frac{4K_1K_3 - K_2^2}{[L_1^2K_3 + L_2^2K_1 - L_1L_2K_2]} = \frac{-1}{\left[(\cosh 2\nu z_0 + 1)\log(1-\nu^2) + \frac{2\nu^2}{1-\nu^2}\right]\frac{(1-a)}{8\nu^2}}. \tag{24}$$

Thus we obtain an approximation to $f(z)$:

$$f^{(1)}(z) = K_1\left[\sinh \nu(z + z_0) + A\left(G_3(\nu, z) + \frac{B}{A}G_2(\nu, z)\right)\right] \tag{25}$$

in which z_0 and $\frac{B}{A}$ are known, and A is still to be determined. In order to determine A we require some additional property of $f(z)$. For example, we can use (6), $f(o) = j(o)\sqrt{\frac{\nu^2}{a}}$, which implies, from (2), the choice of normalization

$$K_1 = j(o)\sqrt{\frac{2\nu^2(1-\nu^2)}{a(\nu^2 - a)}}.$$

So that, making $f^{(1)}(z)$ correct at the boundary we get the equation

$$\sqrt{\frac{\nu^2 - a}{2(1-\nu^2)}} = \sinh \nu z_0 + A\left\{G_3(\nu, o) + \frac{B}{A}G_2(\nu, o)\right\} \tag{26}$$

and
$$A = \frac{\sqrt{\frac{\nu^2 - a}{2(1-\nu^2)}} - \sinh \nu z_0}{-\frac{1-a}{2\nu}\log(1-\nu^2) - \frac{B}{A}}. \tag{27}$$

Method II

Method I has the disadvantage that some additional information regarding $f(z)$, e.g. $f(o)$, is necessary before $f^{(1)}(z)$ can be determined. If we consider

* *The expressions for K_1, K_2, K_3, L_1, L_2 are given in the Appendix.*

Equation (18), an approximation to $f(z)$ can be completely determined from the extremum property of $F(q)$. For Equation (18) we have

$$h(z) = \frac{G_3(\nu, z) + G_2(\nu, z)}{2}.$$

The value of $\int_0^\infty h(z)q_2(z)dz$, in terms of z_0, can be obtained from (20), by making use of the relation (17) between $q_1(z)$ and $q_2(z)$ and also of the equation

$$\int_0^\infty q_2(z)\left[\frac{G_3(\nu, z) - G_2(\nu, z)}{2}\right]dz = \int_0^\infty \frac{e^{-\nu z}[G_3(\nu, z) + G_2(\nu, z)]}{2}dz,$$

which can be obtained from Equation (18) by multiplying by $e^{-\nu z}$ and integrating with respect to z over the range, (o, ∞). We have

$$\int_0^\infty q_2(z)\frac{G_3(\nu, z) + G_2(\nu, z)}{2}dz = \frac{-(1-a)}{2\nu}$$
$$\left[\frac{\log(1-\nu^2)}{2\nu} + \left(\frac{2}{1-\nu^2} - \frac{2}{1-a}\right)e^{-2\nu z_0}\right]. \tag{28}$$

To obtain an approximation to $f(z)$, we start from the trial function

$$\bar{q}_2(z) = k\left[e^{-\nu z} + AG_3(\nu, z) + BG_2(\nu, z)\right], \tag{29}$$

which corresponds to (21). If $k = e^{-2\nu z_0}$, $e^{\nu z} + \bar{q}_2(z)$ has the correct asymptotic behavior. In this case $F(\bar{q}_2)$ is a rather lengthy expression which will not be given here*(6). By minimizing it, one can determine A and B.

The value of z_0 given by this approximation is found from

$$F(\bar{q})_2 = \frac{-1}{\frac{1-a}{2}\left[\frac{\log(1-\nu^2)}{2\nu} + e^{-2\nu z_0}\left(\frac{2}{1-\nu^2} - \frac{2}{1-a}\right)\right]},$$

that is,

$$z_0 = \frac{-1}{2\nu}\log\left\{\frac{\frac{-(1-a)}{4\nu^2}\log(1-\nu^2) - \frac{1}{F(\bar{q}_2)}}{\frac{1-a}{\nu}\left(\frac{1}{1-\nu^2} - \frac{1}{1-a}\right)}\right\}. \tag{30}$$

No numerical work has been attempted with the trial function (29). For the simpler trial function $\bar{q}(z) = e^{-\nu z}$, one obtains an analytical expression for z_0:

$$z_0 = -\frac{1}{2\nu}\log\left\{\frac{\left[\frac{1}{1+\nu} - \frac{1}{\nu}\log(1+\nu)\right]^2 - \frac{1}{4\nu^2}\log^2(1-\nu^2)}{\frac{1}{\nu}\left(\frac{1}{1-\nu^2} - \frac{1}{1-a}\right)\log(1-\nu^2)}\right\}. \tag{31}$$

As will be seen below, this expression represents z_0 within 0.3%.

* *The present paper is based on Montreal Report M.T. 119, which contains the full expression for $F(\bar{q}_2)$. Anyone interested should write to the Theoretical Physics Branch, Chalk River Laboratories, National Research Council, Chalk River, Ont.*

Angular Distribution of Outgoing Neutrons

The angular distribution is related to $f(z)$ by

$$\psi_h(\mu) = \frac{(1-a)}{2\mu}\int_0^\infty f(z')e^{-z'/\mu}dz', \tag{32}$$

where μ is the cosine of the angle between the direction of the neutron and the *outward* normal. Thus the angular distribution corresponding to

$$f(z) = \sqrt{\frac{2\nu^2(1-\nu^2)}{a(\nu^2-a)}}\left[\sinh \nu(z+z_0) + AG_3(\nu, z) + BG_2(\nu, z)\right]$$

is

$$\begin{aligned}\psi_h(\mu) = \frac{1-a}{4}\sqrt{\frac{2\nu^2(1-\nu^2)}{a(\nu^2-a)}}\Bigg[&\frac{e^{\nu z_0}}{1-\mu\nu} - \frac{e^{-\nu z_0}}{1+\mu\nu} \\ &+ \frac{(1-a)A}{(1-\mu^2\nu^2)\nu}\left\{-\log(1-\nu^2) - \frac{2\mu\nu^2}{1-a} + 2\mu^2\nu^2\log\left(1+\frac{1}{\mu}\right)\right\} \\ &+ \frac{(1-a)B}{(1-\mu^2\nu^2)\nu}\left\{-\frac{2\nu}{1-a} - \log(1-\nu^2)\mu\nu + 2\mu\nu\log\left(1+\frac{1}{\mu}\right)\right\}\Bigg]\end{aligned} \tag{33}$$

and

$$\begin{aligned}\int_0^1 \psi_h(\mu)d\mu = \frac{1-a}{4}\sqrt{\frac{2(1-\nu^2)}{a(\nu^2-a)}}\Bigg[&-e^{\nu z_0}\log(1-\nu) - e^{-\nu z_0}\log(1+\nu) \\ &+ \frac{A(1-a)}{\nu}\left\{-4\nu\log 2 + \frac{2\nu}{1-a}\log(1+\nu) + \frac{\pi^2}{6} - 2\sum\frac{(-1)^{n-1}}{n^2}\left(\frac{1-\nu}{1+\nu}\right)^n\right\} \\ &+ \frac{B(1-a)}{\nu}\log(1+\nu)\log(1-\nu)\Bigg].\end{aligned}$$

Numerical Results

It has already been noted that the variational method gives a better approximation to z_0 than to the density function. Table I gives a comparison of the

TABLE I

a	From (31)	From (24)	By Integration
0	0.7083	0.7104	0.7104
0.1	0.7095	0.7106	0.7106
0.2	0.7105	0.7113	0.7113
0.3	0.7121	0.7127	0.7127
0.4	0.7150	0.7154	0.7154
0.5	0.7202	0.7204	0.721
0.6	0.7298	0.7300	0.730
0.7	0.7484	0.7484	0.749
0.8	0.7848	0.7847	0.785
0.9	0.8538	0.8539	0.85
1	1.0000	1.0000	1.0

values for $(1-a)\,z_0$ obtained from the simple expression (31) and the more accurate approximation (24), with the values obtained from numerical integration of the exact expression (4).

The simple expression (31) is thus seen to give a good approximation to z_0. Its maximum error (0.3%) occurs for $a = 0$ and the accuracy increases with increasing a. Equation (24) is of course a much better approximation. For $a > 5$, when the numerical integration is difficult, (24) and even (31) seems to be more accurate than the result of numerical integration.

Method I has been applied to determine $f(z)$ and $\phi(\mu)$ for $a = 0.1, 0.2, 0.3, 0.4, 0.5, 0.6, 0.7, 0.8, 0.9$. We get

$$f(z) = \sinh \nu(z + z_0) + AG_3(\nu, z) + BG_2(\nu, z)$$
$$= \sinh \nu(z + z_0) + \frac{1-a}{2\nu}\left\{(A+B)e^{\nu z}E_1((1+\nu)z) + (A-B)e^{-\nu z}E_1((1-\nu)z) - 2AE_1(z)\right\}, \quad (34)$$

where the constants ν, z_0, A, B, depend on a, and are given in Table II.

TABLE II

a	ν	z_0	$B \div A$	A	B
0.1	0.5254	0.7896	0.5794	0.2581	0.1496
0.2	0.7104	0.8891	0.7883	0.3052	0.2406
0.3	0.8286	1.0181	0.9219	0.3748	0.3456
0.4	0.9073	1.1923	1.0070	0.4868	0.4902
0.5	0.9575	1.4408	1.0531	0.6886	0.7251
0.6	0.9856	1.8249	1.0649	1.1281	1.2014
0.7	0.9974	2.4947	1.0490	2.4727	2.5938
0.8	0.99997	3.9238	1.021	11.48	11.72
0.9	1.00000	8.5394	1.004	1238	1243

$\phi(\mu)$ is given by (33) with the constants as in Table II.
For a near zero, ν approaches zero, and

$$\sinh \nu(z + z_0) \doteqdot \nu(z + z_0)$$
$$G_3(\nu, z_0) \doteqdot \nu E_3(z)$$
$$G_2(\nu, z) \doteqdot -E_2(z)$$
$$\frac{B}{A} \doteqdot 1.0915\nu.$$

Thus for $a = 0$, the expression for $f(z)$ determined by Method I is

$$f(z) = 3\left\{z + z_0 + 0.2248\,E_3(z) - 0.2455\,E_2(z)\right\}. \quad (35)$$

Method II applied to the case $a = 0$ gives

$$f(z) = 3\left\{z + z_0 + 0.2244\,E_3(z) - 0.2436\,E_2(z)\right\}.$$

In the limiting case a and ν near 1, the ratio $\dfrac{B}{A}$ also approaches 1.

$$\frac{B}{A} \doteqdot 1 + \frac{1.1835}{\log^2(1-\nu)} + \ldots\ldots$$

We have also

$$A \doteqdot \frac{\sqrt{1-a}}{4\sqrt{2}} e^{\frac{1}{1-a}}$$

$$\sinh \nu(z+z_0) \doteqdot e^{\nu z} \cdot \frac{\sqrt{1-a}}{2\sqrt{2}} e^{\frac{1}{1-a}} \left(1 + \frac{1-a}{2} \log 2\right)$$

and

$$\sqrt{\frac{2\nu^2(1-\nu^2)}{a(\nu^2-a)}} \doteqdot \frac{2\sqrt{2} \cdot e^{-\frac{1}{1-a}}}{\sqrt{1-a}} \left\{1 + \frac{1-a}{2} + \ldots.\right\}.$$

Thus in the limit for $a \doteqdot 1$, $f(z)$ is

$$f(z) \doteqdot \left\{1 + \frac{1-a}{2}(1 + \log 2) \ldots\right\} e^z - \frac{1-a}{2}\left\{E_1(z) - e^z E_1(2z)\right\} \quad (36)$$

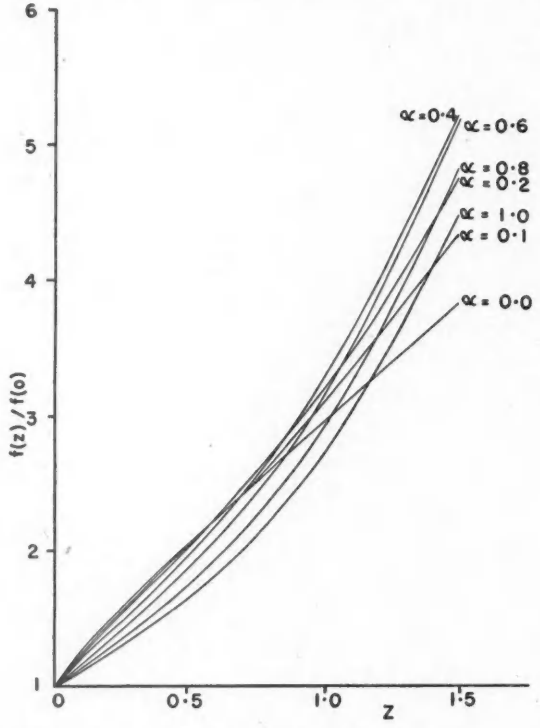

FIG. 1. *Neutron density $f(z)/f(o)$ as a function of distance z from the boundary. Unit of length: total mean free path.*

The angular distribution $\psi_h(\mu)$, given by (33) becomes for $a \doteqdot 1$,

$$\psi_h(\mu) \doteqdot \frac{1-a}{2(1-\nu\mu)}\left\{1+\frac{1-a}{2}\mu\log\left(1+\frac{1}{\mu}\right)+\cdots\right\}.$$

These forms agree with those obtained by the rigorous treatment for $a \doteqdot 1$ [1]

For $a = 0, 0.1, 0.2, 0.3, 0.4, 0.5, 0.6, 0.7, 0.8, 0.9, 1$, the density and the asymptotic density are tabulated, in Tables III and IV, as a function of z, the distance from tne boundary measured in units of total mean free path. In Table III the normalization used is unit outgoing current at the boundary, so that

$$f(z) = \sqrt{\frac{2\nu^2(1-\nu^2)}{a(\nu^2-a)}}\left\{\sinh\nu(z+z_0) + AG_3(\nu,z) + BG_2(\nu,z)\right\}. \quad (37)$$

In Table IV the normalization used is unit density at the boundary:

$$\bar{f}(z) = \sqrt{\frac{a}{\nu^2}}f(z). \quad (38)$$

In each table column (a) gives the density, column (b) the asymptotic density, and column (c) the deviation of the density from the asymptotic density. The figures used for $a = 0$ are those obtained by numerical integration (7).

Fig. 1 is a plot of density normalized to unit density at the boundary (column (a), Table IV) over the region within one and a half mean free paths of the boundary, for $a = 0, 0.1, 0.2, 0.4, 0.6, 0.8, 1$.

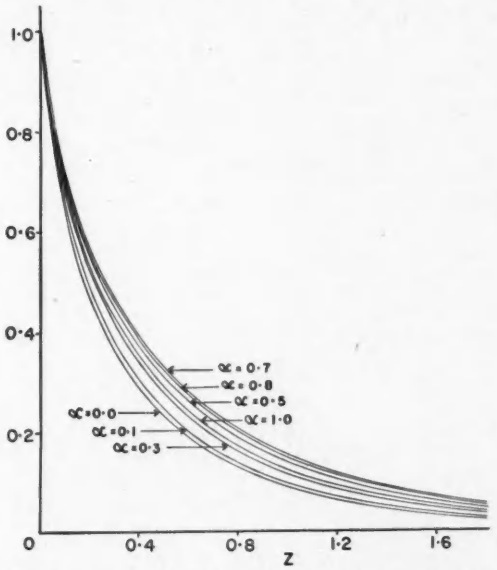

FIG. 2. *Deviation of neutron density from the asymptotic density, normalized to unit deviation at the boundary, as a function of distance z from the boundary. Unit of length: total mean free path.*

The deviation of the true density from the asymptotic density is investigated further in Table V and Fig. 2. Table V gives the deviation normalized to unit deviation at the boundary. The values used for $a = 0$ in this table were obtained from (35). Although, as seen from Tables II and III the deviation from the asymptotic is identically zero for $a = 1$, it is seen from (36) that the deviation normalized to unit deviation at the boundary, approaches, as $a \to 1$, the limit

$$\frac{e^z E_1(2z) - E_1(z)}{-\log 2}.$$

Fig. 2 is a plot of this deviation, for $a = 0, 0.1, 0.3, 0.5\ 0.7, 0.8, 1$. The curve for $a = 0$ is lowest, the curves rise as a increases until $a = 0.7$, and then fall again for larger a, so that the limiting curve $a = 1$, lies slightly below the curve for $a = 0.4$.

The angular distribution of emerging neutrons, $\phi(\mu)$ is tabulated in Table VI. The values for $a = 0$ are obtained by numerical integration and the values for $a = 0.1, 0.2, 0.3, 0.4, 0.5, 0.6, 0.7, 0.8, 0.9$, are obtained from (33). The normalization used is

$$\int_0^1 \phi(\mu) d\mu = 1.$$

TABLE III

DENSITY NORMALIZED TO UNIT CURRENT

z	$a = 0$			$a = 0.1$			$a = 0.2$		
	(*a*)	(*b*)	(*c*)	(*a*)	(*b*)	(*c*)	(*a*)	(*b*)	(*c*)
0	1.7321	2.1312	0.3991	1.6619	2.0340	0.3721	1.5889	1.9320	0.3431
0.1	2.1841	2.4313	0.2472	2.0693	2.3089	0.2396	1.9566	2.1823	0.2257
0.2	2.5485	2.7312	0.1827	2.4114	2.5905	0.1791	2.2731	2.4441	0.1710
0.3	2.8899	3.0312	0.1413	2.7396	2.8792	0.1396	2.5834	2.7180	0.1346
0.4	3.2190	3.3312	0.1122	3.0646	3.1761	0.1115	2.8973	3.0056	0.1083
0.5	3.5406	3.6312	0.0906	3.3905	3.4810	0.0905	3.2198	3.3083	0.0885
1.0	5.0955	5.1312	0.0357	5.1338	5.1701	0.0363	5.0702	5.1066	0.0364
1.5	6.6153	6.6312	0.0159	7.2017	7.2179	0.0162	7.5392	7.5559	0.0167
2.0	8.1237	8.1312	0.0075	9.7593	9.7669	0.0076	10.9604	10.9684	0.0080
3.0	11.1294	11.1312	0.0018	17.1210	17.1229	0.0019	21.7871	21.7891	0.0020

z	$a = 0.3$			$a = 0.4$			$a = 0.5$		
	(*a*)	(*b*)	(*c*)	(*a*)	(*b*)	(*c*)	(*a*)	(*b*)	(*c*)
0	1.5130	1.8246	0.3116	1.4347	1.7116	0.2769	1.3543	1.5921	0.2378
0.1	1.8420	2.0512	0.2092	1.7249	1.9146	0.1897	1.6067	1.7727	0.1660
0.2	2.1311	2.2915	0.1604	1.9860	2.1333	0.1473	1.8393	1.9696	0.1303
0.3	2.4202	2.5477	0.1275	2.2514	2.3696	0.1182	2.0789	2.1845	0.1056
0.4	2.7178	2.8214	0.1036	2.5284	2.6254	0.0970	2.3323	2.4196	0.0873
0.5	3.0293	3.1146	0.0853	2.8228	2.9031	0.0803	2.6037	2.6767	0.0730
1.0	4.9103	4.9468	0.0365	4.6665	4.7018	0.0353	4.3538	4.3868	0.0330
1.5	7.6231	7.6403	0.0172	7.4682	7.4852	0.0170	7.1053	7.1216	0.0163
2.0	11.6557	11.6642	0.0085	11.8271	11.8358	0.0087	11.5116	11.5201	0.0085
3.0	26.8575	26.8599	0.0024	29.3982	29.4006	0.0024	30.0449	30.0473	0.0024

TABLE III—*Concluded*

DENSITY NORMALIZED TO UNIT CURRENT—*concluded*

z	$a = 0.6$			$a = 0.7$			$a = 0.8$		
	(*a*)	(*b*)	(*c*)	(*a*)	(*b*)	(*c*)	(*a*)	(*b*)	(*c*)
0	1.2724	1.4656	0.1932	1.1922	1.3341	0.1419	1.1179	1.2024	0.0845
0.1	1.4889	1.6256	0.1367	1.3750	1.4760	0.1010	1.2695	1.3290	0.0595
0.2	1.6931	1.8014	0.1083	1.5522	1.6324	0.0802	1.4217	1.4688	0.0471
0.3	1.9061	1.9946	0.0885	1.7394	1.8052	0.0658	1.5849	1.6233	0.0384
0.4	2.1337	2.2073	0.0736	1.9410	1.9959	0.0549	1.7622	1.7941	0.0319
0.5	2.3795	2.4415	0.0620	2.1601	2.2065	0.0464	1.9560	1.9829	0.0269
1.0	3.9963	4.0224	0.0288	3.6171	3.6290	0.0219	3.2568	3.2693	0.0125
1.5	6.5855	6.6000	0.0145	5.9843	5.9955	0.0112	5.3838	5.3901	0.0063
2.0	10.8057	10.8133	0.0076	9.8684	9.8743	0.0059	8.8832	8.8866	0.0034
3.0	28.9852	28.9874	0.0022	26.7729	26.7747	0.0018	24.1531	24.1541	0.0010

z	$a = 0.9$			$a = 1.0$		
	(*a*)	(*b*)	(*c*)	(*a*)	(*b*)	(*c*)
0	1.0541	1.0907	0.0366	1.0000	1.0000	0
0.1	1.1799	1.2054	0.0255	1.1052	1.1052	0
0.2	1.3122	1.3321	0.0199	1.2214	1.2214	0
0.3	1.4561	1.4723	0.0162	1.3499	1.3499	0
0.4	1.6138	1.6271	0.0133	1.4918	1.4918	0
0.5	1.7871	1.7982	0.0111	1.6487	1.6487	0
1.0	2.9597	2.9647	0.0050	2.7183	2.7183	0
1.5	4.8855	4.8880	0.0025	4.4817	4.4817	0
2.0	8.0577	8.0590	0.0013	7.3891	7.3891	0
3.0	21.9063	21.9067	0.0004	20.0855	20.0855	0

$$(a) = f(z)$$

$$(b) = \sqrt{\frac{\nu^2 2(1-\nu^2)}{a(\nu^2-a)}}\ \sinh \nu(z+z_0)$$

$$(c) = (b) - (a).$$

TABLE IV

DENSITY NORMALIZED TO UNIT DENSITY AT THE BOUNDARY

z	$a = 0$			$a = 0.1$			$a = 0.2$		
	(*a*)	(*b*)	(*c*)	(*a*)	(*b*)	(*c*)	(*a*)	(*b*)	(*c*)
0	1.0000	1.2304	0.2304	1.0000	1.2239	0.2239	1.0000	1.2159	0.2159
0.1	1.2611	1.4037	0.1426	1.2451	1.3893	0.1442	1.2314	1.3735	0.1421
0.2	1.4714	1.5769	0.1055	1.4510	1.5588	0.1078	1.4306	1.5382	0.1076
0.3	1.6685	1.7501	0.0816	1.6485	1.7325	0.0840	1.6259	1.7106	0.0847
0.4	1.8585	1.9233	0.0648	1.8440	1.9111	0.0671	1.8235	1.8916	0.0681
0.5	2.0442	2.0965	0.0523	2.0401	2.0946	0.0545	2.0264	2.0821	0.0557
1.0	2.9419	2.9625	0.0206	3.0891	3.1110	0.0219	3.1910	3.2139	0.0229
1.5	3.8193	3.8285	0.0092	4.3334	4.3432	0.0098	4.7449	4.7554	0.0105
2.0	4.6902	4.6946	0.0044	5.8724	5.8769	0.0045	6.8981	6.9031	0.0050
3.0	6.4256	6.4266	0.0010	10.3021	10.3032	0.0011	13.7121	13.7133	0.0012

TABLE IV—*Concluded*

DENSITY NORMALIZED TO UNIT DENSITY AT THE BOUNDARY—*concluded*

z	$a = 0.3$			$a = 0.4$			$a = 0.5$		
	(*a*)	(*b*)	(*c*)	(*a*)	(*b*)	(*c*)	(*a*)	(*b*)	(*c*)
0	1.0000	1.2059	0.2059	1.0000	1.1930	0.1930	1.0000	1.1756	0.1756
0.1	1.2174	1.3557	0.1383	1.2023	1.3345	0.1322	1.1864	1.3089	0.1225
0.2	1.4085	1.5145	0.1060	1.3843	1.4869	0.1026	1.3581	1.4543	0.0962
0.3	1.5996	1.6839	0.0843	1.5692	1.6516	0.0824	1.5350	1.6130	0.0780
0.4	1.7963	1.8648	0.0685	1.7623	1.8299	0.0676	1.7221	1.7866	0.0645
0.5	2.0022	2.0586	0.0564	1.9675	2.0235	0.0560	1.9225	1.9764	0.0539
1.0	3.2454	3.2695	0.0241	3.2526	3.2772	0.0246	3.2148	3.2392	0.0244
1.5	5.0384	5.0498	0.0114	5.2054	5.2173	0.0119	5.2465	5.2585	0.0120
2.0	7.7037	7.7093	0.0056	8.2436	8.2497	0.0061	8.500	8.5063	0.0063
3.0	17.7512	17.7527	0.0015	20.4908	20.4925	0.0017	22.1848	22.1866	0.0018

z	$a = 0.6$			$a = 0.7$			$a = 0.8$		
	(*a*)	(*b*)	(*c*)	(*a*)	(*b*)	(*c*)	(*a*)	(*b*)	(*c*)
0	1.0000	1.1518	0.1518	1.0000	1.1190	0.1190	1.0000	1.0756	0.0756
0.1	1.1702	1.2776	0.1074	1.1533	1.2380	0.0847	1.1356	1.1888	0.0532
0.2	1.3306	1.4157	0.0851	1.3020	1.3692	0.0672	1.2718	1.3139	0.0421
0.3	1.4980	1.5676	0.0696	1.4590	1.5142	0.0552	1.4177	1.4521	0.0344
0.4	1.6769	1.7348	0.0579	1.6281	1.6741	0.0460	1.5763	1.6049	0.0286
0.5	1.8701	1.9188	0.0487	1.8119	1.8508	0.0389	1.7497	1.7738	0.0241
1.0	3.1386	3.1613	0.0227	3.0340	3.0523	0.0183	2.9133	2.9245	0.0112
1.5	5.1757	5.1870	0.0113	5.0195	5.0289	0.0094	4.8160	4.8216	0.0056
2.0	8.4924	8.4983	0.0059	8.2775	8.2824	0.0049	7.9463	7.9494	0.0031
3.0	22.7799	22.7817	0.0018	22.4567	22.4582	0.0015	21.6058	21.6067	0.0009

z	$a = 0.9$			$a = 1.0$		
	(*a*)	(*b*)	(*c*)	(*a*)	(*b*)	(*c*)
0	1.0000	1.0347	0.0347	1.0000	1.0000	0
0.1	1.1193	1.1435	0.0242	1.1052	1.1052	0
0.2	1.2449	1.2637	0.0188	1.2214	1.2214	0
0.3	1.3814	1.3967	0.0153	1.3499	1.3499	0
0.4	1.5310	1.5436	0.0126	1.4918	1.4918	0
0.5	1.6954	1.7059	0.0105	1.6487	1.6487	0
1.0	2.8078	2.8125	0.0047	2.7183	2.7183	0
1.5	4.6348	4.6371	0.0023	4.4817	4.4817	0
2.0	7.6442	7.6454	0.0012	7.3891	7.3891	0
3.0	20.7820	20.7824	0.0004	20.0855	20.0855	0

$(a) = f(z)$

$(b) = \sqrt{\frac{2(1-\nu^2)}{(\nu^2-a)}} \sinh \nu(z+z_0)$

$(c) = (b) - (a).$

This normalization would be equivalent to unit density at the boundary if $\phi(\mu)$ were the correct angular distribution. Since

$$\phi(o) = \frac{1-a}{2} \cdot \rho(o)$$

it is evident from the values of $\phi(o)$ given in Table VI that the accuracy of the approximation to $\phi(\mu)$ is such that $\int_0^1 \phi(\mu)d\mu$ is practically equal to its true value.

Fig. 3*a* gives a plot of $\phi(\mu)$ for $\alpha = 0, 0.1, 0.2, 0.3$, and Fig. 3*b* gives $\phi(\mu)$ for $\alpha = 0, 0.3, 0.4, 0.5, 0.6$. In the limit as $\alpha \to 1$, $\phi(\mu)$ is zero for $\mu \neq 1$, and for $\mu = 1$, becomes infinite.

The accuracy of the approximation to the angular distribution is indicated in Tables VII and VIII. Table VII shows, for $\mu = 1$, and $\mu = 0$, and $\alpha = 0.1, 0.2, 0.4, 0.6$, the values of $\phi(\mu)$ obtained by the method of variations, and the

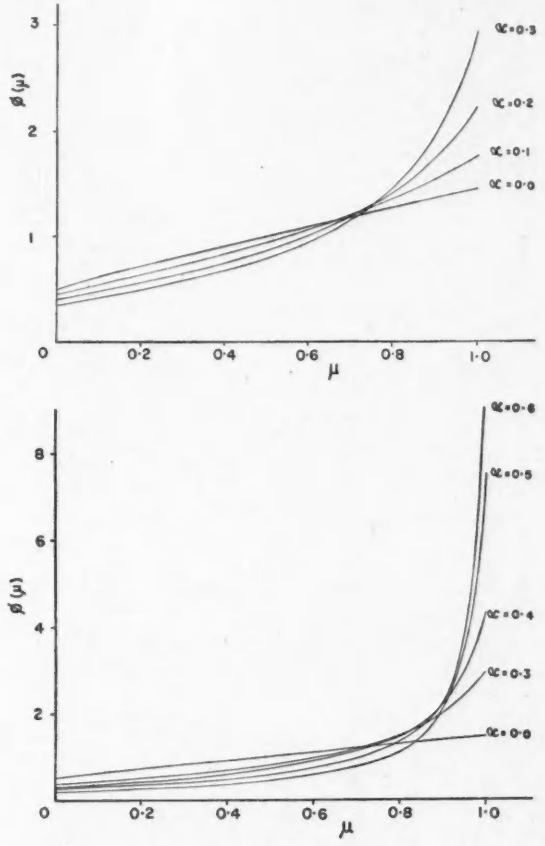

FIGS. 3a AND 3b. *Emerging angular distribution* $\phi(\mu)$, *normalized to unit density:* $\int_0^1 \phi(\mu)d\mu = 1$.

values obtained by numerical integration (2). Table VIII shows the values of $\phi(\mu)$ obtained by the method of variations and those obtained by integration (2), for $a = 0.4$ and $\mu = 0, 0.4, 0.8, 1$.

TABLE V

NEUTRON DENSITY IN MILNE'S PROBLEM WITH CAPTURE
DEVIATION FROM ASYMPTOTIC SOLUTION
NORMALIZED TO UNIT DEVIATION AT THE BOUNDARY
AS A FUNCTION OF DISTANCE FROM THE BOUNDARY

z	$a = 0$	$a = 0.1$	$a = 0.2$	$a = 0.3$	$a = 0.4$	$a = 0.5$
0	1.0000	1.0000	1.0000	1.0000	1.0000	1.0000
0.1	0.6286	0.6435	0.6576	0.6712	0.6852	0.6979
0.2	0.4635	0.4810	0.4977	0.5150	0.5317	0.5476
0.3	0.3573	0.3749	0.3920	0.4091	0.4272	0.4441
0.4	0.2825	0.2992	0.3158	0.3326	0.3501	0.3668
0.5	0.2271	0.2426	0.2577	0.2739	0.2904	0.3068
0.7	0.1520	0.1645	0.1774	0.1911	0.2055	0.2199
1.0	0.0880	0.0971	0.1063	0.1166	0.1276	0.1389
1.5	0.0386	0.0437	0.0486	0.0549	0.0615	0.0686
1.8	0.0244	0.0279	0.0316	0.0359	0.0408	0.0460
2.0	0.0181	0.0209	0.0237	0.0273	0.0312	0.0355
3.0	0.0045	0.0053	0.0062	0.0074	0.0087	0.0102

z	$a = 0.6$	$a = 0.7$	$a = 0.8$	$a = 0.9$	$a = 1$
0	1.0000	1.0000	1.0000	1.0000	1.0000
0.1	0.7077	0.7114	0.7044	0.6970	0.6805
0.2	0.5604	0.5655	0.5570	0.5454	0.5262
0.3	0.4580	0.4637	0.4550	0.4416	0.4217
0.4	0.3809	0.3870	0.3783	0.3645	0.3448
0.5	0.3204	0.3267	0.3185	0.3048	0.2858
0.7	0.2323	0.2383	0.2313	0.2186	0.2016
1.0	0.1489	0.1541	0.1487	0.1384	0.1247
1.5	0.0752	0.0788	0.0757	0.0689	0.0599
1.8	0.0509	0.0538	0.0516	0.0464	0.0396
2.0	0.0396	0.0418	0.0402	0.0359	0.0303
3.0	0.0117	0.0128	0.0122	0.0106	0.0084

TABLE VI

ANGULAR DISTRIBUTION OF NEUTRON EMERGING AT THE BOUNDARY
NORMALIZED TO UNIT DENSITY AT THE BOUNDARY

μ	$a = 0$	$a = 0.1$	$a = 0.2$	$a = 0.3$	$a = 0.4$	$a = 0.5$	$a = 0.6$	$a = 0.7$	$a = 0.8$	$a = 0.9$
0.00	0.5000	0.4502	0.4001	0.3501	0.3000	0.2500	0.2000	0.1500	0.1000	0.0500
0.01	0.5171	0.4642	0.4117	0.3595	0.3074	0.2556	0.2040	0.1526	0.1023	0.0506
0.05	0.5683	0.5077	0.4483	0.3896	0.3315	0.2741	0.2175	0.1618	0.1073	0.0530
0.10	0.6237	0.5562	0.4900	0.4245	0.3599	0.2964	0.2337	0.1733	0.1143	0.0562
0.20	0.7252	0.6490	0.5725	0.4959	0.4195	0.3442	0.2705	0.1989	0.1299	0.0637
0.30	0.8213	0.7430	0.6609	0.5757	0.4887	0.4012	0.3146	0.2304	0.1498	0.0731
0.40	0.9146	0.8423	0.7604	0.6703	0.5738	0.4732	0.3715	0.2716	0.1759	0.0855
0.50	1.0064	0.9497	0.8774	0.7875	0.6841	0.5696	0.4492	0.3284	0.2124	0.1029
0.60	1.0971	1.0686	1.0172	0.9398	0.8354	0.7076	0.5633	0.4129	0.2666	0.1289
0.70	1.1870	1.2027	1.1933	1.1487	1.0598	0.9239	0.7488	0.5527	0.3565	0.1722
0.80	1.2764	1.3569	1.4234	1.4568	1.4297	1.3151	1.1058	0.8296	0.5364	0.2586
0.90	1.3653	1.5378	1.7402	1.9621	2.1622	2.2456	2.0840	1.6455	1.0751	0.5178
0.94	1.4008	1.6196	1.9037	2.2692	2.7073	3.1160	3.2091	2.7013	1.7925	0.8635
0.96	1.4185	1.6629	1.9963	2.4599	3.0946	3.8605	4.3896	3.9728	2.6879	1.2955
0.98	1.4362	1.7079	2.0973	2.6840	3.6087	5.0673	6.9361	7.4954	5.3659	2.5915
1.00	1.4539	1.7548	2.2081	2.9514	4.3237	7.3616	16.464	65.355	1186.5	$1.2578.10^7$

TABLE VII

ANGULAR DISTRIBUTION, $\mu = 0$ AND $\mu = 1$

a	$\mu = 0$		$\mu = 1$	
	Value obtained by variation	True value	Value obtained by variation	Value obtained by integration
0.1	0.4502	0.4500	1.7548	1.7542
0.2	0.4001	0.4000	2.2081	2.2075
0.4	0.3000	0.3000	4.3237	4.3232
0.6	0.2000	0.2000	16.4640	16.4629

TABLE VIII

ANGULAR DISTRIBUTION, $a = 0.4$

μ	Value obtained by method of variation	Value obtained by integration
0	0.3000	0.3000
0.4	0.5738	0.57407
0.8	1.4297	1.4301
1	4.3237	4.3232

Milne Problem with Constant Production

It has been shown by Davison and Placzek (4) that the density and angular distribution in the Milne problem with constant production are simply related to the density and angular distribution in the Milne problem with the same capture and no production. We use the notation of that paper, namely: $f(z)$ and $\psi_h(\mu)$ denote the density and outgoing angular distribution in the Milne problem with no production normalized to unit outgoing current; $\rho_q(z)$ and $\psi_q(z)$ denote the density and angular distribution in the Milne problem with production normalized to unit production; $g(z)$ denotes the fictitious source density,

$$g(z) = (1 - a)\,\rho_q(z) + 1. \tag{39}$$

From Davison and Placzek, we have

$$g(z) = g(o)\frac{\sqrt{a}}{\nu}f(z) - \int_0^z f(t)dt, \tag{40}$$

where the value of $g(o)$ is arbitrary and depends on the conditions at infinity. In particular, if $g(z)$ is bounded at infinity,

$$g(o) = \frac{1}{\sqrt{a}} \tag{41}$$

and

$$g(z) = \frac{f(z)}{\nu} - \int_0^z f(t)dt. \tag{42}$$

Also, under the same assumption,

$$\psi_q(\mu) = \frac{1}{(1 - a)\nu}(1 - \nu\mu)\psi_h(\mu) \tag{43}$$

Using for $f(z)$ the formula (37) obtained by the variational method,

$$g(z) = \frac{1}{a} - \sqrt{\frac{2(1-\nu^2)}{a(\nu^2-a)}}\, e^{-\nu z - \nu z_0} - \frac{1-a}{\nu}\sqrt{\frac{2(1-\nu^2)}{a(\nu^2-a)}}\,\{\nu A E_2(z) + (A-B)E_1(z) - (A-B)e^{-\nu z}E_1((1-\nu)z)\} \tag{44}$$

where ν, z_0, A, and B are given in Table II.

TABLE IX

FICTITIOUS SOURCE DENSITY, MILNE PROBLEM WITH CONSTANT PRODUCTION NORMALIZED TO UNIT PRODUCTION

z	$a = 0.1$			$a = 0.2$		
	(a)	(b)	(c)	(a)	(b)	(c)
0	3.1623	4.0112	0.8489	2.2361	2.8560	0.6199
0.1	3.7498	4.3178	0.5679	2.5750	3.0031	0.4281
0.2	4.1765	4.6086	0.4321	2.8087	3.1400	0.3313
0.3	4.5434	4.8846	0.3412	3.0026	3.2676	0.2650
0.4	4.8714	5.1464	0.2750	3.1704	3.3864	0.2160
0.5	5.1700	5.3949	0.2249	3.3187	3.4970	0.1783
1.0	6.3662	6.4588	0.0926	3.8702	3.9464	0.0762
1.5	7.2346	7.2770	0.0424	4.2256	4.2614	0.0358
2.0	7.8856	7.9061	0.0205	4.4645	4.4822	0.0177
3.0	8.7565	8.7619	0.0054	4.7408	4.7455	0.0047
∞	10.0000	10.0000	0.0000	5.0000	5.0000	0.0000

z	$a = 0.3$			$a = 0.4$		
	(a)	(b)	(c)	(a)	(b)	(c)
0	1.8257	2.3334	0.5077	1.5811	2.0102	0.4291
0.1	2.0533	2.4129	0.3596	1.7415	2.0526	0.3111
0.2	2.2033	2.4861	0.2828	1.8438	2.0915	0.2477
0.3	2.3250	2.5535	0.2285	1.9244	2.1269	0.2025
0.4	2.4272	2.6155	0.1883	1.9900	2.1593	0.1693
0.5	2.5158	2.6726	0.1568	2.0475	2.1888	0.1413
1.0	2.8275	2.8967	0.0692	2.2379	2.3023	0.0644
1.5	3.0115	3.0448	0.0333	2.3426	2.3744	0.0318
2.0	3.1259	3.1427	0.0168	2.4038	2.4202	0.0164
3.0	3.2454	3.2501	0.0047	2.4631	2.4678	0.0047
∞	3.3333	3.3333	0.0000	2.5000	2.5000	0.0000

z	$a = 0.5$			$a = 0.6$		
	(a)	(b)	(c)	(a)	(b)	(c)
0	1.4142	1.7751	0.3609	1.2910	1.5829	0.2919
0.1	1.5288	1.7957	0.2669	1.3718	1.5908	0.2190
0.2	1.5994	1.8143	0.2149	1.4200	1.5979	0.1779
0.3	1.6526	1.8300	0.1774	1.4563	1.6043	0.1481
0.4	1.6980	1.8467	0.1487	1.4853	1.6102	0.1249
0.5	1.7349	1.8607	0.1258	1.5092	1.6155	0.1063
1.0	1.8546	1.9137	0.0591	1.5841	1.6354	0.0513
1.5	1.9167	1.9465	0.0298	1.6211	1.6476	0.0265
2.0	1.9512	1.9669	0.0157	1.6409	1.6550	0.0141
3.0	1.9827	1.9873	0.0046	1.6580	1.6623	0.0043
∞	2.0000	2.0000	0.0000	1.6667	1.6667	0.0000

TABLE IX—*Concluded*

FICTITIOUS SOURCE DENSITY, MILNE PROBLEM WITH CONSTANT PRODUCTION NORMALIZED TO UNIT PRODUCTION—*concluded*

z	$a = 0.7$			$a = 0.8$		
	(*a*)	(*b*)	(*c*)	(*a*)	(*b*)	(*c*)
0	1.1952	1.4100	0.2148	1.1180	1.2491	0.1311
0.1	1.2500	1.4118	0.1618	1.1514	1.2491	0.0977
0.2	1.2813	1.4133	0.1321	1.1698	1.2492	0.0794
0.3	1.3045	1.4148	0.1103	1.1832	1.2493	0.0661
0.4	1.3228	1.4161	0.0933	1.1935	1.2494	0.0559
0.5	1.3376	1.4173	0.0797	1.2019	1.2494	0.0475
1.0	1.3827	1.4217	0.0390	1.2265	1.2497	0.0232
1.5	1.4040	1.4244	0.0204	1.2378	1.2498	0.0120
2.0	1.4150	1.4261	0.0110	1.2434	1.2499	0.0065
3.0	1.4242	1.4276	0.0034	1.2479	1.2500	0.0020
∞	1.4286	1.4286	0.0000	1.2500	1.2500	0.0000

z	$a = 0.9$			$a = 1$		
	(*a*)	(*b*)	(*c*)	(*a*)	(*b*)	(*c*)
0	1.0541	1.1111	0.0570	1	1	0
0.1	1.0689	1.1111	0.0422	1	1	0
0.2	1.0771	1.1111	0.0340	1	1	0
0.3	1.0830	1.1111	0.0281	1	1	0
0.4	1.0876	1.1111	0.0235	1	1	0
0.5	1.0912	1.1111	0.0199	1	1	0
1.0	1.1017	1.1111	0.0094	1	1	0
1.5	1.1063	1.1111	0.0048	1	1	0
2.0	1.1086	1.1111	0.0025	1	1	0
3.0	1.1103	1.1111	0.0008	1	1	0
∞	1.1111	1.1111	0.0000	1	1	0

(*a*) = $g(z)$, (*b*) = $g_{as}(z)$, (*c*) = (*b*) − (*a*).

The values of $g(z)$ determined from (44) are tabulated in Table IX, column (*a*). Column (*b*) of Table IX gives

$$g_{as}(z) = \frac{1}{a} - \sqrt{\frac{2(1-\nu^2)}{a(\nu^2-a)}}\, e^{-\nu z - \nu z_0} \tag{45}$$

and column (*c*) gives the deviation of $g(z)$ from $g_{as}(z)$. For $a = 0$, $g(z)$ is infinite for every z, and for $a = 1$, $g(z) \equiv 1$. Fig. 4 is a plot of $g(z)$.

The density $\rho_q(z)$ can be found easily from (39), which is equivalent to

$$\rho_q(z) = \frac{g(z) - 1}{1 - a}. \tag{46}$$

$\rho_q(z)$ is tabulated in Table X column (*a*). Column (*b*) gives

$$\rho_{q_{as}}(z) = \frac{1}{a} - \frac{1}{1-a}\sqrt{\frac{2(1-\nu^2)}{a(\nu^2-a)}}\, e^{-\nu z - \nu z_0}$$

and column (*c*) gives the deviation from the asymptotic, $\rho_{q_{as}}(z) - \rho_q(z)$. For $a = 0$, $\rho_q(z)$ is infinite, and for $a = 1$

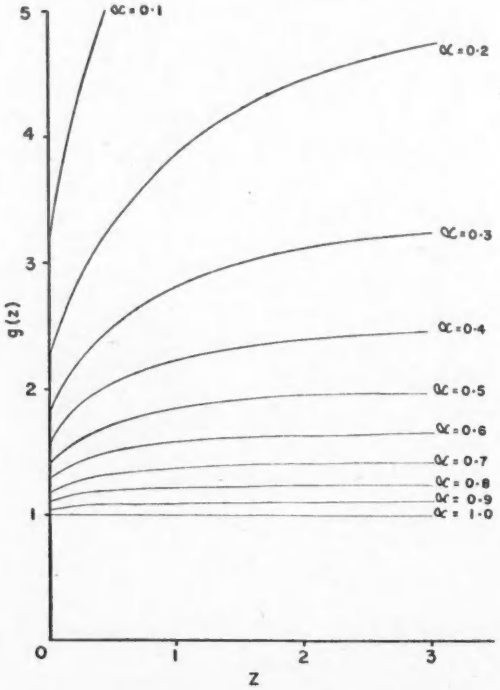

FIG. 4. *Fictitious source density g(z), normalized to unit production per unit length, as a function of distance z from the boundary. Unit of length: total mean free path.*

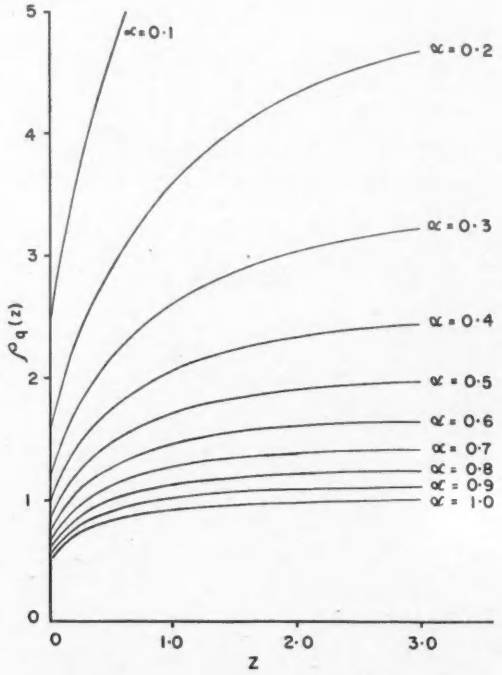

FIG. 5. *Neutron density $\rho_q(z)$, normalized to unit production per unit length, as a function of distance z from the boundary. Unit of length: total mean free path.*

$$\rho_q(z) = 1 - \frac{1}{2} E_2(z). \tag{47}$$

Formula (47) is the limit as $a \to 1$ of $\frac{g(z) - 1}{1 - a}$ with $g(z)$ given by (44). It can easily be shown to be the exact value of $\rho_q(z)$ for $a = 1$. Fig. 5 is a plot of $\rho_q(z)$.

TABLE X

DENSITY, MILNE PROBLEM WITH CONSTANT PRODUCTION NORMALIZED TO UNIT PRODUCTION

z	$a = 0.1$			$a = 0.2$		
	(a)	(b)	(c)	(a)	(b)	(c)
0	2.4025	3.3458	0.9433	1.5451	2.3200	0.7749
0.1	3.0554	3.6864	0.6310	1.9687	2.5038	0.5351
0.2	3.5294	4.0096	0.4802	2.2609	2.6750	0.4141
0.3	3.9372	4.3162	0.3790	2.5032	2.8344	0.3312
0.4	4.3016	4.6071	0.3055	2.7130	2.9830	0.2700
0.5	4.6333	4.8832	0.2499	2.8984	3.1213	0.2229
1.0	5.9624	6.0654	0.1030	3.5878	3.6830	0.0952
1.5	6.9273	6.9744	0.0471	4.0320	4.0767	0.0447
2.0	7.6506	7.6734	0.0228	4.3306	4.3527	0.0221
3.0	8.6184	8.6243	0.0059	4.6760	4.6819	0.0059
∞	10.0000	10.0000	0.0000	5.0000	5.0000	0.0000

z	$a = 0.3$			$a = 0.4$		
	(a)	(b)	(c)	(a)	(b)	(c)
0	1.1796	1.9049	0.7253	0.9686	1.6836	0.7150
0.1	1.5047	2.0185	0.5138	1.2358	1.7544	0.5186
0.2	1.7191	2.1231	0.4040	1.4064	1.8191	0.4127
0.3	1.8929	2.2193	0.3264	1.5406	1.8781	0.3375
0.4	2.0389	2.3079	0.2690	1.6500	1.9321	0.2821
0.5	2.1654	2.3894	0.2240	1.7459	1.9813	0.2354
1.0	2.6107	2.7096	0.0989	2.0631	2.1705	0.1074
1.5	2.8735	2.9212	0.0477	2.2377	2.2907	0.0530
2.0	3.0369	3.0610	0.0241	2.3397	2.3670	0.0273
3.0	3.2078	3.2144	0.0066	2.4386	2.4463	0.0077
∞	3.3333	3.3333	0.0000	2.5000	2.5000	0.0000

z	$a = 0.5$			$a = 0.6$		
	(a)	(b)	(c)	(a)	(b)	(c)
0	0.8284	1.5503	0.7219	0.7275	1.4572	0.7297
0.1	1.0575	1.5913	0.5338	0.9295	1.4769	0.5474
0.2	1.1989	1.6286	0.4297	1.0499	1.4947	0.4448
0.3	1.3051	1.6600	0.3549	1.1407	1.5108	0.3701
0.4	1.3961	1.6934	0.2973	1.2133	1.5255	0.3122
0.5	1.4699	1.7214	0.2515	1.2730	1.5387	0.2657
1.0	1.7092	1.8274	0.1182	1.4603	1.5885	0.1282
1.5	1.8333	1.8930	0.0597	1.5528	1.6189	0.0661
2.0	1.9024	1.9337	0.0313	1.6022	1.6375	0.0353
3.0	1.9654	1.9746	0.0092	1.6451	1.6558	0.0107
∞	2.0000	2.0000	0.0000	1.6667	1.6667	0.0000

TABLE X—*Concluded*

DENSITY, MILNE PROBLEM WITH CONSTANT PRODUCTION NORMALIZED TO UNIT PRODUCTION—*concluded*

z	$\alpha = 0.7$			$\alpha = 0.8$		
	(*a*)	(*b*)	(*c*)	(*a*)	(*b*)	(*c*)
0	0.6508	1.3666	0.7159	0.5902	1.2453	0.6551
0.1	0.8334	1.3725	0.5392	0.7568	1.2457	0.4889
0.2	0.9378	1.3778	0.4400	0.8489	1.2461	0.3972
0.3	1.0151	1.3826	0.3676	0.9158	1.2465	0.3307
0.4	1.0759	1.3870	0.3111	0.9677	1.2468	0.2791
0.5	1.1252	1.3910	0.2657	1.0093	1.2471	0.2378
1.0	1.2756	1.4057	0.1301	1.1327	1.2483	0.1156
1.5	1.3467	1.4147	0.0680	1.1888	1.2489	0.0601
2.0	1.3835	1.4202	0.0367	1.2169	1.2494	0.0325
3.0	1.4141	1.4255	0.0114	1.2397	1.2498	0.0100
∞	1.4286	1.4286	0.0000	1.2500	1.2500	0.0000

z	$\alpha = 0.9$			$\alpha = 1$		
	(*a*)	(*b*)	(*c*)	(*a*)	(*b*)	(*c*)
0	0.5409	1.1111	0.5702	1	0.5000	0.5000
0.1	0.6885	1.1111	0.4226	1	0.6387	0.3613
0.2	0.7712	1.1111	0.3399	1	0.7129	0.2871
0.3	0.8304	1.1111	0.2807	1	0.7654	0.2346
0.4	0.8759	1.1111	0.2352	1	0.8053	0.1947
0.5	0.9120	1.1111	0.1991	1	0.8367	0.1633
1.0	1.0169	1.1111	0.0942	1	0.9258	0.0743
1.5	1.0631	1.1111	0.0480	1	0.9634	0.0365
2.0	1.0856	1.1111	0.0255	1	0.9812	0.0188
3.0	1.1034	1.1111	0.0077	1	0.9947	0.0053
∞	1.1111	1.1111	0.0000	1	1.000	0.0000

$(a) = \rho_q(z)$, $(b) = \rho_{q_{as}}(z)$, $(c) = (b) - (a)$.

TABLE XI

DENSITY, MILNE PROBLEM WITH CONSTANT PRODUCTION NORMALIZED TO UNIT DENSITY AT THE BOUNDARY

z	$\alpha = 0$			$\alpha = 0.1$			$\alpha = 0.2$		
	(*a*)	(*b*)	(*c*)	(*a*)	(*b*)	(*c*)	(*a*)	(*b*)	(*c*)
0	1.0000	1.2306	0.2306	1.0000	1.3926	0.3926	1.0000	1.5016	0.5016
0.1	1.2784	1.4038	0.1254	1.2717	1.5344	0.2627	1.2742	1.6205	0.3463
0.2	1.4715	1.5770	0.1055	1.4691	1.6689	0.1998	1.4633	1.7313	0.2680
0.3	1.6686	1.7502	0.0816	1.6388	1.7965	0.1577	1.6201	1.8345	0.2144
0.4	1.8587	1.9234	0.0648	1.7904	1.9176	0.1272	1.7559	1.9306	0.1747
0.5	2.0443	2.0967	0.0523	1.9285	2.0325	0.1041	1.8759	2.0201	0.1442
1.0	2.9421	2.9628	0.0206	2.4817	2.5246	0.0429	2.3220	2.3837	0.0617
1.5	3.8197	3.8289	0.0092	2.8833	2.9029	0.0196	2.6095	2.6385	0.0290
2.0	4.6906	4.6950	0.0043	3.1844	3.1937	0.0095	2.8028	2.8172	0.0144
3.0	6.4261	6.4272	0.0010	3.5872	3.5897	0.0025	3.0264	3.0302	0.0038
∞	∞	∞	0.0000	4.1623	4.1623	0.0000	3.2360	3.2360	0.0000

TABLE XI—*Concluded*

DENSITY, MILNE PROBLEM WITH CONSTANT PRODUCTION NORMALIZED TO UNIT DENSITY AT THE BOUNDARY—*concluded*

z	$a = 0.3$			$a = 0.4$			$a = 0.5$		
	(*a*)	(*b*)	(*c*)	(*a*)	(*b*)	(*c*)	(*a*)	(*b*)	(*c*)
0	1.0000	1.6148	0.6148	1.0000	1.7382	0.7382	1.0000	1.8713	0.8713
0.1	1.2756	1.7111	0.4355	1.2758	1.8114	0.5355	1.2766	1.9209	0.6443
0.2	1.4573	1.7998	0.3425	1.4520	1.8781	0.4261	1.4472	1.9659	0.5188
0.3	1.6047	1.8814	0.2767	1.5906	1.9391	0.3485	1.5754	2.0038	0.4284
0.4	1.7284	1.9565	0.2281	1.7036	1.9948	0.2912	1.6852	2.0441	0.3589
0.5	1.8357	2.0256	0.1899	1.8026	2.0457	0.2431	1.7743	2.0779	0.3036
1.0	2.2131	2.2970	0.0839	2.1301	2.2409	0.1108	2.0631	2.2058	0.1427
1.5	2.4359	2.4764	0.0405	2.3103	2.3650	0.0547	2.2130	2.2851	0.0721
2.0	2.5745	2.5949	0.0204	2.4157	2.4438	0.0281	2.2964	2.3342	0.0378
3.0	2.7193	2.7249	0.0056	2.5177	2.5257	0.0079	2.3724	2.3835	0.0111
∞	2.8258	2.8258	0.0000	2.5810	2.5810	0.0000	2.4143	2.4143	0.0000

z	$a = 0.6$			$a = 0.7$			$a = 0.8$		
	(*a*)	(*b*)	(*c*)	(*a*)	(*b*)	(*c*)	(*a*)	(*b*)	(*c*)
0	1.0000	2.0031	1.0031	1.0000	2.1000	1.1000	1.0000	2.1100	1.1100
0.1	1.2776	2.0301	0.7525	1.2806	2.1091	0.8285	1.2823	2.1108	0.8285
0.2	1.4432	2.0546	0.6114	1.4411	2.1173	0.6762	1.4383	2.1115	0.6732
0.3	1.5680	2.0768	0.5088	1.5598	2.1247	0.5649	1.5517	2.1121	0.5604
0.4	1.6677	2.0969	0.4292	1.6532	2.1314	0.4782	1.6397	2.1127	0.4730
0.5	1.7498	2.1151	0.3653	1.7291	2.1374	0.4083	1.7102	2.1132	0.4030
1.0	2.0074	2.1836	0.1762	1.9601	2.1601	0.2000	1.9193	2.1151	0.1958
1.5	2.1345	2.2254	0.0909	2.0694	2.1739	0.1045	2.0143	2.1163	0.1020
2.0	2.2024	2.2509	0.0485	2.1259	2.1823	0.0564	2.0620	2.1170	0.0550
3.0	2.2613	2.2760	0.0147	2.1730	2.1905	0.0175	2.1006	2.1176	0.0170
∞	2.2910	2.2910	0.0000	2.1951	2.1951	0.0000	2.1179	2.1179	0.0000

z	$a = 0.9$			$a = 1$		
	(*a*)	(*b*)	(*c*)	(*a*)	(*b*)	(*c*)
0	1.0000	2.0541	1.0541	1.0000	2	1.0000
0.1	1.2728	2.0541	0.7813	1.2775	2	0.7225
0.2	1.4257	2.0541	0.6284	1.4258	2	0.5742
0.3	1.5351	2.0541	0.5190	1.5309	2	0.4691
0.4	1.6192	2.0541	0.4349	1.6106	2	0.3894
0.5	1.6860	2.0541	0.3681	1.6734	2	0.3266
1.0	1.8799	2.0541	0.1742	1.8515	2	0.1485
1.5	1.9652	2.0541	0.0889	1.9269	2	0.0731
2.0	2.0070	2.0541	0.0471	1.9625	2	0.0375
3.0	2.0399	2.0541	0.0142	1.9894	2	0.0106
∞	2.0542	2.0542	0.0000	2.0000	2	0.0000

$(a) = \bar{\rho}_q(z)$, $(b) = \bar{\rho}_{q_{as}}(z)$, $(c) = (b) - (a)$.

It follows also from (46) and (41) that

$$\rho_q(o) = \frac{1}{\sqrt{a}\,(1+\sqrt{a})}. \tag{48}$$

If, instead of normalizing to unit production we normalize to unit density at the boundary, we obtain

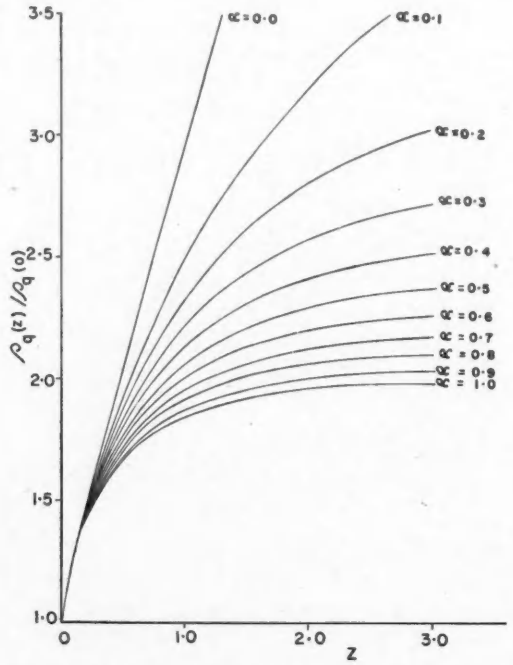

FIG. 6. *Neutron density $\rho_q(z)/\rho_q(o)$ as a function of distance z from the boundary. Unit of length: total mean free path.*

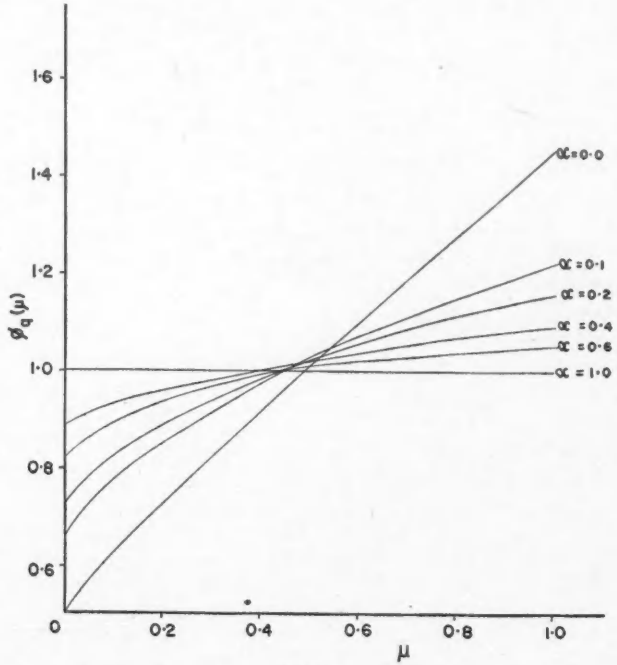

FIG. 7. *Emerging angular distribution $\phi_q(\mu)$, normalized to unit density: $\int_0^1 \phi_q(\mu)d\mu = 1$.*

$$\bar{\rho}_q(z) = \frac{\rho_q(z)}{\rho_q(o)} = \frac{\sqrt{a}g(z) - \sqrt{a}}{1 - \sqrt{a}}. \tag{49}$$

The values of $\bar{\rho}_q(z)$, $\bar{\rho}_{q_{as}}(z)$, and $\bar{\rho}_{q_{as}}(z) - \bar{\rho}_q(z)$ are tabulated in columns (a), (b), (c) of Table XI, with $g(z)$ given by (44). For $a = 0$, $\bar{\rho}_q(z)$ exists and is equal to $\frac{1}{\sqrt{3}} f(z)$. Fig. 6 is a plot of $\bar{\rho}_q(z)$.

The normalization to unit density is convenient in discussing the angular distribution. We have

$$\phi_q(\mu) = \frac{1 - \mu\nu}{1 - \sqrt{a}}\,\phi(\mu), \tag{50}$$

where $\phi(\mu)$ is the angular distribution for the Milne problem with no production, normalized to unit density (Table VI). ϕ_q is tabulated in Table XII and plotted in Fig. 7.

TABLE XII

EMERGING ANGULAR DISTRIBUTION MILNE PROBLEM WITH CONSTANT PRODUCTION NORMALIZED TO UNIT DENSITY AT THE BOUNDARY

μ	$a=0$	$a=0.1$	$a=0.2$	$a=0.3$	$a=0.4$	$a=0.5$	$a=0.6$	$a=0.7$	$a=0.8$	$a=0.9$
0.00	0.5000	0.6584	0.2738	0.7741	0.8162	0.8536	0.8873	0.9183	0.9472	0.9745
0.01	0.5171	0.6753	0.7395	0.7883	0.8289	0.8643	0.8962	0.9251	0.9590	0.9762
0.05	0.5683	0.7230	0.7821	0.8257	0.8611	0.8910	0.9174	0.9412	0.9653	0.9830
0.10	0.6237	0.7707	0.8234	0.8608	0.8905	0.9150	0.9346	0.9551	0.9740	0.9867
0.20	0.7252	0.8494	0.8885	0.9147	0.9342	0.9501	0.9635	0.9748	0.9844	0.9930
0.30	0.8213	0.9153	0.9408	0.9565	0.9677	0.9763	0.9830	0.9885	0.9933	0.9971
0.40	0.9146	0.9729	0.9847	0.9908	0.9946	0.9968	0.9984	0.9994	0.9997	0.9997
0.50	1.0064	1.0240	1.0234	1.0198	1.0170	1.0137	1.0108	1.0080	1.0059	1.0028
0.60	1.0971	1.0701	1.0558	1.0446	1.0356	1.0279	1.0212	1.0151	1.0101	1.0048
0.70	1.1870	1.1120	1.0852	1.0666	1.0521	1.0402	1.0300	1.0212	1.0133	1.0067
0.80	1.2764	1.1503	1.1115	1.0858	1.0663	1.0507	1.0376	1.0263	1.0165	1.0079
0.90	1.3653	1.1855	1.1353	1.1029	1.0792	1.0599	1.0443	1.0308	1.0192	1.0093
0.94	1.4008	1.1987	1.1441	1.1092	1.0837	1.0632	1.0465	1.0325	1.0202	1.0098
0.96	1.4185	1.2053	1.1485	1.1124	1.0859	1.0647	1.0478	1.0333	1.0206	1.0100
0.98	1.4362	1.2116	1.1527	1.1152	1.0880	1.0667	1.0487	1.0340	1.0210	1.0102
1.00	1.4539	1.2178	1.1568	1.1183	1.0904	1.0682	1.0501	1.0347	1.0215	1.0104

Acknowledgments

The research in this report was undertaken at the suggestion of Dr. George Placzek who offered valuable help and encouragement throughout. The computations and graphs included were prepared under the direction of Mr. Bengt Carlson. The author wishes to express her gratitude to Dr. Placzek and to Mr. Carlson and his staff.

References

1. ADLER, F. T. and MARK, C. Phys. Rev. To be published.
2. DAVISON, B. Can. J. Research, A, 28: 303. 1950.
3. DAVISON, B. Phys. Rev. 71: 694. 1947.
4. DAVISON, B. and PLACZEK, G. Phys. Rev. To be published.
5. LECAINE, J. Phys. Rev. 72: 564. 1947.
6. LECAINE, J. Montreal Report, MT-119, 1945.
7. MARK, C. Phys. Rev. 72: 558. 1947.
8. MARSHAK, R. E. Phys. Rev. 71: 688. 1947.

(*The Appendix follows on the next page*)

APPENDIX

The explicit expressions for the constants L_1, L_2, K_1, K_2, K_3, are listed below.

$$L_1 = \frac{\cosh \nu z_0}{2}\int_0^\infty G_3^2(\nu, z)dz + \frac{\sinh \nu z_0}{2}\int_0^\infty G_2(\nu, z)G_3(\nu, z)dz$$

$$= \frac{(1-a)^2}{8\nu^3}\Bigg[e^{\nu z_0}\Bigg\{-\frac{\pi^2}{4} + \frac{(6-4\nu^2)\nu\log 2}{1-\nu^2} - \frac{\nu\left(\log(1-\nu^2) + \dfrac{2\nu^2}{1-a}\right)}{1-\nu^2}$$

$$- \frac{2\nu\log(1+\nu)}{1-a} + 3\sum_{n=1}^{\infty}\frac{(-1)^{n-1}}{n^2}\left(\frac{1-\nu}{1+\nu}\right)^n - \log^2(1+\nu)\Bigg\}$$

$$+ e^{-\nu z_0}\Bigg\{-\frac{\pi^2}{4} + \frac{(6-4\nu^2)\nu\log 2}{1-\nu^2} - \frac{\nu\left(\log(1-\nu^2) + \dfrac{2\nu^2}{1-a}\right)}{1-\nu^2}$$

$$- \frac{2\nu\log(1+\nu)}{1-a} + 3\sum_{n=1}^{\infty}\frac{(-1)^{n-1}}{n^2}\left(\frac{1-\nu}{1+\nu}\right)^n - \frac{\nu\log(1-\nu^2)}{1-a}$$

$$+ \log(1+\nu)\log(1-\nu)\Bigg\}\Bigg].$$

$$L_2 = \frac{\cosh \nu z_0}{2}\int_0^\infty G_2(\nu, z)G_3(\nu, z)dz + \frac{\sinh \nu z_0}{2}\int_0^\infty G_2^2(\nu, z)dz = \frac{(1-a)^2}{8\nu^3}\Bigg[e^{\nu z_0}\Bigg\{\frac{\pi^2}{12}$$

$$- \frac{2\nu\log 2}{1-\nu^2} + \frac{\nu\left(\log(1-\nu^2) + \dfrac{2\nu^2}{1-a}\right)}{1-\nu^2} - \log(1+\nu)\log(1-\nu)$$

$$- \sum_{n=1}^{\infty}\frac{(-1)^{n-1}}{n^2}\left(\frac{1-\nu}{1+\nu}\right)^n\Bigg\} - e^{-\nu z_0}\Bigg\{\frac{\pi^2}{12} - \frac{2\nu\log 2}{1-\nu^2} + \frac{\nu\left(\log(1-\nu^2) + \dfrac{2\nu^2}{1-a}\right)}{1-\nu^2}$$

$$+ \frac{\log^2(1-\nu)}{2} + \frac{\log^2(1+\nu)}{2} - \sum_{n=1}^{\infty}\frac{(-1)^{n-1}}{n^2}\left(\frac{1-\nu}{1+\nu}\right)^n\Bigg\}\Bigg].$$

$$K_1 = \int_0^\infty G_3^2(\nu, z)dz - \frac{1-a}{2}\int_0^\infty G_3(\nu, z)\int_0^\infty G_3(\nu, z')E_1(|z-z'|)dz'dz$$

$$= \frac{(1-a)^2}{4\nu^4}\Bigg[2\nu\Bigg(-\frac{\pi^2}{4} + \frac{(6-4\nu^2)\nu\log 2}{1-\nu^2} - \frac{\nu\left(\log(1-\nu^2) + \dfrac{2\nu^2}{1-a}\right)}{1-\nu^2}$$

$$- \frac{2\nu\log(1+\nu)}{1-a} + 3\sum_{n=1}^{\infty}\frac{(-1)^{n-1}}{n^2}\left(\frac{1-\nu}{1+\nu}\right)^n\Bigg) - \frac{\nu^2\log(1-\nu^2)}{1-a} - \frac{2\nu^2\log(1+\nu)}{1-a}$$

$$- \frac{1-a}{2}\Bigg\{-\frac{2}{3}\pi^2\nu^2 + \frac{2\nu\pi^2}{3(1+\nu)} - \frac{16a\nu^2}{1-a}\log 2 + \frac{8}{3}\pi^2\log 2 - 16\log^3 2$$

$$+ 8\log^2 2\log(1-\nu^2) + \frac{\pi^2\nu}{1-a} - \frac{8\nu^2(\log 2 - \log(1+\nu))}{(1-a)(1-\nu^2)}$$

$$+\frac{6\nu}{1-a}\log^2(1+\nu)-\frac{2\nu}{1-a}\log(1+\nu)\log(1-\nu)-4\log^2(1+\nu)\log(1-\nu)$$
$$-\left(\frac{12\nu}{1-a}+\frac{8\nu}{1-\nu^2}\right)\sum_{n=1}^{\infty}\frac{(-1)^{n-1}}{n^2}\left(\frac{1-\nu}{1+\nu}\right)^n+32\sum_{n=1}^{\infty}\frac{1}{n^3 2^n}$$
$$-16\sum_{n=1}^{\infty}\left(\frac{1}{n}+\log 2\right)\left[\frac{(1-\nu)^n}{2^n n^2}+\frac{(1+\nu)^n}{2^n n^2}\right]\Bigg\}\Bigg].$$

$$K_2=2\int_0^{\infty}G_2(\nu,z)G_3(\nu,z)dz-(1-a)\int_0^{\infty}G_2(\nu,z)\int_0^{\infty}G_3(\nu,z')\,E_1(|z-z'|)\,dz'dz$$
$$=-\frac{(1-a)^2}{4}\Bigg[\frac{(\log(1-\nu^2))^2}{\nu^3}+\frac{2(1-a)\log(1-\nu^2)}{\nu^4}\left\{\frac{\pi^2}{12}+\frac{\nu\log(1+\nu)}{1-a}\right.$$
$$\left.-2\nu\log 2-\sum_{n=1}^{\infty}\frac{(-1)^{n-1}}{n^2}\left(\frac{1-\nu}{1+\nu}\right)^n\right\}\Bigg].$$

$$K_3=\int_0^{\infty}G_2^2(\nu,z)dz-(1-a)\int_0^{\infty}G_2(\nu,z)\int_0^{\infty}G_2(\nu,z')\,E_1(|z-z'|)\,dz'dz$$
$$=\frac{(1-a)^2}{4}\Bigg[\frac{2}{\nu^3}\left\{\frac{\pi^2}{12}-\frac{2\nu\log 2}{1-\nu^2}+\frac{\nu\left(\log(1-\nu^2)+\dfrac{2\nu^2}{1-a}\right)}{1-\nu^2}\right.$$
$$\left.-\sum_{n=1}^{\infty}\frac{(-1)^{n-1}}{n^2}\left(\frac{1-\nu}{1+\nu}\right)^n\right\}+\frac{2}{\nu(1-a)^2}-\frac{2(1-a)}{\nu^4}\left\{2\log^3 2\right.$$
$$-\log^2 2\log(1-\nu^2)-\frac{\pi^2}{3}\log 2-\frac{\pi^2\nu}{6(1+\nu)}-\frac{\pi^2\nu}{12(1-a)}$$
$$+\frac{2\nu^2\log 2-2\nu^2\log(1+\nu)}{(1-\nu^2)(1-a)}-\frac{\nu\log^2(1+\nu)}{2(1-a)}+\frac{1}{2}\log^2(1+\nu)\log(1-\nu)$$
$$+\frac{1}{4}\log(1+\nu)\log(1-\nu)\log(1-\nu^2)+\left(\frac{2\nu}{1-\nu^2}+\frac{\nu}{1-a}\right)\sum_{n=1}^{\infty}\frac{(-1)^{n-1}}{n^2}\left(\frac{1-\nu}{1+\nu}\right)^n$$
$$-4\sum_{n=1}^{\infty}\frac{1}{n^3 2^n}+2\sum_{n-1}^{\infty}\left(\frac{1}{n}+\log 2\right)\left[\frac{(1-\nu)^n}{2^n n^2}+\frac{(1+\nu)^n}{2^n n^2}\right]\Bigg\}\Bigg].$$

A GEOMETRIC TREATMENT OF "DIMENSIONS" IN PHYSICS[1]

By Parry Moon and Domina Eberle Spencer

Abstract

"Dimensional analysis" is an established and venerable subject, associated with such names as Fourier, Maxwell, and Lord Rayleigh. But only a genius can obtain dependable results with it, a state of affairs that is caused by the vague, intuitionalistic way in which the subject has always been presented. The purpose of this paper is to formulate a precise theory.

An *idon* or complete physical quantity is an entity with two attributes: quality and quantity. Formal rules are given for the manipulation of idons, and it is shown that they can be pictured as vectors in a k-dimensional space. This geometrization is not necessary, of course, but it often gives added grasp of the subject; just as vector analysis is never necessary in physics, though it is often convenient. There are six practical applications of the theory, all of which are handled in a precise and dependable way by the geometric method.

Introduction

The "dimensional" theory of physical quantities seems to have been first used by Fourier in his celebrated treatise (9), *Théorie analytique de la chaleur* (1822). It was further developed by Maxwell (11, 12) (1863); and Lord Rayleigh (15) was one of its ablest supporters. The subject has been extended by Vaschy (20), Riabouchinsky (16, 17), Buckingham (3), Bridgman (1), Ehrenfest-Afanassjewa (7, 8), Tolman (19), Campbell (4, 5), Hill (10), and others.

Despite the effort that has been expended on "dimensions," however, the theory has remained in an unsatisfactory state, as evidenced by the endless and largely meaningless disputes that have taken place. (2, 4, 5, 6, 14, 17, 21). The difficulty is primarily semantic; for in reading the voluminous and conflicting literature on the subject, one can never be sure of the exact meaning attached to such words as "dimension", "unit", "magnitude", "quantity". And this difficulty is not solely an academic question. The complaint is often made that it takes the physical intuition of a Lord Rayleigh to apply "dimensional analysis" with any certainty, a situation that is caused at least partially by the lack of precision in the traditional treatment of the subject.

Within recent years, there has been progress toward greater exactness in "dimension" theory. The present paper attempts to contribute toward that end by showing how the subject can be treated as a branch of geometry.

Fundamentals

Maxwell stressed the use of "dimensions" in changing from one set of units to another. Thus he associated "dimensions" with units; and this conception of the subject has persisted down to the present day, despite the fact that

[1] *Manuscript received in original form September 23, 1949, and as revised, January 26, 1950. Contribution from the Massachusetts Institute of Technology, Cambridge, Mass., and Brown University, Providence, R.I.*

change of units is now one of the least important applications of "dimension" theory.

The modern approach associates "dimensions" with physical *concepts* rather than with *units*, and one of the principal applications of the subject is the classification and correlation of concepts.* Concepts may be classed as *primary* and *secondary*. We prefer these names to *fundamental* and *derived* because of the idea of uniqueness that is often associated with the latter terminology. In mechanics, *length*, *mass*, and *time* are usually chosen as primary concepts, but there is nothing unique about this choice. It is now generally realized that the number and selection of primary concepts is largely arbitrary: we choose a set of primary concepts that is convenient for the problem in hand.

Secondary concepts are specified in terms of primary concepts by use of the defining equations for the secondary concepts. For example, if l, m, t are chosen as primary concepts,** then velocity may be designated as lt^{-1} and force as $lmt.^{-2}$ An alternative specification is obtained by writing only the exponents, as was done by Fourier. Then a concept is designated by writing the exponents of l, m, and t in order. The concept of velocity is designated as $[1, 0, -1]$, while force is $[1, 1, -2]$. These bracketed quantities are called *designation symbols* and provide a convenient way of specifying concepts. Physical concepts should be so chosen that, for a given set of primary concepts, there is a 1:1 relation between concept and designation symbol.

Consider now a *physical quantity* or *physical magnitude*. It differs from a concept inasmuch as it represents a specific amount, as 4.5 kgm. Evidently a physical quantity can be designated in either of two ways:

(*a*) By specifying the number of units and the kind of unit (as 4.5 kgm.); or, if m.k.s. units are presupposed,

(*b*) By specifying the number of units and the concept (as a mass of 4.5).

For most purposes, (*a*) is the more convenient since it leaves no doubt about the system of units employed. Maxwell and his followers used (*a*) also for "dimensional" specification. The modern treatment of "dimensions," however, employs (*b*) so that the emphasis throughout can be on *concepts*, not on *units*. We indicate a specific physical quantity, expressed as in (*b*), by a letter enclosed in curly brackets:

$$\{A\} = A[a^1, a^2, \ldots a^k]. \tag{1}$$

This quantity is called an *idon* (From Gk εἶδος = class, species) and the study of these quantities is called *idon theory* or *idonics*. In Equation (1), the magnitude of the physical quantity $\{A\}$ is denoted by A (a pure number). The bracketed quantity is the designation symbol, which specifies what con-

*The operational definition of concepts is treated by P. W. Bridgman in "The logic of modern physics" (The Macmillan Co., New York, 1927).

**The advisability of considering two fundamental lengths (l_r and l_l) instead of one is considered elsewhere:

Moon and Spencer, "Modern terminology in physics," Amer. J. Phys., 16 : 100. 1948; "A modern approach to 'dimensions' ", J. Franklin Institute, 248, 495. 1949.

cept is being considered. For instance, a mass of 4.5 kgm. is written $\{m\} = 4.5\,[0, 1, 0]$.

A serious attempt was made to employ the traditional notation and names, but the semantic difficulties were found to be almost insuperable. How can one distinguish, for instance, between the "dimensions" (length, width, and height) of a model and the "dimensions" (length, mass, time), which may be referred to in the same sentence? And do the latter "dimensions" refer to the concept, the unit, or the complete physical quantity? In the interest of precision, therefore, we were forced to use a new word to represent the one particular meaning of "dimensions" that we wished to present.

Geometry

The foregoing notation suggests a geometric interpretation. A vector in 3-space is often specified by writing a number-triple or ordered set $[x, y, z]$, where the three numbers represent the co-ordinates of the vector.* Similarly, a vector in k-space is written $[a^1, a^2, \ldots a^k]$, or in tensor notation (17),

$$a^i = [a^1, a^2, \ldots a^k], \qquad i = 1, 2, \ldots k.$$

Comparing with Equation (1), one sees that the idon $\{A\}$ may be regarded as a vector in k-space. The designation symbol $[a^1, a^2, \ldots a^k]$ is a *base vector* which fixes the direction of $\{A\}$, while the length of the vector $\{A\}$ is given by the scalar quantity A. The numbers $a^1, a^2, \ldots a^k$ are the *co-ordinates* of the base vector. The fictitious space in which the idon vectors lie is called *idon space*. The dimensionality k of this space is equal to the number of primary concepts employed in the problem under consideration.

In kinematics, for example, *length* and *time* are usually taken as primary concepts. Then idon space is two-dimensional with co-ordinate axes l and t. Any specific distance is represented by a vector** $\{l\}$:

$$\{l\} = l\,[1, 0],$$

which is in the direction of the l-axis. A definite value of time is another vector,

$$\{t\} = t\,[0, 1],$$

while a specific velocity is

$$\{v\} = v\,[1, -1].$$

Evidently each concept is associated with a definite direction in idon space, this direction being specified by the base vector a^i. An increase in the magnitude of the physical quantity merely stretches the idon vector, whose direction remains that of the base vector a^i.

*See, for instance, L. E. Dickson, Linear algebras (Cambridge Univ. Press, 1930) or Algebras and their arithmetics (G. E. Stechert, New York, 1938).

**Needless to say, the vector nature of the physical quantity in idon space is distinct from its possible vector nature in the euclidean space of the phenomena. We assume without loss of generality that the physical quantity in euclidean space is a scalar. If it is actually a tensor, we deal in idon theory with only the magnitude.

Note that with a suitable choice of primary concepts, each base vector has a different direction in idon space, and thus each distinct concept is distinguished geometrically from all others. Of course this desirable condition will not obtain unless the investigator has exercised due care in the selection of his primary concepts. The subject is discussed in detail in another paper (J. Franklin Institute, Dec. 1949). In the present paper, we assume that such an unambiguous selection of primary concepts has been made.

Idon space is a fictitious space; moreover it does not have all the properties of ordinary euclidean space. For example, the "length" of the base vector a^i cannot be obtained by taking the square root of the sum of the squares of its co-ordinates $a^1, a^2, \ldots a^k$. By definition,

$$\{A\} = Aa^i$$

and the magnitude of any idon vector $\{A\}$ is A, irrespective of what numbers may appear in the designation symbol $[a^1, a^2, \ldots a^k] = a^i$. Thus a^i always acts as a *unit vector*.

This principle may be stated in another way: in general, lengths in different directions in idon space cannot be compared. It is evident also that angles in idon space have no physical significance. These characteristics lead one to suspect that idon space is similar in many respects to *affine space*,* a fact that will be elaborated later.

Algebra

The following operations will be postulated:

(1) *Addition.* Given two idons $\{A\}$ and $\{B\}$:

$$\{A\} = Aa^i, \quad \{B\} = Bb^i.$$

Then $\{A\} + \{B\}$ is defined only if the two vectors are collinear.** If this condition is satisfied, then the sum is defined as

$$\{A\} + \{B\} = (A + B)\, a^i. \tag{2}$$

Subtraction is defined by

$$\{A\} - \{B\} = (A - B)\, a^i.$$

If $A - B = 0$, the result of the subtraction signifies zero amount of the concept denoted by a^i. Addition and subtraction are commutative and associative. Like addition, subtraction is defined only for vectors in the same direction.

(2) *Multiplication by a pure number* (*idonic scalar*). Given an idon $\{A\}$ and a pure number k, then the product is

$$k\,\{A\} = k\,A\,a^i. \tag{3}$$

**A very readable account of spaces is given in Felix Klein, Elementarmathematik vom höheren Standpunkte aus (Springer, Berlin, 1925, Vol. II); English translation by E. R. Hedrick and C. A. Noble (The Macmillan Co., New York, 1939).*

***This corresponds to the well known principle of "dimensional" homogeneity.*

Multiplication by a scalar is commutative:

$$k\{A\} = \{A\}k.$$

(3) *Multiplication.* The multiplication of two idons is effected by multiplying their magnitudes to obtain the magnitude of the product, and adding the co-ordinates of their base vectors to obtain the co-ordinates of the new base vector:

$$\{C\} = \{A\}\{B\} = AB[a^i + b^i]. \tag{4}$$

Multiplication is commutative and associative, and is distributive with respect to addition as defined in (1).

(4) *Division.* The division of two idons is effected by taking the quotient of the two magnitudes to obtain the new magnitude, and taking the difference of the co-ordinates of the base vectors to obtain the co-ordinates of the new base vector:

$$\{D\} = \frac{\{A\}}{\{B\}} = \frac{A}{B}[a^i - b^i]. \tag{5}$$

These four are the only operations in idon theory. They are called *allowable operations.* An idon can be raised to an integer power by repeated use of Equation (4), and this idea can be extended to a noninteger power γ by the following definition:

$$\{A\}^\gamma = A^\gamma[\gamma a^i]. \tag{6}$$

Of particular interest is the fact that if $\alpha a^i + \beta b^i + \gamma c^i + \ldots + \nu n^i = 0$, the product of vectors in idon space is a scalar:

$$\{A\}^\alpha\{B\}^\beta \ldots \{N\}^\nu = A^\alpha B^\beta \ldots N^\nu[0, 0, \ldots 0]$$
$$= A^\alpha B^\beta \ldots N^\nu[0].$$

Geometrically, this condition results when the sum of the base vectors a^i, $b^i \ldots n^i$, multiplied by suitable scalars $\alpha, \beta, \ldots \nu$, is zero. Such quantities, $\Pi = \{A\}^\alpha\{B\}^\beta \ldots \{N\}^\nu$, are called "dimensionless products" or *idonic scalars.*

The determination of idonic scalars is one of the important applications of idon theory. For a given physical problem, however, the idonic scalars are not unique but may exist in an infinite number of forms. A set of idonic scalars is said to be *equivalent* to any other set that can be obtained from the original set by allowable operations (assuming, of course, that the original set can again be obtained by allowable operations from the final set).

Any equation of physics may be written in idon form by merely replacing each numerical magnitude by a vector in idon space. For example, Newton's relation,

$$F = ma$$

may be written

$$\{F\} = \{m\}\{a\}$$

and since

$$\{F\} = Fa^i, \{m\} = mb^i, \{a\} = ac^i,$$

$$Fa^i = ma[b^i + c^i].$$

This breaks into the original equation which deals with magnitudes only, and the relation among base vectors:

$$a^i = b^i + c^i.$$

The latter equation gives the designation symbol for *force*.

Differentiation and Integration

It is convenient to have rules also for the differentiation and integration of idons. By the customary definition of differentiation with respect to an arbitrary variable ξ,

$$\frac{d\{A\}}{d\{\xi\}} = \lim_{\Delta\xi \to 0} \left(\frac{\{\Delta A\}}{\{\Delta\xi\}} \right).$$

But $\{A\} = A\, a^i$; and since $\{\Delta A\}$ is the difference of two idon vectors, which has significance only if a^i is the same for both, $\{\Delta A\} = A\, a^i$. Similarly, since $\{\xi\} = \xi b^i$, $\{\Delta\xi\} = \Delta\xi \cdot b^i$.

Therefore

$$\frac{\{\Delta A\}}{\{\Delta\xi\}} = \frac{\Delta A}{\Delta\xi}[a^i - b^i],$$

and

$$\frac{d\{A\}}{d\{\xi\}} = [a^i - b^i] \lim_{\Delta\xi \to 0} \left(\frac{\Delta A}{\Delta\xi} \right) \tag{7}$$

$$= [a^i - b^i] \frac{dA}{d\xi}.$$

In other words, to differentiate an idon we differentiate the scalar magnitude, and subtract the designation symbols.

Similarly, integration is a process of addition and multiplication. Thus

$$\int \{A\}\, d\{\xi\} = [a^i + b^i] \int A\, d\xi. \tag{8}$$

The integration of one idon with respect to another is the integral of the corresponding scalar magnitudes but the resulting designation symbol is the sum of the original designation symbols.

As an example, consider the equation

$$F = \frac{d}{dt}(mv).$$

In idon form, it becomes

$$\{F\} = \frac{d}{d\{t\}}(\{m\}\ \{v\}),$$

where

$$\{m\} = ma^i,$$

$$\{v\} = vb^i$$

$$\{t\} = tc^i, \text{ and } \{F\} = Fd^i.$$

Substitution gives

$$Fd^i = [a^i + b^i - c^i] \frac{d}{dt}(mv).$$

Thus the base vector for force is equal to the sum of the base vectors for mass and velocity minus the base vector for time:

$$d^i = a^i + b^i - c^i.$$

With l, m, t as axes,

$$a^i = [0, 1, 0],\ b^i = [1, 0, -1],\ c^i = [0, 0, 1].$$

Therefore, $$d^i = [1, 1, -2],$$

which is the designation symbol for the concept of force.

As a second illustration, take the potential difference V between two points, $x = a$ and $x = b$:

$$V = \int_a^b \frac{F}{Q} dx.$$

The corresponding idon equation is

$$\{V\} = \int_a^b \frac{\{F\}}{\{Q\}} d\{x\},$$

where $\{V\} = Va^i$, $\{F\} = Fb^i$, $\{Q\} = Qc^i$ and $\{x\} = xd^i$.

By the rules enunciated above,

$$Va^i = [b^i - c^i + d^i] \int_a^b \frac{F}{Q} dx$$

so $$a^i = b^i - c^i + d^i.$$

If the primary concepts are chosen as l, m, t, Q, then

$$b^i = [1, 1, -2, 0],\ c_i = [0, 0, 0, 1],\ d^i = [1, 0, 0, 0]$$

and therefore the designation symbol for potential difference must be

$$a^i = [2, 1, -2, -1].$$

Of course these same results would have been obtained intuitively from the customary "dimension" theory, but it seems safer to base them on an exact procedure.

The Π Theorem

What is the most general relation among idons? Evidently it is the equation that is obtained by employing the four allowable operations in all possible ways, or

$$\sum_{i=1}^{j} K_i \{A\}^{\alpha}{}_i \{B\}^{\beta}{}_i \ldots \{N\}^{\nu}{}_i = 0, \tag{9}$$

where K_i are scalar coefficients, which may themselves be arbitrary functions of idonic scalars.

Examination of the equations of physics shows that all of them can be written in this form. There are a few cases where the foregoing principle seems to be violated, but further examination shows that such equations can be rewritten in the form of Equation (9). If transcendental functions occur, their arguments

are always idonic scalars ("dimensionless" quantities). With idons that represent physical quantities having "dimensions," the only function that can occur is a power function. *Equation* (9) *therefore represents the most general equation of physics.*

The most general equation of physics will now be written in an alternative form which often has advantages. Divide Equation (9) by one of its terms. The result is of the form,

$$\sum k_l \{A\}^{\rho}{}_l \{B\}^{\sigma}{}_l \ldots \{N\}^{\omega}{}_l + 1 = 0. \tag{10}$$

But addition is only allowable for idons having the same base vectors. Since 1 is a scalar in idon space, all other terms must also be scalars. Therefore any equation of physics can be expressed in terms of *idonic scalars*:

$$\Pi_i = \{A\}^{\rho}{}_i \{B\}^{\sigma}{}_i \ldots \{N\}^{\omega}{}_i \tag{11}$$

Since the Π's are scalars, any function of them is allowable, and we have as an expression of the most general physical equation,

$$\varphi(\Pi_1, \Pi_2, \ldots \Pi_m) = 0. \tag{12}$$

This is the Π *theorem*, stated in 1896 by Vaschy (20), in 1911 by Riabouchinsky (16), and in 1914 by Buckingham (3).

Derivation of New Equations

The Π theorem is utilized in the derivation of equations where there is insufficient information to allow a derivation in the ordinary manner. The result is usually less complete and less satisfactory than an equation derived from a thorough analysis, but it often gives a broad view of the subject that can hardly be obtained in another way.

In using the Π theorem, one decides (on physical grounds) on the n variables that enter the problem: $\{A\}$, $\{B\}$, . . . $\{N\}$. A choice is also made of k primary concepts (l, m, t, for instance). Then an idonic scalar may be written

$$\begin{aligned} \Pi &= \{A\}^{\alpha} \{B\}^{\beta} \ldots \{N\}^{\nu} \\ &= A^{\alpha} B^{\beta} \ldots N^{\nu} [\alpha a^i + \beta b^i + \ldots + \nu n^i], \end{aligned} \tag{13}$$

where $i = 1, 2, \ldots k$. Since Π is a scalar, the bracketed quantity must be equal to zero, giving the vector equation:

$$\alpha a^i + \beta b^i + \ldots \nu n^i = 0. \tag{14}$$

Equation (14) is equivalent to a set of k homogeneous algebraic equations which the n exponents $\alpha, \beta, \ldots \nu$ must satisfy. The matrix is written immediately from the known co-ordinates of the base vectors, $a^i = [a^1, a^2, \ldots a^k]$, $b^i = [b^1, b^2, \ldots b^k]$, etc. and is

$$\begin{bmatrix} a^1 & b^1 & c^1 & \ldots & n^1 \\ a^2 & b^2 & c^2 & \ldots & n^2 \\ \ldots & \ldots & \ldots & \ldots & \ldots \\ a^k & b^k & c^k & \ldots & n^k \end{bmatrix}.$$

The rank of this matrix will be denoted* by r. The only case of physical interest is where $r < n$; in which case $(n - r)$ of the unknowns $(\alpha, \beta, \ldots \nu)$ may be given arbitrary values, and the remaining unknowns are uniquely determined. Equation (14) is rewritten

$$\underbrace{\alpha a^i + \beta b^i + \ldots + \kappa k^i}_{r \text{ terms}} = \underbrace{\lambda l^i + \ldots + \nu n^i}_{(n-r) \text{ terms}}.$$

The simplest procedure is to set one of the unknowns on the right (say, λ) equal to unity, with the remainder of them zero. The solution of Equation (14) then evaluates $\alpha, \beta, \ldots \nu$, and Equation (13) gives an idonic scalar, say Π_1.

Now set $\nu = 1$ and $\lambda, \ldots \mu = 0$ to obtain Π_2. Evidently there are $(n - r)$ of these independent Π's, and the final solution is

$$\varphi(\Pi_1, \Pi_2, \ldots \Pi_{n-r}) = 0. \tag{12a}$$

If other arbitrary values had been assigned to $\lambda, \ldots \nu$, different idonic scalars would usually have been obtained. These Π's, however, would have been *equivalent* to those of Equation (12a). As a matter of fact, the latter set of Π's may not be the simplest and most convenient; so it is often advisable to transform them by use of the *allowable operations* and select the set best suited to the problem.

As an example, consider thermionic emission from a plane cathode. On the usual basis, using l, m, t, and Q as primary concepts, one writes down the pertinent quantities:

	Symbol	"Dimensions"
Current density	J	$l^{-2}t^{-1}Q$
Potential difference between electrodes	V	$l^2mt^{-2}Q^{-1}$
Charge of electrons	Q	Q
Mass of electron	m	m
Distance between electrodes	l	l
Permittivity	ϵ	$l^{-3}m^{-1}t^2Q^2$

Then, according to the Π-theorem,

$$\Pi = J^\alpha V^\beta Q^\gamma m^\delta l^\mu \epsilon^\nu$$
$$= (l^{-2}t^{-1}Q)^\alpha (l^2mt^{-2}Q^{-1})^\beta Q^\gamma m^\delta l^\mu (l^{-3}m^{-1}t^2Q^2)^\nu.$$

Thus we have four equations,

$$\begin{cases} -2\alpha + 2\beta + \mu - 3\nu = 0 \\ \beta + \delta - \nu = 0 \\ -\alpha - 2\beta + 2\nu = 0 \\ \alpha - \beta + \gamma + 2\nu = 0. \end{cases}$$

Since there are six unknowns, two may be assigned arbitrarily and (if the rank of the coefficient matrix is four) there are two Π's.

**If the n concepts are distinct, each base vector being in a different direction in idon space, then $r = k$.*

Let $a = 1, \nu = 0$. Then $\beta = -\frac{1}{2}, \gamma = -3/2, \delta = 1/2, \mu = 3$ and

$$\Pi_1 = \frac{Jm^{\frac{1}{2}}l^3}{V^{\frac{1}{2}}Q^{3/2}}.$$

Now let $a = 0, \nu = 1$. We now find $\beta = 1, \gamma = -1, \delta = 0, \mu = 1$ and

$$\Pi_2 = \frac{Vl\epsilon}{Q}.$$

Therefore the usual "dimensional" solution is

$$J = \sqrt{\frac{V}{m}}\frac{Q^{3/2}}{l^3} \cdot F\left(\frac{Vl\epsilon}{Q}\right)$$

where $F\left(\frac{Vl\epsilon}{Q}\right)$ is an unknown function.

Now consider the same problem, but in idonic notation with l_r, l_t, m, t, Q as primary concepts. The idons are written (See Table IV of Moon and Spencer, "A modern approach to 'dimensions' ", J. Franklin Institute, Dec. 1949.)

$$\begin{aligned}
\{J\} &= J[-1, -1, 0, -1, 1] \\
\{V\} &= V[0, 2, 1, -2, -1] \\
\{Q\} &= Q[0, 0, 0, 0, 1] \\
\{m\} &= m[0, 0, 1, 0, 0] \\
\{l\} &= l[0, 1, 0, 0, 0] \\
\{\epsilon\} &= \epsilon[-1, -2, -1, 2, 2].
\end{aligned}$$

Let $\{J\} = \text{const}\ \{V\}^a \{Q\}^\beta \{m\}^\gamma \{l\}^\delta \{\epsilon\}^\mu$.

Substitution of the above evaluation of the idons leads to an equation for the base vectors:

$$\begin{aligned}
[-1, -1, 0, -1, 1] = {} & [0, 2a, a, -2a, -a] \\
& + [0, 0, 0, 0, \beta] \\
& + [0, 0, \gamma, 0, 0] \\
& + [0, \delta, 0, 0, 0] \\
& + [-\mu, -2\mu, -\mu, 2\mu, 2\mu]
\end{aligned}$$

from which we obtain the five simultaneous equations,

$$\begin{cases}
-1 = -\mu \\
-1 = 2a + \delta - 2\mu \\
0 = a + \gamma - \mu \\
-1 = -2a + 2\mu \\
1 = -a + \beta + 2\mu.
\end{cases}$$

Thus, $a = 3/2, \beta = 1/2, \gamma = -1/2, \delta = -2, \mu = 1$ and

$$J = \text{const}\sqrt{\frac{Q}{m}}\frac{\epsilon V^{3/2}}{l^2},$$

which is the usual formulation of Child's equation.

Change of Units

Another application of idon theory occurs when physical units are changed from one system to another (British to c.g.s. units, for instance). Such a transformation is equivalent to a change of scales along the co-ordinate axes. Consider a k-space with vectors $\{A\}, \{B\}, \ldots \{K\}$ in the directions of the axes:

$$\begin{aligned} \{A\} &= A[1, 0, 0, \ldots 0] \\ \{B\} &= B[0, 1, 0, \ldots 0] \\ &\cdots\cdots\cdots \\ \{K\} &= K[0, 0, 0, \ldots 1]. \end{aligned}$$

Any other vector is expressible in terms of the foregoing, or*

$$\begin{aligned} \{L\} &= \Theta\{A\}^{\alpha}\{B\}^{\beta}\ldots\{K\}^{\kappa} \\ &= \Theta A^{\alpha}B^{\beta}\ldots K^{\kappa}[\alpha a^i + \beta b^i + \ldots + \kappa k^i], \\ &\qquad\qquad i = 1, \ldots k. \end{aligned} \tag{15}$$

Now suppose that the scales along the axes are changed in the ratios $u_1, u_2, \ldots u_k$:

$$u_i = \frac{\text{old unit}}{\text{new unit}}.$$

Then in terms of the new units,

$$\begin{aligned} \{A'\} &= u_1 A[1, 0, 0, \ldots 0] \\ \{B'\} &= u_2 B[0, 1, 0, \ldots 0] \\ &\cdots\cdots\cdots \\ \{K'\} &= u_k K[0, 0, 0, \ldots 1]. \end{aligned}$$

Since the form of Equation (15) must be invariant with respect to a change of units,

$$\begin{aligned} \{L'\} &= \Theta'\{A'\}^{\alpha}\{B'\}^{\beta}\ldots\{K'\}^{\kappa} \\ &= u_1^{\alpha}u_2^{\beta}\ldots u_k^{\kappa}\frac{\Theta'}{\Theta}\{L\}. \end{aligned} \tag{16}$$

Equation (16) allows units to be changed in a systematic manner. Many of the older writers on the subject considered this to be the primary use of "dimensions." The modern view, however, is that change of units is a rather trivial application, particularly since any change of units is unproductive, a complete waste of time which can be eliminated by the universal use of the m.k.s. system (12).

Transformation of Co-ordinate Axes

The old idea that l, m, and t, are sacrosanct has been abandoned (1). Numerous choices are possible. Select a set of k primary concepts, which corresponds to a choice of rectilinear co-ordinate axes in idon k-space. Any idon is then represented by the vector

$$\{A\} = Aa^i.$$

*Here Θ is a scalar constant, which allows the use of peculiar units for $\{L\}$. For example, if axes are l, m, t, and $\{L\}$ represents energy, then m.k.s. unit of $\{L\}$ is obtained directly from the three fundamental units and is $m^2kg\ sec^{-2}$ = joule. In this case, $\Theta = 1$. But if L is expressed in calories, $\Theta = 1/4.182$.

Now make a different choice of primary concepts, keeping the number equal to k as before. Then the above idon is written

$$\{A'\} = Aa^{i'}.$$

The use of the same base letters (A and a) indicates that the idon vector is unaltered (18), while the primes show that the co-ordinate axes have changed. Geometrically, we have a given vector $\{A\}$ which remains fixed as the co-ordinate axes are rotated to new positions. The co-ordinates of the base vector $a^{i'}$ are different from those of a^i, but both are unit vectors. The length A is identical in both cases and need not be primed.

It is well known (18) that the transformation from one set of rectilinear axes to another is always accomplished by a linear homogeneous transformation, so

$$\begin{cases} a^{1'} = B_1^{1'} a^1 + B_2^{1'} a^2 + \ldots + B_k^{1'} a^k \\ a^{2'} = B_1^{2'} a^1 + B_2^{2'} a^2 + \ldots + B_k^{2'} a^k \\ \quad \ldots \quad \ldots \quad \ldots \quad \ldots \quad \ldots \quad \ldots \quad \ldots \\ a^{k'} = B_1^{k'} a^1 + B_2^{k'} a^2 + \ldots + B_k^{k'} a^k. \end{cases}$$

In index notation (18), this set of equations is written

$$a^{i'} = B_i^{i'} a^i, \quad (i, i' = 1, 2, \ldots k), \tag{17}$$

which is the equation of an *affine transformation* of co-ordinate axes. Consequently, idon space has *affine* properties.

For instance, consider the transformation from l, m, t axes to l, P, t axes. In terms of l, m, t, we have idons of the form

$$\{A\} = Aa^i, \text{ or specifically,}$$

$\{l\} = l[1, 0, 0]$, $\{P\} = P[2, 1, -3]$, $\{t\} = t[0, 0, 1]$.

In terms of l, P, t,

$$\{A'\} = Aa^{i'}, \text{ or}$$

$$\{l'\} = l[1, 0, 0], \{P'\} = P[0, 1, 0], \{t'\} = t[0, 0, 1].$$

Substitution in Equation (14) evaluates the co-ordinates of $A_i^{i'}$, which are

$$\begin{bmatrix} 1 & -2 & 0 \\ 0 & 1 & 0 \\ 0 & 3 & 1 \end{bmatrix}.$$

Any quantity expressed in terms of l, m, t can then be transformed to the l, P, t, system by means of Equation (14).

Energy, for example, has the base vector $a^i = [2, 1, -2]$ in the l, m, t system. Substitution into Equation (14) leads to the new specification,

$$a^{i'} = [0, 1, 1].$$

Acknowledgment

In conclusion, we gratefully acknowledge the helpful comments of Royal M. Frye, Phillipe Le Corbeiller, Dirk J. Struik, and Joseph L. Walsh.

References

1. BRIDGMAN, P. W. Dimensional analysis. Yale University Press, New Haven. 1931.
2. BROWN, G. B. Phil. Mag. 33:367. 1942.
3. BUCKINGHAM, E. Phys. Rev. 4:345. 1914.
4. CAMPBELL, NORMAN. Physics, the elements. Chaps. XIV, XV. Cambridge University Press. 1920.
5. CAMPBELL, NORMAN. Phil. Mag. 47:481. 1924.
6. DINGLE, H. Phil. Mag. 35:296. 1944.
7. EHRENFEST-AFANASSJEWA, T. Math. Ann. 77:259. 1915.
8. EHRENFEST-AFANASSJEWA, T. Phil. Mag. 1:257. 1926.
9. FOURIER, J. B. J. Théorie analytique de la chaleur. Section 160. Paris, 1822. *English translation by* A. Freeman, p. 128. Cambridge University Press. 1878.
10. HILL, W. S. Teoria general de las magnitudes. Montevideo. 1941.
11. MAXWELL, J. C. A treatise on electricity and magnetism. Vol. 1, p. 46. Oxford University Press. 1904.
12. MAXWELL, J. C. and JENKIN, F. British Association Report for 1863, p. 130; Report of the Committee on Electrical Standards, p. 59. London, 1873.
13. MOON, P. and SPENCER, D. E. Am. J. Phys. 16:25. 1948.
14. O'RAHILLY, ALFRED. Electromagnetics, p. 672. Longmans, Green and Co., London. 1938.
15. LORD RAYLEIGH. Nature, 95:66. 1915.
16. RIABOUCHINSKY, D. Aerophile, 19:407. 1911.
17. RIABOUCHINSKY, D. Nature, 95:591. 1915.
18. SCHOUTEN, J. A. and STRUIK, D. J. Einführung in die neueren Methoden der Differentialgeometrie. Vol. 1. P. Noordhoff, Groningen, 1935.
19. TOLMAN, R. C. Phys. Rev. 6:219. 1915.
20. VASCHY, O. Théorie de l'électricité, p. 13. Paris. 1896.
21. WILSON, W. Phil. Mag. 35:420. 1944.

COMPARATIVE HEAT LOSSES FROM BARE AND ANODIZED ALUMINUM SURFACES TO STILL AIR[1]

By A. C. Burr and Robert H. Hay

Abstract

The effect of anodic films on the total heat losses to still air from the surfaces of cylindrical aluminum containers maintained at temperatures between 23°C. and 100°C. has been studied by recording the power required to maintain the containers at various temperatures above ambient. Anodic coats of the order of 20μ thick required increases in power of 43% to 60% at 30°C. and 68% to 79% at 90°C., the variations at any one temperature being due to variations in thickness and color of the coating. The emissivity coefficient for the clear anodic coats used is estimated from the data to be about 0.80.

Introduction and Theory

Recent consideration of the heat loss problems involved in the design of certain aluminum tanks revealed the lack of reliable heat-loss information in the literature for aluminum surfaces at temperatures between 20°C. and 100°C., particularly if the aluminum has been anodized or anodized and dyed black. It was therefore decided to perform simple experiments which might lead to reasonably reliable information on such heat losses.

A body in air and at a temperature higher than that of its surroundings will lose heat to them by conduction, convection, and radiation. In the first two cases, particularly for the conditions of this experiment, the heat loss will be at a rate approximately proportional to the temperature difference between the body and surrounding air. In the last case, however, rate of heat loss is proportional to the fourth power of the temperature, i.e.,

$$Q \propto \epsilon (T_r^4 - T_s^4), \tag{1}$$

where ϵ is the emissivity of the surface and T_r and T_s are respectively the absolute temperatures of the radiating body and of its surroundings. Heat transfer by radiation is, of course, unaffected by the presence or absence of air. As the quantity proportional to the amount of heat lost in unit time by the surface by all three of the above mentioned modes of heat transfer, the writers chose the electrical power used by an immersion heater to hold the water in an aluminum tank at a given temperature. Different surface treatments can be applied to any one tank and the different power inputs to the heater will be a measure of the ability of the various surfaces to dissipate heat.

Some measure of the emissivity of anodized surfaces can be gained by comparing the power input for an anodic coat with that for a similar coat dyed black on the same tank. Since the nature of the surfaces in the two cases would be almost exactly similar (i.e., conduction plus convection would be equal for the

[1] *Manuscript received January 20, 1950.*
Contribution from the Physics Division, Aluminium Laboratories, Limited, Kingston, Ont.

two cases) the difference in power would be due to a difference in radiation alone. Using the subscript a for the anodized tank and b for the anodized tank dyed black and somewhat arbitrarily taking the emissivity for the dyed tank to be 90% (the emissivity of a "black body" is 100%), the total heat loss per second in watts for each of the two cases would be,

$$Q_a = \epsilon\sigma A(T_r^4 - T_s^4) + q, \tag{2}$$

$$\text{and} \quad Q_b = 0.9\sigma A(T_r^4 - T_s^4) + q, \tag{3}$$

where σ = 5.74×10^{-12} watts cm.$^{-2}$ deg.$^{-4}$ (Stefan's constant),

and ϵ = coefficient of emissivity ($\epsilon = 1$ for a perfect black body),

A radiating area in square centimeters (taken as surface area of the tank),

T_r = temperature of radiating surface in degrees absolute,

T_s = temperature of surroundings in degrees absolute,

q, = a term to represent heat loss by conduction plus convection.

q, can be calculated from Equation (3) and substituted in (2). The value for ϵ can thus be calculated from observed heat losses and temperature differences.

Experimental

Two cylindrical tanks were made up, each nominally 4 in. in diameter and 9 in. high. One tank was made from Alcan 57S* alloy sheet 0.040 in. thick and the other of Alcan 2S* alloy sheet 0.062 in. thick. The top end of each cylinder was closed by a flat plate which carried three diametrically located holes over which were brazed "chimneys", or 3-in. long cylinders, through which a knife-type immersion heater, a stirring mechanism, and a thermometer and thermocouple lead wires were inserted. The amount of water surface exposed to the air was thus kept at a minimum. All anodizing was done in 15% (by weight) sulphuric acid at 21°C. with a current density of 18 amp. per sq. ft. and sealing by immersion in boiling water. Coatings were stripped after each test by immersion for 10 to 15 min. in a phosphoric–chromic acid bath** at 95–100°C. Black dyeing was accomplished by immersing the coated but unsealed tanks for 10 min. in a solution of Nigrosene Black—12525 (National Aniline Co.) made up to a 12 gm. per liter concentration and a pH of 6.1 and maintained at 65°C. For test, a tank was filled with distilled water to within 1/2 in. to 3/4 in. of the top of the chimney tubes. The knife-type immersion heater was fed by a variac transformer which in turn was fed from a Sola constant voltage transformer on the 60-cycle main. Power in watts was calculated from voltage and current readings on Westinghouse type Py-5 one-half per cent meters. The center opening admitted a mercury thermometer to obtain readings of water temperature and a thermocouple connected to a sensitive potentiometer to read small temperature differences when approaching the equilibrium temperature of the water. A second mercury thermometer was used to read the

* *Aluminum Company of Canada designations. Corresponding Alcoa designations are 52S and 2S respectively.*

** *ASTM Designation B 137-45.*

temperature of the surrounding air. A propeller type stirrer was used to agitate the water. An initial test was run to see if there was any heating effect due to the agitation of the stirrer, but no rise in water temperature could be noted from this cause in several hours' operation.

The procedure of the experiment was to obtain the equilibrium temperature for a given amount of power input to the heater. Power steps were adjusted to give appropriate temperature intervals. The time necessary to reach equilibrium for any one steady power input was from two to four hours, but the experiment needed only occasional adjustment and readings taken. When the water temperature reached equilibrium for any one power this temperature was reduced or increased for plotting by the amount that the room temperature was above or below 23.0°C. respectively, as 23.0°C. was the average room temperature. The amount of this correction was never more than 2° and since most of the heat transfer is by conduction and convection (which are roughly proportional to the first power of the temperature difference) the resulting error would be small.

Results

Fig. 1 gives the power necessary to hold the water in a 57S tank at various temperatures for different surface finishes while Fig. 2 gives the same data for a 2S tank. All figures are for a room temperature of 23.0°C. The two tanks used in these tests are of the same shape and of approximately the same size but

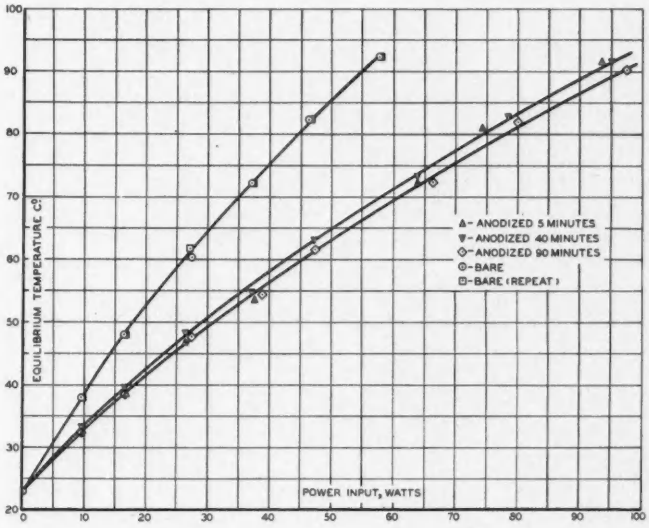

FIG. 1. *Heat loss from an aluminum water tank to its surroundings as measured by power necessary to maintain equilibrium temperature above ambient; Alloy 57S bare and anodized; ambient temperature, 23°C.*

they are not nearly enough identical to permit comparison to be made of losses from surface finishes on different alloys.

In Fig. 3 is shown the increase in power input in per cent for tanks anodized on the outside over the power input for the same tanks bare and polished on the outside. The power figures for Fig. 3 are taken from curves in Figs. 1 and 2.

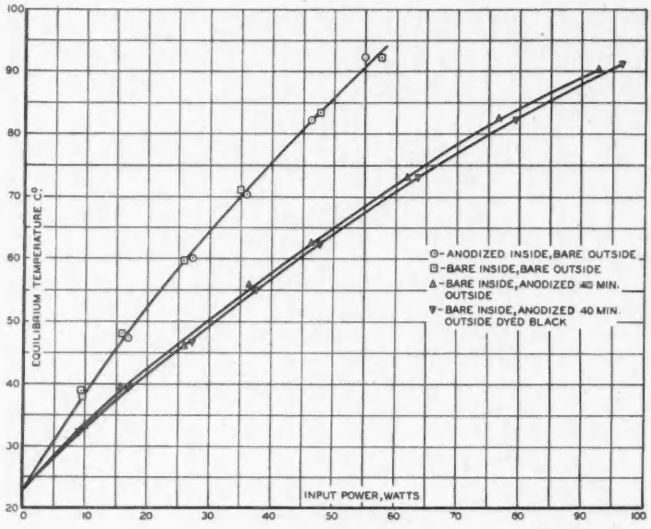

FIG. 2. *Heat loss from an aluminum water tank to its surroundings as measured by power necessary to maintain equilibrium temperature above ambient; Alloy 2S bare, anodized, anodized and dyed black; ambient temperature, 23°C.*

On the assumption that an emissivity value of 90% can be given to the 2S tank anodized 40 min. and dyed black, then values for the 40 min. anodized undyed finish were calculated and are given in Table I. The average ϵ of these

TABLE I

EMISSIVIVITY IN % FOR 2S ANODIZED 40 MIN. WHEN 2S ANODIZED 40 MIN. PLUS BLACK DYE IS TAKEN AS 90%

Water temp., °C.	Heat loss, watts		% Emissivity	
	Anodized 40 min.	Anodized 40 min. plus black dye	Anodized 40 min. plus black dye	Anodized 40 min.
90.0	88.9	93.3	90.0	81.1
80.0	72.5	74.7	90.0	84.5
70.0	56.5	57.9	90.0	85.5
60.0	42.0	43.2	90.0	84.9
50.0	28.8	29.6	90.0	85.1

values is 84.2%. A 40 min. anodic coat on 2S with conditions as given above would be of the order of 15 to 20μ in thickness, so that a figure of 84% for emissivity is in fair agreement with other published figures for anodic films (3), provided the published curves are extrapolated slightly. Additional valuable reference material is contained in papers by Draper (1) and Lux (2).

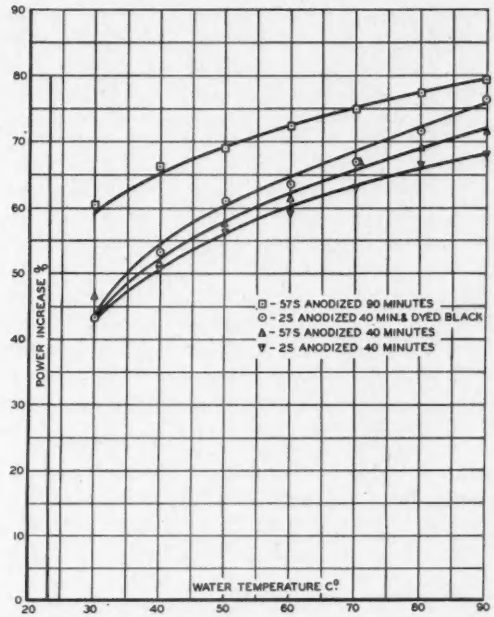

FIG. 3. *Curves for anodized tanks showing extra power input required to maintain given water temperature as percentage increase over power necessary to maintain same temperature in bare tank.*

In the formulas given above for calculating emissivity, T_r is the temperature of the radiating surface. This temperature was not measured, the water temperature being used instead. It would be slightly higher than the actual temperature of the radiating surface. However, a 5-degree error in T_r at 90°C. has approximately 1% effect on the value of ϵ while at 50°C. a 2.5-degree change in T_r alters ϵ by about 0.7%. Since calculations showed that the difference between the water temperature and the temperature of the radiating surface would be of the order of 0.5°C. and not more than 1°C., the error arising from the assumption that T_r equals water temperature has been neglected.

Discussion of Results

The curves of Figs. 1 and 2 give all the data obtained. From them have been constructed the curves of Fig. 3. These show clearly the most interesting conclusions to be drawn from the experiment.

The agreement between values obtained for the two runs with the bare surfaces is very good, the second run being made after anodic coatings had been stripped off and the bare aluminum repolished. From Fig. 1 (or Fig. 2) we see that the heat losses for the various thicknesses of anodic coating (thickness being taken, to a first-order approximation, to vary directly with anodizing time) are of the same order of magnitude and that they all differ very much from those for a bare, polished aluminum surface. Even as thin a coat as is obtained with five minutes anodizing time has a marked effect on heat loss. It is clear, also, that though in general heat loss depends on some factor related to the time of anodizing and also is greater for black than for clear surfaces, the differences we have observed due to these factors are small.

From Fig. 3, referring to the 57S alloy curves, it is seen that the heat loss is distinctly higher for a 90 min. coating than for the thinner 40 min. coating, and that the two curves show a greater difference in heat loss at the lower equilibrium temperatures than at the higher, even though the loss difference is not very great. At first glance there appear to be consistent differences between the heat loss for the 57S alloy tank and for the 2S alloy tank. It is well known that each alloy has its own anodizing characteristics, and it may be that a difference in heat loss could be attributed to this difference in anodic film character. However, the two tanks used are sufficiently different in size to rule out drawing any such conclusion from the data presented here.

Applications may occur for which the temperatures are well above 100°C. It would be unwise to extrapolate the curves given here for more than 10° or 20°C., and further experimental work would have to be done in the region of interest if it lay outside such an extrapolation range.

References

1. DRAPER, C. R. Light metals, 10: 656. 1947.
2. LUX, L. Aluminium, 19 (5): 334. 1947.
3. TAYLOR, C. S. and EDWARDS, J. D. Heating, Piping, Air Conditioning, 11: 59. 1939.

A 60 db. NONLINEAR AMPLIFIER[1]

By J. A. Carruthers

Abstract

A nonlinear amplifier is described which has been used to drive an Esterline Angus 0–1 ma. recording galvanometer as part of the automatic recording apparatus set up for taking microwave antenna patterns. The amplifier output is approximately proportional to the logarithm of the input voltage, and permits plotting a 60 db. variation in input signal. The speed of response is limited by the galvanometer movement but is adequate for obtaining a pattern through 100 degrees of azimuth in about two minutes. The plotting accuracy is better than 1 db. if care is taken to check calibration frequently.

Introduction

In the investigation of fundamental properties of microwave diffraction, as well as in the routine measurement of antenna directivity characteristics, it is necessary to measure the power transmitted between the system under test and a distant point, as a function of the angle of rotation of the test apparatus. In order to eliminate much of the time required for a point-by-point plot of such patterns an inexpensive automatic recording system has been built which permits obtaining the complete information in a few minutes.

The essential parts of the apparatus are an Esterline Angus 0–1 ma. recording galvanometer and a distorting amplifier which is described here. The amplifier must be nonlinear since it is desirable to plot up to a 30 db. range of radio-frequency power picked up at the receiver; because a square detector (bolometer or crystal) is used at the receiver, it follows that a 60 db. variation in the signal from the detector must be recorded. To cover this plotting range, an approximately logarithmic characteristic has been obtained by the use of automatic volume control (A.V.C.) bias on supercontrol tubes whose gain is thereby decreased as the signal level increases. Amplification takes place at 600 cycles, which is the frequency used to amplitude modulate the R.F. carrier and which therefore appears at the output of the detector. The 600 cycle voltage is converted to d.c. to actuate the galvanometer.

Since an amplifier cannot be truly logarithmic starting from zero output, it is designed to have a characteristic which is lin-log, i.e., linear for small signals up to a crossover point beyond which the output increases in proportion to the logarithm of the input. This is expressed by the following relations:

$$E_0 = k\,E_i \qquad E_i < E_c \tag{1}$$

$$E_0 = k\,E_c\left(1 + \log_e \frac{E_i}{E_c}\right) \qquad E_i > E_c \tag{2}$$

[1] *Manuscript received December 23, 1949.*
Contribution from the Department of Physics, McGill University, Montreal, Que.

where $E_0 \equiv$ output voltage,

$E_i \equiv$ input voltage,

$E_c \equiv$ crossover voltage which is a constant of the design of the amplifier.

The constant, k, is related to the voltage amplification of the amplifier as follows:—

From (1) $V.A. = \dfrac{E_0}{E_i} = k$ $\qquad E_i < E_c$ (3)

(2) $V.A. = \dfrac{E_0}{E_i} = k\dfrac{E_c}{E_i}\left(1 + \log_e \dfrac{E_i}{E_c}\right)$ $\qquad E_i > E_c$ (4)

If it is considered that E_c is the lower extreme of the plotting range, then for a 60 db. increase in signal $E_i(\text{max.}) = 1000\ E_c$. Substitution in Equation (4) shows that the A.V.C. bias must act to decrease the gain of the amplifier by a factor of 130 in order to cover the desired plotting range.

Description of the Amplifier

Fig. 1 shows the circuit diagram of the amplifier which is described below in detail.

(1) *The Input Stage*

The cathode following V_1 was found necessary to isolate the gain controls from the main amplifier. Any change in the impedance of the grid circuit of V_2 brought about a change in calibration, an effect which was eliminated by the cathode follower. The controls permit a 12 db. variation in gain in 3 db. steps as well as a 3 db. continuous adjustment. The amplifier has been used either as a termination on a 500 ohm line or in parallel with a terminated line. For this reason the input impedance can be altered from 500 ohms to high impedance.

(2) *The Main Amplifier*

The two amplifier stages V_2 and V_3 have A.V.C. bias applied to the grids in order to decrease the gain with increasing signal. V_4 is an A.V.C. amplifier which is isolated from the A.V.C. diode (V_{6-1}) by a cathode follower stage (V_{5-2}). The signal to be measured is coupled to the detector V_{6-2} through V_{5-1}, which is a triode amplifier whose gain has been adjusted to give the most desirable shape to the cramping characteristic of the amplifier, without affecting the feed-back loop. This is particularly helpful since it allows a control on the crossover point without danger of setting the amplifier into oscillation.

The time constants have been adjusted to allow as rapid a response as possible while maintaining stability. It requires approximately one second for the amplifier to reach a sensibly steady state for a 60 db. change in the input signal. The 2.2 megohm resistor, and the 0.05 and 0.01μf. condensers between V_3 and V_4 were found to decrease the tendency to oscillate by reducing the low frequency gain without introducing large phase shifts at the low frequencies.

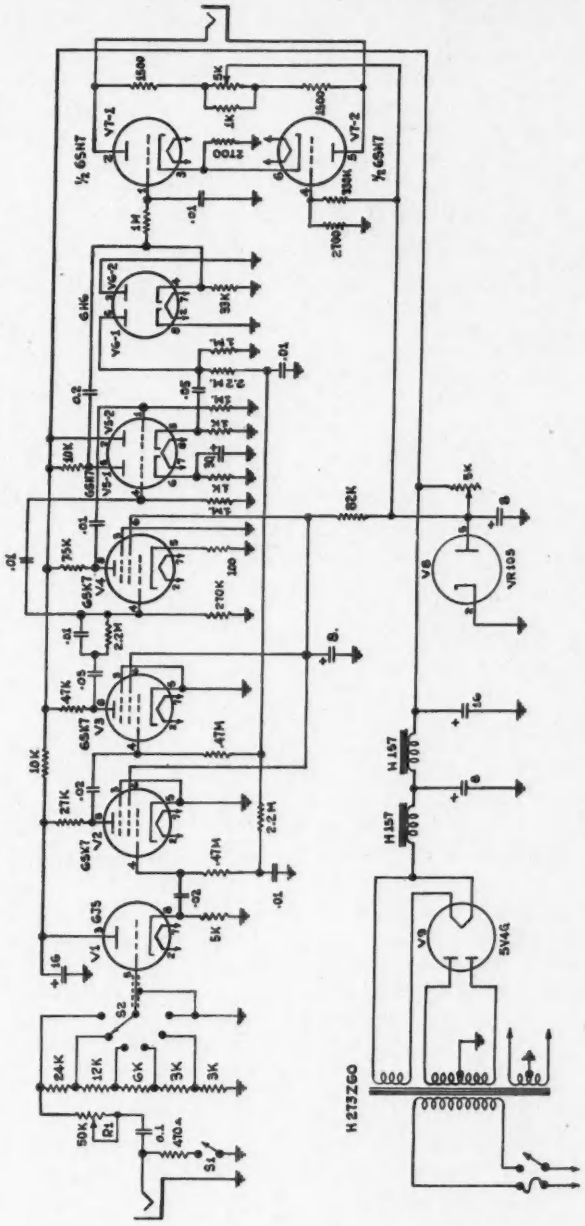

FIG. 1. *Circuit diagram of the nonlinear amplifier.*

(3) *The Metering Circuit*

The remaining stages make up the detector and balanced voltmeter circuits which drive the d-c. meter. The output impedance of the voltmeter stage has been adjusted to give optimum speed of response of the galvanometer without overshooting. The 5K potentiometer between the plates of V_{7-1} and V_{7-2} is for setting the meter to zero at no signal.

Operation and Performance

Fig. 2 is a plot of relative meter deflection versus change in input voltage, expressed in decibels. Allowing for the square law detector ahead of the amplifier it is seen that a 30 db. plotting range is feasible. Full scale deflection requires an input of 0.05 v.

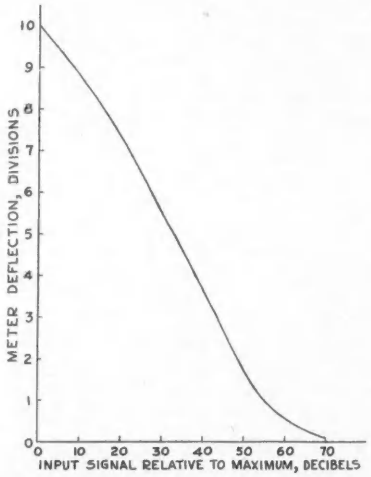

FIG. 2. *Over-all calibration curve for amplifier and recording galvanometer.*

The calibration has been found to vary somewhat with tube temperature and age, but a half-hour warm-up period is sufficient to ensure a precision of 1 db. after a thorough initial break-in of all tubes. For maximum precision, a 500 ohm attenuator box has been used in the line feeding the amplifier so that calibration can be checked very rapidly: after completing a pattern the antenna is rotated to the angle of maximum signal and the attenuation is varied in 10 db. steps to give six points on the calibration curve.

The response time for large changes in signal is less than two seconds, which allows taking a normal horn pattern through 100° of azimuth in about two minutes. The accuracy in following small changes in intensity is limited by the friction between the pen and the chart. This friction was decreased considerably by rebalancing the galvanometer needle so as to exert minimum

pressure on the paper, although this requires keeping the inkwell filled to the same level at all times in order to maintain constant buoyancy effect from the part of the needle in the ink.

Fig. 3 shows a comparison of the curves obtained for a horn pattern when replotted from the recorder chart, and when obtained by a point-by-point plot (hand pattern). A plotting accuracy of about 1 db. is indicated. Fig. 4 shows

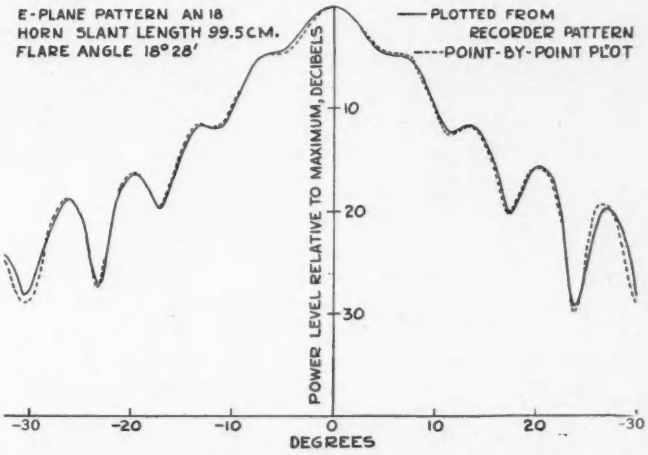

FIG. 3. *Comparison of replotted recorder trace and hand pattern.*

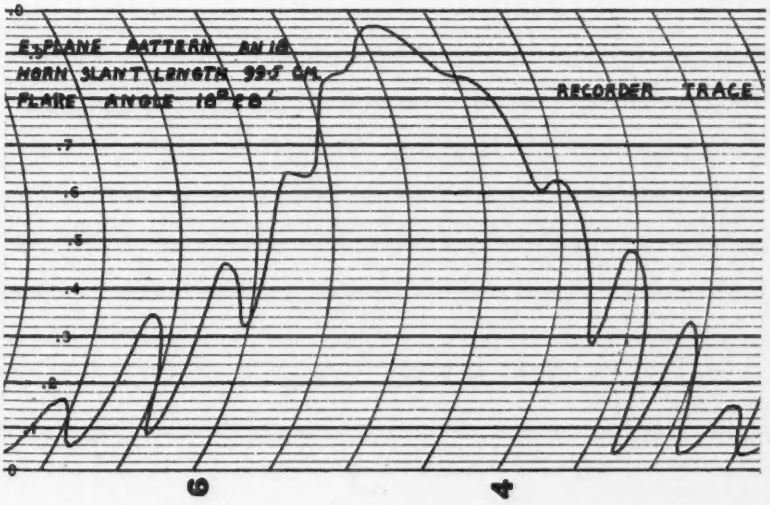

FIG. 4. *Section of recorder chart showing the actual trace.*

the trace of the recorder chart from which the graph in Fig. 3 was obtained. Although this trace is distorted by the curved arc of the pen and the departure from logarithmic response of the amplifier, it is often necessary only to observe the effects of varying some part of the antenna system, and replotting the trace is not required.

Acknowledgments

The program of research for which this amplifier was constructed was made possible by grants from the Defence Research Board. The author wishes to express his appreciation to Prof. G. A. Woonton for valuable suggestions, and to Mr. E. G. Ross for technical assistance in building the amplifier.

DEFLECTIONS OF AN INFINITE PLATE[1]

By Max Wyman

Abstract

Problems associated with the thickness of ice sheets on Canadian lakes led the author to investigate mathematically the deflection of a loaded plate resting upon an elastic foundation. Certain simplifying assumptions, which appear to be not unreasonable, permit the solutions obtained to be applied to the strength of a floating ice sheet. Relations for maximum stress and maximum deflections in terms of known functions are derived, both for a concentrated load and a uniform load distributed over a circular area. The resulting expressions should be tested experimentally to determine their domain of validity. Owing to similarity of conditions, these results may also be applied to the design of concrete roadways and airport runways.

Introduction

During the last war considerable activity took place in the northern part of Canada. The problem of transporting heavy equipment over frozen lakes became important and Prof. I. F. Morrison of the University of Alberta received several requests for a formula which would give the thickness of ice required to support loads of various proportions. Engineers interested in the problem had no accurate formulas and were using rough charts whose validity seemed doubtful. In addition to the requests made to Professor Morrison several other members of the Faculty of Engineering were asked to consider the problem of landing aircraft on frozen lakes. Here again the problem was to determine the thickness of ice in order to make a safe landing.

A rigorous mathematical solution of the problems enunciated would be very complicated. Some of the factors which would require consideration are that ice is a nonisotropic elastic medium and that its elastic properties show wide variability under different conditions. In addition the problems of transportation involve moving loads which are of course much more difficult to treat than the corresponding problem involving only stationary loads.

In order to make a start toward the solution of the above problem we shall make several simplifying assumptions which will enable us to carry out a mathematical analysis. The final formulas which we shall obtain should be tested experimentally in order to obtain their domain of validity.

As the ice deflects into the water there is a restoring force due to the water pressure which is proportional to the deflection. For this reason the mathematical problem to be solved resolves itself into determining the deflection of a loaded plate resting on an elastic foundation. Since we are considering a frozen lake there is no serious error in considering the ice plate to be of infinite extent. More serious is the assumption that we shall make that ice is an iso-

[1]*Manuscript received in original form August 13, 1949, and, as revised, January 10, 1950. Contribution from the University of Alberta, Edmonton, Alberta.*

tropic elastic medium. In order to overcome some of the error introduced by this assumption we shall be conservative in choosing the values of our elastic constants and in this way we hope that the numerical values which we shall obtain for the safe thickness of ice will be on the conservative side. Finally we shall deal only with stationary loads and shall assume that these loads are big enough to make the weight of the ice itself negligible.

On the basis of the above assumptions the problem has been considered to some extent by others (3, pp. 275-282). In most cases the final form of solution has been left as an infinite series which does not lend itself to easy numerical calculations. For this reason we shall treat the problem from the beginning and shall be able to show that the final form of solution can be expressed in terms of known functions for which tables of values exist.

The fundamental differential equations, upon which our mathematical problem is based, are all readily available in Timoshenko's book on Plates and Shells. For this reason we shall try, as far as possible, to restrict our notation to that used in this book.

Section 1—Concentrated Load

In Fig. 1 we consider an infinite isotropic plate of thickness h resting on a liquid of density ρ. If we let w be the deflection of the middle plane of the plate then it is known (3, p. 58) that w must satisfy the differential equation.

$$\frac{1}{r}\frac{d}{dr}\left\{r\frac{d}{dr}\left[\frac{1}{r}\frac{d}{dr}\left(r\frac{dw}{dr}\right)\right]\right\} = \frac{q}{D}, \tag{1.1}$$

where q is the intensity of the external load and D is the flexural rigidity of the plate. For a concentrated load P the intensity q at every point, except the origin, is entirely due to the pressure of the liquid on the plate. Its magnitude is equal to $-\rho g w$. Thus the differential equation to be solved is

$$\frac{1}{r}\frac{d}{dr}\left\{r\frac{d}{dr}\left[\frac{1}{r}\frac{d}{dr}\left(r\frac{dw}{dr}\right)\right]\right\} + \frac{\rho g w}{D} = 0. \tag{1.2}$$

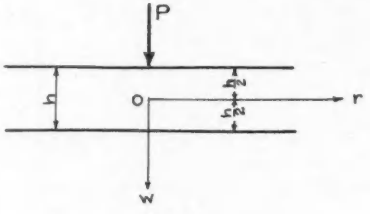

FIG. 1.

If we let $r = lx$, where $l = (D/\rho g)^{1/4}$, we find that (1.2) can be put into the form

$$\left(\frac{d^2}{dx^2}+\frac{1}{x}\frac{d}{dx}\right)\left(\frac{d^2w}{dx^2}+\frac{1}{x}\frac{dw}{dx}\right)+w=0. \tag{1.3}$$

In order to find the general solution of (1.3) we note that any solution of

$$\frac{d^2w}{dx^2}+\frac{1}{x}\frac{dw}{dx}+aw=0. \tag{1.4}$$

will satisfy (1.3) providing $a=\pm\sqrt{-1}=\pm i$. However, for these values of a it is well known that the Bessel Functions

$$J_0(i^{3/2}x),\ J_0((-i)^{3/2}x),\ K_0(i^{1/2}x),\ K_0((-i)^{1/2}x)$$

are all solutions of (1.4). Since

$$\begin{aligned}
J_0(i^{3/2}x) &= \operatorname{ber} x + i \operatorname{bei} x\\
J_0((-i)^{3/2}x) &= \operatorname{ber} x - i \operatorname{bei} x\\
K_0(i^{1/2}x) &= \ker x + i \operatorname{kei} x\\
K_0((-1)^{1/2}x) &= \ker x - i \operatorname{kei} x
\end{aligned}$$

we see that the modified Bessel Functions ber x, bei x, ker x, kei x provide four linearly independent solutions of (1.3) and hence the general solution of (1.3) is

$$w=A_1 \operatorname{ber} x + A_2 \operatorname{bei} x + A_3 \ker x + A_4 \operatorname{kei} x, \tag{1.5}$$

where A_1, A_2, A_3, A_4 are arbitrary constants. This gives the general solution of (1.2) to be

$$w=A_1 \operatorname{ber}(r/l) + A_2 \operatorname{bei}(r/l) + A_3 \ker(r/l) + A_4 \operatorname{kei}(r/l). \tag{1.6}$$

The modified Bessel Functions in (1.6) are discussed in great detail in McLachlan's book, Bessel Functions for Engineers (2). Many of the formulas involving these functions are given on pages 168-172 of this book and numerical tables are given on pages 177-178. Since we shall be using these formulas and tables throughout the rest of the paper we shall refer to it by the abbreviation M in the remaining part of this paper.

From M, page 169, formulas 185, 186 we see that both ber x and bei x increase without limit as $x\to\infty$. Similarly formula 203 shows that ker $x\to\infty$ as $x\to 0$. Since our displacement w must be finite at $r=0$ and $r=\infty$ we see that $A_1=A_2=A_3=0$. Hence

$$w=A_4 \operatorname{kei}(r/l). \tag{1.7}$$

From the fact that our plate is in equilibrium we can conclude that the total restoring force of the water must equal the concentrated load P. Hence

$$\int_0^\infty \rho g w\, 2\pi r\, dr = P. \tag{1.8}$$

Thus,

$$2\pi\rho g A_4 \int_0^\infty r \operatorname{kei}(r/l)\, dr = P. \tag{1.9}$$

From M, p. 172, formula (235), this integral can be evaluated to give

$$-2\pi\rho g A_4 l \left[r \ker'(r/l) \right]_0^\infty = P. \tag{1.10}$$

Since M, p. 172, formula (232) implies $\lim_{r\to\infty} [r \ker'(r/l)] = 0$ and M, p. 170, formula (203) gives $\lim_{r\to 0} [r \ker'(r/l)] = -l$ we find that

$$A_4 = -P/2\pi\rho g l^2. \tag{1.11}$$

Thus the deflection, at any point, due to a concentrated load P is given by

$$w = -P \operatorname{kei}(r/l)/2\pi\rho g l^2. \tag{1.12}$$

This immediately implies that the maximum deflection is at the origin and is given by

$$w_{max} = P/8\,\rho g l^2.$$

Section 2—Arbitrary Loading

In Fig. 2 we are considering the top of the plate and shall assume that the plate has been loaded in an arbitrary manner over the region enclosed by a closed curve. We desire to find the deflection at an arbitrary point Q due to this load. It should be noted that although Q is shown as an external point to the area of loading, the following derivation also applies if it is an interior point.

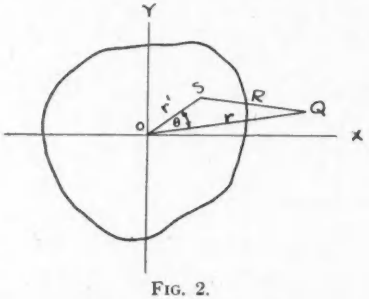

FIG. 2.

Let us take polar co-ordinates with respect to the line OQ with O as the polar origin. Let S be any interior point with polar co-ordinates (r', θ). Further suppose that $SQ = R$ and that the density of loading at S is given by some function $q(r', \theta)$. Thus the concentrated load at S is given by $q(r',\theta)r'\,dr'\,d\theta$ and hence the deflection dw at Q due to this load is given by (1.12) to be

$$dw = -q(r', \theta) \operatorname{kei}(R/l)\, r' dr' d\theta / 2\pi\rho g l^2, \tag{2.1}$$

where $R^2 = r'^2 + r^2 - 2rr' \cos\theta$. Thus the total deflection can be obtained by

$$w = -\int_A\int q(r', \theta)r' \operatorname{kei}(R/l)dr'd\theta/2\pi pgl^2, \tag{2.2}$$

where A is the region of loading.

Although (2.2) gives the general expression for the deflection due to any type of loading, it will be difficult to evaluate the integrals involved in most cases. For complicated boundaries it will be necessary to use numerical integration. However, in a few cases it is possible to carry out the integration in terms of known functions. We shall show in a later section that (2.2) can be used to find an exact expression for the deflection due to a uniform loading over a circular region. Before doing this however it is necessary to obtain the so-called addition theorem for the function kei x and an identity satisfied by the modified Bessel Functions.

Section 3—The Addition Theorem for kei x and an Identity

It is quite possible that the addition theorem for kei x and the identity, involving the modified Bessel Functions, which we shall prove, are already known. However we have not been able to find them in print and, since the proofs are short, we felt it advisable to include the proofs in this paper.

Addition Theorem

It is well known (4, p. 361) that the function $K_0(x)$ satisfies the addition theorem

$$K_0(x) = \sum_{m=-\infty}^{\infty} K_m(Z)\, I_m(z) \cos m\,\theta, \tag{3.1}$$

where $x^2 = Z^2 + z^2 - 2Zz\cos\theta$. Moreover the expression (3.1) is valid as long as $|z| \leqslant |Z|$. Replacing x, Z, z in the above expression by $i^{\frac{1}{2}}x$, $i^{\frac{1}{2}}Z$, $i^{\frac{1}{2}}z$ respectively we have

$$K_0(i^{1/2}x) = \sum_{m=-\infty}^{\infty} K_m(i^{1/2}Z)\, I_m(i^{1/2}z) \cos m\theta, \tag{3.2}$$

where again, $x^2 = Z^2 + z^2 - 2Zz\cos\theta$. From M, formulas 201, 205 and 163 we have

$$K_0(i^{1/2}x) = \ker x + i \operatorname{kei} x \tag{3.3}$$

$$K_m(i^{1/2}Z) = i^m(\ker_m Z + i \operatorname{kei}_m Z) \tag{3.4}$$

$$I_m(i^{1/2}z) = i^{-m}(\operatorname{ber}_m z + i \operatorname{bei}_m z). \tag{3.5}$$

Thus

$$\ker x + i \operatorname{kei} x = \sum_{m=-\infty}^{\infty} (\ker_m Z + i \operatorname{kei}_m Z)(\operatorname{ber}_m z + i \operatorname{bei}_m z)\cos m\theta \tag{3.6}$$

If we assume x, Z, z are all real, we can, by equating imaginary parts, find that

$$\operatorname{kei} x = \sum_{m=-\infty}^{\infty} (\operatorname{kei}_m Z \operatorname{ber}_m z + \ker_m Z \operatorname{bei}_m z)\cos m\theta. \tag{3.7}$$

Expression (3.7) is the so-called addition theorem for kei x and will hold as

long as $|z| \leqslant |Z|$. From the symmetry of the expression $x^2 = Z^2 + z^2 - 2Zz \cos\theta$, it is obvious that

$$\text{kei}\, x = \sum_{m=-\infty}^{\infty} (\text{kei}_m z \, \text{ber}_m Z + \text{ker}_m z \, \text{bei}_m Z) \cos m\theta \qquad (3.8)$$

if $|Z| \leqslant |z|$.

Since $$\int_0^{2\pi} \cos m\theta \, d\theta = 0, \; m = \pm 1, \pm 2, \pm 3, \ldots$$
$$= 2\pi, \quad m = 0$$

we have that

$$\int_0^{2\pi} \text{kei}\, x \, d\theta = 2\pi \, (\text{kei}\, Z \, \text{ber}\, z + \text{ker}\, Z \, \text{bei}\, z), \text{ if } |z| \leqslant |Z| \text{ and} \qquad (3.9)$$

$$\int_0^{2\pi} \text{kei}\, x \, d\theta = 2\pi \, (\text{kei}\, z \, \text{ber}\, Z + \text{ker}\, z \, \text{bei}\, Z), \text{ if } |Z| \leqslant |z|. \qquad (3.10)$$

We shall make use of these relationships in evaluating the integral (2.2).

An Identity

From M, page 156, problem 60, we have

$$z\left[K_0(z)\frac{d}{dz}I_0(z) - I_0(z)\frac{d}{dz}K_0(z)\right] = 1. \qquad (3.11)$$

Replacing z by $i^{1/2}z$ we have

$$z\left[K_0(i^{1/2}z)\frac{d}{dz}I_0(i^{1/2}z) - I_0(i^{1/2}z)\frac{d}{dz}K_0(i^{1/2}z)\right] = 1.$$

From Relations (3.3) and (3.5) of the present paper we find

$$z\Big[(\ker z + i\,\text{kei}\, z)\Big(\frac{d}{dz}\text{ber}\, z + i\frac{d}{dz}\text{bei}\, z\Big) -$$
$$(\text{ber}\, z + i\,\text{bei}\, z)\Big(\frac{d}{dz}\ker z + i\frac{d}{dz}\text{kei}\, z\Big)\Big] = 1.$$

Assuming z is real, we can equate real and imaginary parts and find that

$$z\left[\ker z\frac{d}{dz}\text{ber}\, z - \text{kei}\, z\frac{d}{dz}\text{bei}\, z - \text{ber}\, z\frac{d}{dz}\ker z + \text{bei}\, z\frac{d}{dz}\text{kei}\, z\right] = 1 \qquad (3.12)$$

and

$$\text{kei}\, z\frac{d}{dz}\text{ber}\, z + \ker z\frac{d}{dz}\text{bei}\, z - \text{bei}\, z\frac{d}{dz}\ker z - \text{ber}\, z\frac{d}{dz}\text{kei}\, z = 0. \qquad (3.13)$$

Denoting differentiation by the prime notation these identities may be written

$$z\,[\ker z \, \text{ber}' z - \text{kei}\, z \, \text{bei}' z - \text{ber}\, z \, \ker' z + \text{bei}\, z \, \text{kei}' z] = 1 \qquad (3.14)$$

$$\text{kei}\, z \, \text{ber}'\, z + \ker z \, \text{bei}'\, z - \text{bei}\, z \, \ker'\, z - \text{ber}\, z \, \text{kei}'\, z = 0 \qquad (3.15)$$

Here again we shall make use of these identities in the next section.

Section 4—Uniform Circular Loading

We shall assume that the loading is uniform over a circular area of radius a. Since the loading is uniform $q(r', \theta)$ is a constant which we abbreviate to q. Thus (2.2) gives us the deflection to be

$$w = -\frac{q}{2\pi\rho g l^2}\left(\int_0^a\int_0^{2\pi} r' \operatorname{kei}(R/l)dr'\,d\theta\right). \tag{4.1}$$

In evaluating this integral we distinguish two different cases.

Case 1 *External Point* — $r' < r$.

For this case (3.9) applies and

$$w = -\frac{q}{\rho g l^2}\int_0^a r' [\operatorname{kei}(r/l)\operatorname{ber}(r'/l) + \operatorname{ker}(r/l)\operatorname{bei}(r'/l)]\,dr'.$$

Evaluating the integrals by means of M, p. 170, formulas 189, 190 we have

$$w = \frac{qb}{\rho g}[\operatorname{ber}'(b)\operatorname{ker}(r/l) - \operatorname{bei}'(b)\operatorname{kei}(r/l)], \tag{4.2}$$

where $b = a/l$.

Thus (4.2) gives the deflection at any external point.

Case 2. *Internal Point* — $0 \leqslant r \leqslant a$.

As before, the deflection at any interior point is given by

$$w = -\frac{q}{2\pi\rho g l^2}\int\int_A r' \operatorname{kei}(R/l)\,dr'\,d\theta. \tag{4.3}$$

This can be split up into two integrals as

$$w = -\frac{q}{2\pi\rho g l^2}\left[\int_0^r\int_0^{2\pi} r' \operatorname{kei}(R/l)dr'\,d\theta + \int_r^a\int_0^{2\pi} r' \operatorname{kei}(R/l)dr'd\theta\right]. \tag{4.4}$$

In the first integral (3.9) applies and for the second (3.10) may be used. Thus

$$w = -\frac{q}{\rho g l^2}\left\{\int_0^r r' [\operatorname{kei}(r/l)\operatorname{ber}(r'/l) + \operatorname{ker}(r/l)\operatorname{bei}(r'/l)]\,dr' + \int_r^a r' [\operatorname{kei}(r/l)\operatorname{ber}(r/l) + \operatorname{ker}(r'/l)\operatorname{bei}(r/l)]\,dr'\right\}.$$

These integrals may be evaluated as before and the terms rearranged to give

$$w = \frac{qr}{\rho g l}[\operatorname{ker}(r/l)\operatorname{ber}'(r/l) - \operatorname{bei}'(r/l)\operatorname{kei}(r/l) + \operatorname{kei}'(r/l)\operatorname{bei}(r/l) - \operatorname{ker}'(r/l)\operatorname{ber}(r/l)] + \frac{qb}{\rho g}[\operatorname{ker}'(b)\operatorname{ber}(r/l) - \operatorname{kei}'(b)\operatorname{bei}(r/l)].$$

Using (3.14) we find

$$w = \frac{q}{\rho g} + \frac{qb}{\rho g}[\ker'(b)\mathrm{ber}(r/l) - \mathrm{kei}'(b)\mathrm{bei}(r/l)] \tag{4.5}$$

and that (4.5) will give the deflection at any interior point. The maximum deflection occurs at $r = 0$ and is given by

$$w_{\max} = q(1 + b\ \ker'(b))/\rho g. \tag{4.6}$$

Section 5—Application to Safe Thickness of Ice

Once the deflection function is known then it is possible to determine the stress distribution in the plate. From these it should be possible, from the rupture theories available, to determine the thickness at which the ice plate will break. We shall assume that the ice plate will break when the tensile stress reaches a certain maximum.

Using Timoshenko's notation we let M_r and M_t denote the bending moments per unit length and σ_r the tensile stress. The expressions given by him are

$$M_r = -D\left(\frac{d^2w}{dr^2} + \frac{\nu}{r}\frac{dw}{dr}\right)$$

$$M_t = -D\left(\frac{1}{r}\frac{dw}{dr} + \nu\frac{d^2w}{dr^2}\right)$$

$$(\sigma_r)_{\max} = -6\frac{(M_r)}{h^2}\ \max.$$

It is not difficult from (4.5) to show that $(M_r)_{\max}$ occurs at $r = 0$ and at this point $M_r = M_t$. Calculating from (4.5) we find

$$(\sigma_r)_{\max} = \frac{3qbD(1+\nu)\ \mathrm{kei}'\ b}{\rho g h^2 l^2}. \tag{5.1}$$

Since the load is uniform the total load P over the circular area is given by $P = \pi a^2 q$. Thus

$$(\sigma_r)_{\max} = \frac{3PbD(1+\nu)\ \mathrm{kei}'\ b}{\pi a^2 \rho g h^2 l^2}.$$

Since $D/\rho g = l^4$, and $b = a/l$

$$P = \frac{\pi(\sigma_r)_{\max}\, bh^2}{3(1+\nu)\ \mathrm{kei}'\ b}. \tag{5.2}$$

Formula (5.2) thus relates the maximum load P to the thickness h of ice.

It should be pointed out that the flexural rigidity D is given by

$$D = Eh^3/12(1 - \nu^2)$$

and hence b will also depend on h.

Numerical Analysis

It was pointed out that the elastic properties of ice show wide variability under different conditions. For this reason the values we choose for the elastic

constants are definitely on the conservative side. From work done by Hess (1, pp. 49, 214) and others we take

$$E = 320{,}000 \text{ lb. per in}^2.$$
$$(\sigma_r)_{\max} = 140 \text{ lb. per in}^2.$$
$$\nu = 1/3$$
$$\rho = 0.0361 \text{ lb. per in}^3$$

For ice 1.5 in. thick we find the formula

$$D = Eh^3/12(1 - \nu^2)$$

that

$$D = 1.01 \times 10^5 \text{ lb. in.}$$

Hence $$l = (D/\rho g)^{1/4} = 40.8 \text{ in.}$$

For a circular loading area of diameter 1ft. we find

$$b = a/l = 0.147.$$

From M page 180

$$\text{kei}' b = (0.6159 - \log_e b)(b/2) + \pi b^3/64 + \ldots$$

This gives for $b = 0.147$ that

$$\text{kei}' b = 0.186.$$

From Formula (5.2) we thus find

$$P = 195 \text{ lb.}$$

This result seems to be in agreement with the statement made by Barnes that ice 1.5 in. thick will hold a man.

From M, page 180, we have

$$\text{ker}' b = -\frac{1}{2v} + \tfrac{1}{4}\pi v - \tfrac{1}{2}(1.3659 - \log_e b)v^3 + \ldots,$$

where $v = b/2$. Thus

$$1 + b \text{ ker}' b = \tfrac{1}{2}\pi v^2 - (1.3659 - \log_e b)v^4 + \ldots.$$

For $b = 0.147$ we find

$$1 + b \text{ ker}' b = \tfrac{1}{2}\pi(0.0735)^2$$

is a satisfactory approximation. Thus $w_{\max}$ as given by (4.6) is

$$w_{\max} = \pi q(0.0735)^2/2\rho g = P(0.0735)^2/2a^2\rho g$$

Hence $w_{\max} = 0.4$ in.

Conclusion

In the introduction of our paper we gave a brief outline of the motivating problems for the present paper. Throughout the paper we have tried to point out the simplifying assumptions that we have made in order to obtain a mathematical analysis. The present work should be considered at best a start toward the solution of the motivating problems and that a satisfactory solution will be obtained only by taking into account some of the factors which we have neglected.

It is hoped that formulas (4.6) and (5.2) will soon be tested experimentally and that their domain of validity will be established. When this is done these formulas may prove of some value in determining some of the elastic properties of ice.

In our present work we have dealt at some length with the cases of a single concentrated load and also a single loading over a circular area. From these solutions it is easy to determine the deflection due to any number of concentrated forces or any number of loadings of circular areas. These solutions will of course be required in determining the thickness of ice for vehicles of different types.

Finally we would like to point out that our solutions may have applications in a different field. Our solutions will of course be valid for any isotropic plate resting on an elastic foundation. The constant ρg is simply replaced by the modulus of the foundation. As such the solutions which we have determined for the deflection of the plate may prove of value in the design of concrete roads or airport runways.

References

1. BARNES, H. T. Ice engineering. Renouf Publishing Co., Montreal. 1928.
2. MCLACHLAN, N. W. Bessel functions for engineers. Oxford University Press, London, New York, Toronto. 1934.
3. TIMOSHENKO, S. Theory of plates and shells. McGraw-Hill Book Co., Inc., New York. 1940.
4. WATSON, G. N. Theory of Bessel functions. Cambridge University Press, 1944.

ANGULAR DISTRIBUTION OF NEUTRONS AT THE INTERFACE OF TWO ADJOINING MEDIA[1]

By B. Davison[2]

Abstract

Two media separated by a plane interface and each filling an infinite half-space are considered. Neutrons come in infinite number from infinity in one medium and the neutron density vanishes at infinity in the other medium. Isotropic scattering in the laboratory system of co-ordinates in both media is assumed and all neutrons are assumed to have the same speed. The angular distribution of neutrons emerging from either medium into the other is obtained in terms of the angular distribution of neutrons for the Milne problem, that is, the angular distribution of neutrons emerging from a scattering medium into a vacuum. The latter angular distribution is tabulated in the preceding paper by LeCaine.

1. The preceding paper (1) (hereafter referred to as A) contains the tabulation of the angular distribution of neutrons emerging into a vacuum from a half-space filled with a scattering material. One may also be interested in the angular distribution of neutrons emerging from one into another scattering medium. The purpose of the present paper is to show that this can also easily be obtained from the tabulations of A.

With regard to each of the two media we make the same assumptions as are made in A with regard to the single medium considered there: we assume that one-velocity theory is applicable to both media (i.e., all neutrons have the same velocity and are scattered without loss of energy), that scattering is isotropic in the laboratory system of co-ordinates in both media and that we are dealing with plane geometry, each medium occupying an entire half-space, with the neutron density in it depending only on the distance from the interface.

The case of the neutron density's tending in one medium to zero at large distance from the interface would seem to be of greater interest than the more general case when the neutron density does not tend to zero at large distances in either medium. The former case is also simpler in the sense that the solution is unique, apart from a multiplicative constant, while in the latter case the solution can be looked upon as a sum of two linearly independent solutions with arbitrary coefficients. In view of this we limit ourselves in the present note to the former case.

Since we assume plane geometry, it is immaterial whether the total mean free paths in the two media are the same or not. For in the one-velocity theory in plane geometry we may use different units of length in the two

[1] *Manuscript received October 27, 1949.*
Contribution of the Chalk River Laboratories of the National Research Council of Canada. Issued as N. R. C. No. 2136.
[2] *Present address: Atomic Energy Research Establishment, Harwell, England.*

media without changing the form of the equations governing the distribution of neutrons. Thus we take the total mean free path to be unity in each medium. The media then differ only in their absorptive or multiplicative properties.

Let c be the probable number of secondary neutrons per collision in any medium and $a = 1 - c$; so that $a > 0$ for media in which capture predominates over multiplication and $a < 0$ for media in which multiplication predominates over capture. If capture and scattering are the only processes possible then

$$a = \frac{\text{Total mean free path}}{\text{Mean free path for capture}}.$$

2. Take the interface as the plane $x = 0$ and characterize the spaces $x > 0$ and $x < 0$ by subscripts 1 and 2 respectively. Let neutrons come in infinite number from infinity in the first medium and let their density vanish at infinity in the second medium. This implies that $a_2 > 0$. We impose no restrictions upon the sign of a_1, or upon the comparative values of a_1 and a_2* We require the angular distribution of the particles entering the second medium.

Let $f(x)$ be the density in our problem, $n(x)$, be the density which would exist in the first medium if the second medium were replaced by a vacuum, and $t(x)$ be the density which would exist if the second medium occupied the half-space $x > 0$ with an infinite number of particles comimg from infinity and with vacuum in the half-space $x < 0$. Let $\psi_f(x, \mu)$, $\psi_n(x, \mu)$ and $\psi_t(x, \mu)$ be the angular distributions corresponding to $f(x)$, $n(x)$, and $t(x)$ respectively, μ being the cosine of the angle between the velocity of a neutron and the normal to the interface drawn into the first medium. Also let ν_1 and ν_2 be the roots of the equations

$$\frac{1}{1 - a_1} = \frac{1}{2\nu_1} \log \frac{1 + \nu_1}{1 - \nu_1}; \quad \frac{1}{1 - a_2} = \frac{1}{2\nu_2} \log \frac{1 + \nu_2}{1 - \nu_2}. \tag{1}$$

Since a_2 is positive, the roots of the second of these are real. We shall understand by ν_2 the positive root.

The densities $f(x)$, $n(x)$, and $t(x)$ satisfy the integral equations

$$\left.\begin{aligned} f(x) &= \frac{1 - a_1}{2} \int_0^\infty f(y)\, E(|x - y|)dy + \frac{1 - a_2}{2} \int_{-\infty}^0 f(y)\, E(|x - y|)dy \\ n(x) &= \frac{1 - a_1}{2} \int_0^\infty n(y)\, E(|x - y|)dy \\ t(x) &= \frac{1 - a_2}{2} \int_0^\infty t(y)\, E(|x - y|)dy \end{aligned}\right\} \tag{2}$$

in which $E(x) = \int_1^\infty e^{-xt}\, dt/t.$

*Except that the description "neutrons come in infinite number from infinity in the first medium" is applicable only for $a_1 > 0$. For $a_1 < 0$ it should be replaced by "neutron density be a bounded oscillating function of position in the first medium."

Taking the Fourier transforms, and denoting, following Titchmarsh (2), these Fourier transforms by the corresponding capital letters we have

$$\left.\begin{aligned} &F^+(u)\left[1-(1-a_1)\frac{\tan^{-1}u}{u}\right]+F^-(u)\left[1-(1-a_2)\frac{\tan^{-1}u}{u}\right]=0\\ &N^+(u)\left[1-(1-a_1)\frac{\tan^{-1}u}{u}\right]+N^-(u)=0\\ &T^+(u)\left[1-(1-a_2)\frac{\tan^{-1}u}{u}\right]+T^-(u)=0 \end{aligned}\right\} \tag{3}$$

in which, according to the definitions, $F^+(u)$, $N^+(u)$, and $T^+(u)$ are regular in the half-planes, $I(u) > R(\nu_1)$, $I(u) > R(\nu_1)$, and $I(u) > \nu_2$ respectively, while $F^-(u)$, $N^-(u)$, and $T^-(u)$ are regular in the half-plane $I(u) < 0$. Also, all these functions are quadratically summable over the lines parallel to the real axis situated within the half-planes in which they are regular. Notice next that we can put

$$1-(1-a_i)\frac{\tan^{-1}u}{u}=\frac{u^2+\nu_i^2}{u^2+1}\,\frac{\rho_{\nu_i}^+(u)}{\rho_{\nu_i}^-(u)}\,. \qquad (i=1,2) \tag{4}$$

in which $\rho_{\nu_i}^+(u)$ is regular in the half-plane $I(u) > -1$, $\rho_{\nu_i}^-(u)$ is regular in the half-plane $I(u) < 1$, and both are zero-free in the whole plane. Equation (3) can now be rewritten as

$$\begin{aligned} F^+(u)\,(u^2+\nu_1^2)\,\frac{\rho_{\nu_1}^+(u)}{\rho_{\nu_2}^+(u)} &= -\,F^-(u)\,(u^2+\nu_2^2)\,\frac{\rho_{\nu_1}^-(u)}{\rho_{\nu_2}^-(u)}\\ N^+(u)\,(u^2+\nu_1^2)\;\rho_{\nu_2}^+(u) &= -\,N^-(u)\,(u^2+1)\;\rho_{\nu_1}^-(u)\\ T^+(u)\,(u^2+\nu_2^2)\;\rho_{\nu_2}^+(u) &= -\,T^-(u)\,(u^2+1)\;\rho_{\nu_2}^-(u). \end{aligned} \tag{5}$$

One easily sees that the left sides of (5) are regular in the whole plane. Also, for u tending to infinity, they behave as u^2 times a quadratically summable function, i.e., they can only be linear functions of u. Next, since $F^-(u)$, $N^-(u)$, and $T^-(u)$ are regular in the lower half-plane, the linear functions in question vanish at $u = -i\nu_2$, $u = -i$, and $u = -i$ respectively. Thus (5) gives

$$\left.\begin{aligned} F^+(u)\,(u^2+\nu_1^2)\,\frac{\rho_{\nu_1}^+(u)}{\rho_{\nu_2}^+(u)} &= A_f(u+i\nu_2)\\ N^+(u)\,(u^2+\nu_1^2)\;\rho_{\nu_1}^+(u) &= A_n(u+i)\\ T^+(u)\,(u^2+\nu_2^2)\;\rho_{\nu_2}^+(u) &= A_t(u+i) \end{aligned}\right\} \tag{6}$$

in which A_f, A_n, and A_t are some constants. Eliminating $\rho_{\nu_2}^+(u)$ and $\rho_{\nu_2}^+(u)$ between the equations (6) gives

$$F^+(u)=\frac{\tilde{C}}{u-i\nu_2}\,\frac{N^+(u)}{T^+(u)} \tag{7}$$

in which $\tilde{C}$ is some constant.

The formula (7) can easily be reinterpreted in terms of the angular distribution at the interface. For we have, for $\mu > 0$,

$$\psi_f(0, -\mu) = \frac{1 - a_1}{2} \int_0^\infty f(|\mu|R)e^{-R}dR = \frac{1 - a_1}{2\mu} \int_0^\infty f(x)e^{-x/\mu}dx$$

$$= (1 - a_1) \sqrt{\frac{\pi}{2}} \frac{1}{\mu} F^+\left(\frac{i}{\mu}\right) \tag{8}$$

and similar expressions for $\psi_n(0, -\mu)$ and $\psi_t(0, -\mu)$. Using these expressions we rewrite (7) as

$$\psi_f(0, -\mu) = \frac{C}{1 - \mu\nu_2} \frac{\psi_n(0, -\mu)}{\psi_t(0, -\mu)}, \tag{9}$$

the constant C depending, of course, upon the normalizations used.

Suppose, for the sake of definiteness, that $f(x)$, $n(x)$, and $t(x)$ are normalized so as to be associated each with unit current at the interface, i.e.,

$$\int_{-1}^1 \mu\psi_f(0, \mu)d\mu = \int_{-1}^1 \mu\psi_n(0, \mu)d\mu = \int_{-1}^1 \mu\psi_t(0, \mu)d\mu = -1, \tag{10}$$

and determine, for this normalization, the values of $T^+(u)$, $N^+(u)$, and $F^+(u)$ in the vicinity of $u = 0$. Consider first $T^+(0)$. $T^+(u)$ is defined, for $I(u) > \nu_2$, by

$$T^+(u) = \frac{1}{\sqrt{2\pi}} \int_0^\infty e^{iux} t(x)dx \tag{11}$$

and for $I(u) \leqslant \nu_2$ it is the analytical continuation of (11). Now it is known that for large values of x the asymptotic behaviour of $t(x)$ is given by

$$t(x) = Be^{\nu_2 x} + 0(e^{-x}) = t_{as}(x) + t_{suppl}(x) \tag{12}$$

say, in which B is some numerical coefficient. Thus (11) becomes

$$T^+(u) = \frac{1}{\sqrt{2\pi}} \left\{ \frac{B}{-\nu_2 - iu} + \int_0^\infty e^{iuz} t_{suppl}(x)dx \right\},$$

which gives at once the analytical continuation of the definition (11) into the region $I(u) > -\nu_2$, and in particular

$$T^+(0) = \frac{1}{\sqrt{2\pi}} \left\{ -\frac{B}{\nu_2} + \int_0^\infty t_{suppl}(x)dx \right\}. \tag{13}$$

Consider now the current associated with $t(x)$. Following (12) we can also split the current into two parts, one associated with $t_{as}(x)$ and the other with $t_{suppl}(x)$. From the transport equation we have at once

$$\psi_1(x) - \psi_1(x_0) = a_2 \int_x^{x_0} \psi_0(x')dx', \tag{14}$$

in which ψ_1 denotes the first moment, i.e., the current, and ψ is the density.

For $t_{\text{suppl}}(x)$ the current vanishes at $x = \infty$, and consequently the current corresponding to $t_{\text{suppl}}(x)$ at $x = 0$ is given by

$$a_2 \int_0^\infty t_{\text{suppl}}(x)\, dx.$$

For $t_{as}(x)$ the current would vanish at $x = -\infty$, and consequently the current corresponding to $t_{as}(x)$ at $x = 0$ will be given by

$$a_2 \int_0^{-\infty} t_{as}(x)dx = a_2 B \int_0^\infty e^{\nu_2 x}\, dx = -\frac{a_2 B}{\nu_2}.$$

Combining these expressions and remembering that according to the normalization conditions (10) the total current is equal to -1, we have

$$-\frac{a_2 B}{\nu_2} + a_2 \int_0^\infty t_{\text{suppl}}(x)dx = -1. \tag{15}$$

Comparing this with (13) we obtain

$$T^+(0) = \frac{-1}{a_2\sqrt{2\pi}}. \tag{16}$$

If a_1 is positive the same argument can be applied to $N^+(u)$ and $F^+(u)$ giving

$$F^+(0) = N^+(0) = \frac{-1}{a_1\sqrt{2\pi}}. \tag{17}$$

We can now rewrite (6) more explicitly as

$$\left.\begin{aligned} F^+(u)\,(u^2+\nu_1^2)\,\frac{\rho^+_{\nu_1}(u)}{\rho^+_{\nu_2}(u)} &= \frac{-1}{a_1\sqrt{2\pi}}\,\nu_1^2\,\frac{\rho^+_{\nu_1}(0)}{\rho^+_{\nu_2}(0)}\left(1 - i\frac{u}{\nu_2}\right) \\ N^+(u)\,(u^2+\nu_1^2)\,\rho^+_{\nu_1}(u) &= \frac{-1}{a_1\sqrt{2\pi}}\,\nu_1^2\,\rho^+_{\nu_1}(0)\,(1-iu) \\ T^+(u)\,(u^2+\nu_2^2)\,\rho^+_{\nu_2}(u) &= \frac{-1}{a_2\sqrt{2\pi}}\,\nu_2^2\,\rho^+_{\nu_2}(0)\,(1-iu). \end{aligned}\right\} \tag{18}$$

The formula (7) thus becomes

$$F^+(u) = -\frac{1}{a_2\sqrt{2\pi}}\,\frac{\nu_2}{\nu_2 + iu}\,\frac{N^+(u)}{T^+(u)} \tag{19}$$

and (9)

$$\psi_f(0, -\mu) = \frac{1-a_2}{2a_2}\,\frac{\nu_2}{1-\mu\nu_2}\,\frac{\psi_n(0,-\mu)}{\psi_t(0,-\mu)}. \tag{20}$$

As in A let $\varphi(a, \mu)$ denote the angular distribution of neutrons emerging into a vacuum from a medium whose capture is characterized by a, normalized to unit density at the surface. μ is defined as in A, i.e., having a sign opposite to ours. Then using (6) of A we easily see that our $\psi_n(0, -\mu)$ and $\psi_t(0, -\mu)$ are connected with $\varphi(a, \mu)$ by the relationships

$$\psi_n(0, -\mu) = \frac{\nu_1}{\sqrt{a_1}}\varphi(a_1, \mu)$$

$$\psi_t(0, -\mu) = \frac{\nu_2}{\sqrt{a_2}}\varphi(a_2, \mu),$$

and that (20) becomes

$$\psi_f(0, -\mu) = \frac{1 - a_2}{2\sqrt{a_1 a_2}} \frac{\nu_1}{1 - \mu\nu_2} \frac{\varphi(a_1, \mu)}{\varphi(a_2, \mu)}, \tag{21}$$

in which $\varphi(a, \mu)$ is the function tabulated in Table VI of A.

Turn now to the case of $a_1 \leqslant 0$. Since the coefficient appearing in (20) is independent of a_1 for $a_1 > 0$, one might expect it to be independent of a_1 altogether. We verify this surmise first for $a_1 = 0$. In this case, in the half-space $x > 0$, the solutions $f(x)$ and $n(x)$ will be associated with constant current and, remembering the normalization condition (10) and the fact that in absence of capture the current is equal to one third of the asymptotic value of the density gradient taken with the opposite sign, we have, for $x \to \infty$,

$$\left.\begin{aligned} f(x) &= 3x + \text{a bounded function} \\ n(x) &= 3x + \text{a bounded function.} \end{aligned}\right\} \tag{22}$$

Hence, in the vicinity of $u = 0$,

$$\left.\begin{aligned} F^+(u) &= -\frac{3}{u^2\sqrt{2\pi}} + 0\left(\frac{1}{u}\right) \\ N^+(u) &= -\frac{3}{u^2\sqrt{2\pi}} + 0\left(\frac{1}{u}\right) \end{aligned}\right\}, \tag{23}$$

so that the first two of (12) are replaced by

$$\left.\begin{aligned} u^2F^+(u)\ \frac{\rho_0^+(u)}{\rho_{\nu_2}^+(u)} &= -\frac{3}{\sqrt{2\pi}}\ \frac{\rho_0^+(0)}{\rho_{\nu_2}^+(0)}\left(1 - i\frac{u}{\nu_2}\right) \\ u^2N^+(u)\ \rho_0^+(u) &= -\frac{3}{\sqrt{2\pi}}\ \rho_0^+(0)\ (1 - iu), \end{aligned}\right\}, \tag{24}$$

while (19), (20), and (21) obviously remain unaltered. Consider finally the case of $a_1 < 0$ (i.e., the medium filling the half-space $x > 0$ is a multiplying medium.) Now $f(x)$ and $n(x)$ for $x > 0$ are bounded oscillating functions, and the integrals

$$\int_0^\infty f(x)dx \text{ and } \int_0^\infty n(x)dx$$

exist in the Cesaro-summability sense. However it is known that by applying the Cesaro summability we obtain the correct values of the Fourier transforms, so that we have

$$F^+(0) = \frac{1}{\sqrt{2\pi}}\int_0^\infty f(x)\,dx;\ N^+(0) = \frac{1}{\sqrt{2\pi}}\int_0^\infty n(x)dx, \tag{25}$$

the integrals being understood in the Cesaro-summability sense. On the other hand the first moment at large distances from the interface will behave, both for $f(x)$ and for $n(x)$, as $A \sin \{|\nu_1|(x - x_0)\}$, ($A$ and x_0 being, of course, different for $n(x)$ and $f(x)$) so that on the average there will be no current at large distances, either for $f(x)$ or for $n(x)$, (though at any particular cross section there will be some current). Then the current at $x = 0$ associated with $f(x)$ will be, on account of (14),

$$a_1 \{ \text{ average with respect to } x_0 \text{ of } \int_0^{x_0} f(X)\, dX \} .$$

But this is exactly the definition of the value of a divergent integral in the sense of Cesaro summability. Thus we obtain from the normalization conditions (10), exactly as in the case of $a_1 > 0$,

$$F^+(0) = N^+(0) = \frac{-1}{a_1\sqrt{2\pi}},$$

which is identical with (17), so that (18), (19), (20), and (21) are applicable to the case $a_1 < 0$ without any alterations.

So far we have discussed the angular distribution of neutrons entering medium 2. The angular distribution of neutrons entering medium 1 from medium 2 can be also obtained without difficulty. For this purpose notice first that, according to (4), $\frac{\rho^+_{\nu_1}(u)}{\rho^-_{\nu_1}(u)}$ is an even function of u. Then, using the definitions of $\rho^+_{\nu_1}(u)$ and $\rho^-_{\nu_1}(u)$, one easily sees that

$$\rho^+_{\nu_1}(u) = \frac{1}{\rho^-_{\nu_1}(-u)} . \tag{26}$$

Combining this with (5) and (6) one derives

$$F^+(u)F^-(-u)\,(u^2 + \nu_1^2) = A_f^2. \tag{27}$$

On the other hand, similarly to (16) and (17), one obtains

$$F^-(0) = \frac{1}{a_2\sqrt{2\pi}}$$

and (27) becomes, more explicitly,

$$F^+(u)F^-(-u)\,(u^2 + \nu_1^2) = -\frac{\nu_1^2}{2\pi a_1 a_2} . \tag{28}$$

Further, similarly to (8), we have

$$\psi_f(0, \mu) = (1 - a_2)\sqrt{\pi/2}\,\frac{1}{\mu}\,F^-\left(\frac{-i}{\mu}\right)$$

and combining this with (8) and (28) gives

$$\psi_f(0, \mu)\,\psi_f(0, -\mu) = \frac{1}{4}\,\frac{(1 - a_1)(1 - a_2)}{a_2 a_1}\,\frac{\nu_1^2}{1 - \mu^2\nu_1^2} .$$

Thus from (20)

$$\psi_f(0, \mu) = \frac{(1 - a_1)}{2a_1} \frac{1 - \mu\nu_2}{\nu_2} \frac{{\nu_1}^2}{1 - \mu^2{\nu_1}^2} \frac{\psi_t(0, -\mu)}{\psi_n(0, -\mu)} \tag{29}$$

or, from (21)

$$\psi_f(0, \mu) = \frac{1 - a_1}{2\sqrt{a_1 a_2}} \frac{\nu_1(1 - \mu\nu_2)}{1 - \mu^2{\nu_1}^2} \frac{\varphi(a_2, \mu)}{\varphi(a_1, \mu)}. \tag{30}$$

Thus the angular distributions of neutrons entering medium 2 from 1, $\psi_f(0, -\mu)$, and of neutrons entering medium 1 from 2, $\psi_f(0, \mu)$ can both be found from the angular distributions of neutrons emerging from mediums 1 and 2 into a vacuum.

APPENDIX A

Elementary Derivation of the Formula Connecting Neutron Density and Neutron Current at the Interface

In passing from (20) to (21) we have used the relationship, quoted in A,

$$f(0) = \frac{\nu}{\sqrt{a}} j(0), \tag{A.1}$$

which gives the relation between the neutron density and the neutron current at the free surface of a half-space. However the formula (A.1) is not derived there, but reference is made to a paper which has not, so far, been published. In view of this it appears desirable to append the derivation of (A.1) to the present report.

Actually we shall prove a slightly more general result, namely that at the interface between two isotropically scattering media, each occupying a half-space, the neutron density and the neutron current are connected by the relationship

$$f(0) = \frac{\nu_1}{\sqrt{a_1 a_2}} j(0), \tag{A.2}$$

provided the neutron density vanishes at infinity in the medium (2). Here $f(x)$ is the neutron density at the optical distance x from the interface, $j(0)$ is the current at the interface, the positive direction of the current being taken from the medium (1) into the medium (2), a_1 and a_2 characterize the absorption in the two media respectively, and ν_1 is the solution of the equation

$$\frac{1}{2\nu_1} \log \frac{1 + \nu_1}{1 - \nu_1} = \frac{1}{1 - a_1} \tag{A.3}$$

(a_2 will be assumed positive, but a_1 can have either sign or be zero).

A free surface can be treated as the surface of a medium absorbing all neutrons, in which case $a_2 = 1$, and the formula (A.2) goes over into (A.1).

The function $f(x)$ is known to satisfy the integral equation

$$f(x) = \frac{1-a_1}{2}\int_0^\infty f(y)E(|x-y|)dy + \frac{1-a_2}{2}\int_{-\infty}^0 f(y)E(|x-y|)dy$$

(the medium (1) occupies the half-space $x > 0$, and the medium (2) the half-space $x < 0$). Putting, for brevity,

$$\Lambda\varphi(x) = \frac{1-a_1}{2}\int_0^\infty \varphi(y)E(|x-y|)dy + \frac{1-a_2}{2}\int_{-\infty}^0 \varphi(y)E(|x-y|)dy \quad \text{(A.4)}$$

we can rewrite the above equation as

$$(1-\Lambda)f(x) = 0. \quad \text{(A.5)}$$

The expression for $j(0)$ is given by

$$j(0) = a_2\int_{-\infty}^0 f(x)dx \quad \text{(A.6)}$$

since the current through the interface should be equal to the number of neutrons captured in the medium (2) in unit time. On the grounds of (A.5), the expression for $j(0)$ can also be written as

$$j(0) = a_2\int_{-\infty}^0 \Lambda f(x)dx.$$

On changing the order of integration and slightly rearranging we get a further expression for $j(0)$, namely

$$j(0) = \frac{1-a_1}{2}\int_0^\infty f(x)E_2(x)dx - \frac{1-a_2}{2}\int_{-\infty}^0 f(x)E_2(|x|)dx. \quad \text{(A.7)}$$

(In the above

$$E(x) = \int_1^\infty \frac{e^{-xt}}{t}dt; \qquad E_2(x) = \int_1^\infty \frac{e^{-xt}}{t^2}dt.\ )$$

In order to prove (A.2) it is convenient to consider an auxiliary function $Q(x)$ defined by

$$Q(x) = f'(x) - \nu_1^2\int_0^x f(y)dy - \frac{\nu_1^2 j(0)}{a_1}. \quad \text{(A.8)}$$

Let us construct the integral equation satisfied by $Q(x)$. If $\varphi(x)$ is any differentiable function such that $\Lambda\varphi(x)$ exists (i.e., the integrals involved in (A.4) converge) then differentiating (A.4) and eliminating the derivatives of the E functions by integration by parts gives

$$\frac{d}{dx}\Lambda\varphi(x) = \frac{a_2-a_1}{2}\varphi(0)E(|x|) + \Lambda\varphi'(x). \quad \text{(A.9)}$$

Taking here $\varphi(x) = \int_0^x f(y)dy$ and remembering (A.5) we see at once that

$$\frac{d}{dx}\left[(1-\Lambda)\int_0^x f(y)dy\right] = 0,$$

so that $(1 - \Lambda)\int_0^x f(y)dy$ is a constant. To determine this constant take $x = 0$. Then

$$\left[(1 - \Lambda)\int_0^x f(y)dy\right]_{x=0} = -\left\{\frac{1 - a_1}{2}\int_0^\infty E(y)dy\int_y f(x)dx - \frac{1 - a_2}{2}\int_{-\infty}^0 E(|y|)dy\int_y^0 f(x)dx\right\}.$$

By changing the order of integration and using (A.7) we see at once that this is equal to $-j(0)$. Thus

$$(1 - \Lambda)\int_0^x f(y)dy = -j(0).$$

On the other hand, differentiating (A.5), and using (A.9) again, but with $\varphi(x) = f(x)$, gives

$$(1 - \Lambda)f'(x) = \frac{a_2 - a_1}{2}f(0)E(|x|)$$

while $\Lambda(1)$ can be easily worked out directly from (A.4).

Combining these results gives

$$(1 - \Lambda)Q(x) = H(x), \text{ say,} \tag{A.10}$$

in which

$$H(x) = \begin{cases} \dfrac{a_2 - a_1}{2}f(0)E(x) - \nu_1^2 j(0)\dfrac{a_2 - a_1}{2a_1}E_2(x) & \text{for } x > 0 \\ \dfrac{a_2 - a_1}{2}f(0)E(|x|) - \nu_1^2 j(0)\dfrac{a_2 - a_1}{2a_1}\{2 - E_2(|x|)\} & \text{for } x < 0. \end{cases} \tag{A.11}$$

Let us examine now the behavior of $Q(x)$ for large positive x. It is known that, considering say the half-space $x > 0$, we can present $f(x)$ in the form

$$f(x) = f_{as}(x) + \tilde{f}(x), \qquad x > 0 \tag{A.12}$$

in which $f_{as}(x)$ is a solution of

$$f''_{as}(x) - \nu_1^2 f_{as}(x) = 0$$

while $\tilde{f}(x)$ is a small quantity of the order of $0(e^{-x})$. Hence

$$f''(x) - \nu_1^2 f(x) = \tilde{f}''(x) - \nu_1^2\tilde{f}(x) = 0(e^{-x}).$$

Integration of the last relationship and comparison with the definition of $Q(x)$ shows that

$$Q(x) = \text{const} + 0(e^{-x}) = Q(\infty) + 0(e^{-x}), \quad (x > 0). \tag{A.13}$$

On the other hand, once $Q(x)$ tends to a definite limit for $x \to \infty$, (A.10) gives

$$a_1 Q(\infty) = H(\infty).$$

But according to (A.11), for positive x, $H(x) = 0(e^{-x})$. Hence $H(\infty) = 0$ and consequently $Q(\infty) = 0$. Thus (A.13) reduces to

$$Q(x) = 0(e^{-x}). \tag{A.14}$$

Notice now that $H(x)$ is the free term of an inhomogeneous equation possessing a solution, the corresponding homogeneous equation also having a solution. If we were dealing with bounded functions and the range of integration were finite, this would immediately imply that $H(x)$ is orthogonal to the solution of the transposed homogeneous equation. In our case this would mean

$$\frac{1-a_1}{2}\int_0^\infty H(x)f(x)dx + \frac{1-a_2}{2}\int_{-\infty}^0 H(x)f(x)dx = 0 \tag{A.15}$$

since the solution of the transposed homogeneous equation in our case is

$$\begin{aligned} &(1-a_1)f(x) && \text{for } x > 0 \\ &(1-a_2)f(x) && \text{for } x < 0\,. \end{aligned}$$

Actually in our case the range of integration is infinite. For an infinite range of integration the orthogonality of a possible free term to the solution of the transposed homogeneous equation does not always hold. But (A.15) can easily be proved directly, using (A.14) and the fact that $f(x)$ is assumed to tend to zero for $x \to -\infty$.

For, similarly to (A.12), for negative x we have quite generally

$$f(x) = Ae^{\nu_2|x|} + Be^{-\nu_2|x|} + 0(e^{-|x|}) \quad (x < 0),$$

in which ν_2 is the positive root of the equation similar to (A.3) (ν_2 is necessarily real since a_2 is assumed to be positive.) If for $x \to -\infty$ $f(x)$ tends to zero, the coefficient accompanying $e^{\nu_2|x|}$ should vanish, and the above formula gives

$$f(x) = 0(e^{-\nu_2|x|}). \qquad (x < 0) \tag{A.16}$$

Consider now the left side of (A.15). Substitute for $H(x)$ its expression in terms of $Q(x)$, i.e., rewrite the left side of (A.15) in the form

$$\frac{1-a_1}{2}\int_0^\infty f(x)\,(1-\Lambda)\,Q(x)dx + \frac{1-a_2}{2}\int_{-\infty}^0 f(x)(1-\Lambda)Q(x)dx. \tag{A.17}$$

In the double integrals which appear if (A.17) is written out explicitly, one can interchange the order of integration, as one can easily verify directly from (A.14) and (A.16). Interchanging also the role of the two variables of integration we see that (A.17) is identical with

$$\frac{1-a_1}{2}\int_0^\infty Q(x)(1-\Lambda)f(x)dx + \frac{1-a_2}{2}\int_{-\infty}^0 Q(x)\,(1-\Lambda)f(x)dx,$$

which vanishes in view of (A.5). This proves (A.15).

On the other hand, substitution into (A.15) for $H(x)$ from (A.11) gives

$$0 = \frac{a_2 - a_1}{2} f(0) \left[\frac{1 - a_1}{2} \int_0^\infty f(x)E(x)dx + \frac{1 - a_2}{2} \int_{-\infty}^0 f(x)E(|x|)dx \right.$$

$$- \nu_1^2 j(0) \frac{a_2 - a_1}{2a_1} \left[\frac{1 - a_1}{2} \int_0^\infty f(x)E_2(x)dx - \frac{1 - a_2}{2} \int_{-\infty}^0 f(x)E_2(|x|)dx \right.$$

$$\left. - \nu_1^2 j(0) \frac{a_2 - a_1}{a_1} \frac{1 - a_2}{2} \int_{-\infty}^0 f(x)dx \right]. \qquad \text{(A.18)}$$

Now the content of the first square bracket in (A.18) is, from (A.5), equal to $f(0)$, of the second square bracket is, from (A.7), equal to $j(0)$; finally the integral appearing in the last term is also expressible in terms of $j(0)$ by means of (A.6).

Thus we get

$$\frac{a_2 - a_1}{2} f^2(0) - \nu_1^2 j^2(0) \left[\frac{a_2 - a_1}{2a_1} + \frac{(a_2 - a_1)(1 - a_2)}{2a_1 a_2} \right] = 0$$

from which (A.2) follows at once.

References

1. LeCaine, J. Can. J. Research, A, 28: 242. 1950.
2. Titchmarsh E. C. Introduction to the theory of Fourier integrals. Oxford University Press. 1937.

PARTICLE IDENTIFICATION IN PHOTOGRAPHIC EMULSIONS BY THE DELTA-RAY METHOD[1]

By L. Voyvodic

Abstract

A comparison is made in this study between the δ-ray densities expected theoretically and those observed experimentally on charged particle tracks in Ilford G5 emulsions. The energies of δ-rays are determined here by means of grain-counting measurements and energy-loss considerations. Using this method of energy determination and the theoretical formula for δ-ray density, good agreement has been found with the experimental distributions on proton, μ-meson, deuteron, and α-particle tracks. The agreement is satisfactory both in absolute value and in the shape of the δ-ray density distribution. These results are considered to show that the δ-ray technique is suitable as an absolute method of charged particle identification in photographic emulsions.

Introduction

The study of δ-rays, or "knock-on" electrons, in photographic emulsions has proved to be a valuable technique in identifying energetic heavy nuclei in the primary cosmic radiation (2, 4), and the energetic fragments (8) occasionally emitted in nuclear disintegrations or "stars". The tracks of these heavy particles appear under the microscope as solid filaments of continuous developed grains, accompanied by large numbers of short spurs due to "knock-on" electrons.

Heretofore, the theoretical distribution of δ-rays along the tracks of charged particle has been assumed as valid for photographic emulsions. For comparison with the δ-rays observed on experimental tracks, theoretical curves have been normalized by calibration with α-particles of known energy (2, 4), or with recognizable protons and mesons (8). In the present study a more detailed comparison is made between the calculated and observed δ-rays on recognizable tracks in Ilford G5 electron sensitive emulsions. In particular, the absolute values of the δ-ray densities are used in this comparison in order to test the validity of the δ-ray technique as an absolute method of charged particle identification.

Theory

The theoretical production of δ-rays may be derived from the differential collision probability $\chi(E, E')dE'dx$, which is the probability for a particle of charge Z, energy E, and velocity βc, traversing a thickness dx, to transfer an amount of energy between E' and $E' + dE'$ to a free electron. In the classical treatment $\chi(E, E')$ is given by the Rutherford formula (7) as

$$\chi(E, E')\,dE'dx = \frac{2\mu_e \rho Z^2 C dx}{\beta^2} \frac{dE'}{(E')^2}, \qquad (1)$$

[1] *Manuscript received February 2, 1950.*
Contribution from the Physics Division, National Research Laboratories, Ottawa, Canada. Issued as N.R.C. No. 2135.

where μ_e is the electron mass, ρ is the density, and $C = 0.150 \times \frac{(Z')}{(A)}$ for the material traversed.

The δ-ray density n, or the number of δ-rays per unit length, involving energy transfers $\geqslant E'_{min}$, is obtained by integrating $\chi(E, E')dE'$ over the energy region E'_{min} to E'_{max} (where $E'_{max} = \frac{2\mu_e\beta^2}{1-\beta^2}$ Mev.). Using the values $\delta = 4.0$ gm. per cm.^{3}, $\frac{Z'}{A} = 0.45$ for Ilford emulsions (3), one obtains the formula

$$n = \frac{27 \times 10^{-4} Z^2}{\beta^2}\left[\frac{1}{E'_{min}} - \frac{1-\beta^2}{1.02\beta^2}\right] \delta\text{-rays/100 microns.} \qquad (2)$$

The quantum mechanical treatment of $\chi(E, E')$ given by Bhabha (7) leads to a small correction term in the above formula for n. In the case of $E'_{min} = 10$ kev. this correction is not more than 3%, and it is ignored in the present study.

From Formula (2) above it is seen that the δ-ray density is dependent on the velocity βc of the primary particle and on the minimum energy E'_{min} chosen for the δ-rays. For comparison with experiment, the velocity may readily be related to the observed residual range of the particle by means of the experimental proton range–energy data (1, 5) for photographic emulsions. However, no satisfactory range–energy results for slow electrons are yet available for determining E'_{min}. Recent measurements by Ross and Zajac (6) with a β-ray spectrograph cover the electron energy region 30 to 100 kev., but, as will be seen in the following sections, the δ-ray energies concerned in this study lie below 30 kev. To overcome this difficulty, a method has been developed for relating the number of grains in a δ-ray track with the electron energy. This method makes use of grain-density measurements on protons and mesons, together with theoretical energy-loss calculations for charged particles in photographic emulsions.

Experimental Method

Illustrations of δ-rays are seen in the photomicrographs of Fig. 1. Fig. 1*a* shows a section of a proton track and its δ-rays at about 1000 microns from the end of the proton range. Some of the δ-rays are difficult to identify in the photograph, their ranges being only a few microns and Coulomb scattering very pronounced. Several δ-rays lie in the same direction as the proton track. Under the microscope one can follow each δ-ray by focusing on the individual grains, and in fact grain-counting is much more convenient and also more reliable than range measurements on these very short electron tracks. The long δ-rays shown in Figs. 1*b* and 1*c* were observed along the track of a long-range proton, at 5.4 and 3.4 mm. from the end of its range. Unfortunately, clear δ-rays of this type are very rare and so have little statistical significance in the study of the δ-ray density distribution. Fig. 1*d* shows a section of an α-particle track with its more numerous δ-rays. Here again range measurements on the recoil electrons are very difficult whereas grain-counting is more feasible.

From experience it has been found that an optimum criterion exists for counting δ-rays. This empirical criterion in the present Ilford G5 emulsions requires that the electron track contains four or more developed grains, assuming that one of the δ-ray grains lies inside the track of the primary particle. Under these conditions enough δ-rays are counted for satisfactory statistics, and at the same time the δ-rays are counted with good reproducibility after one has gained a reasonable amount of experience. Similar procedures for the selection of δ-rays have been used by other authors (2, 8).

FIG. 1. *Photomicrographs of delta-rays on charged particle tracks.*

Energy Determination of δ-rays

In order to relate a chosen minimum number of grains in a δ-ray with its corresponding energy E'_{min}, the energy-loss per developed grain has been

investigated. Fig. 2 shows the results of grain-density observations on the charged particles whose δ-rays were also studied. For regions of track containing more than 160 grains per 100 microns, the method of counting gaps rather than grains was used in these observations. Fig. 3 shows the grain-density results plotted versus E/M rather than residual range, and also the

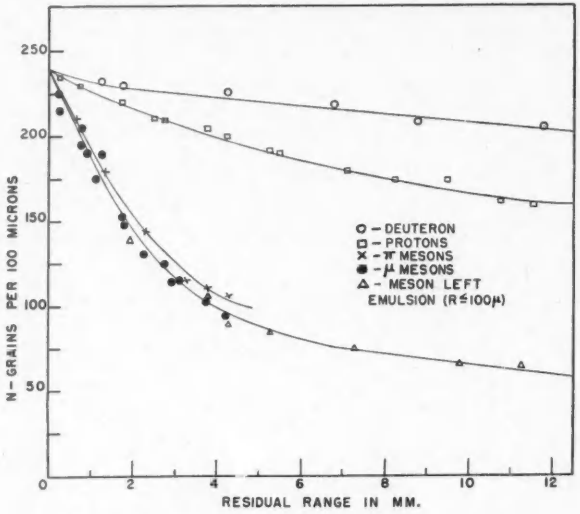

FIG. 2. *Grain-density observations on long range tracks.*

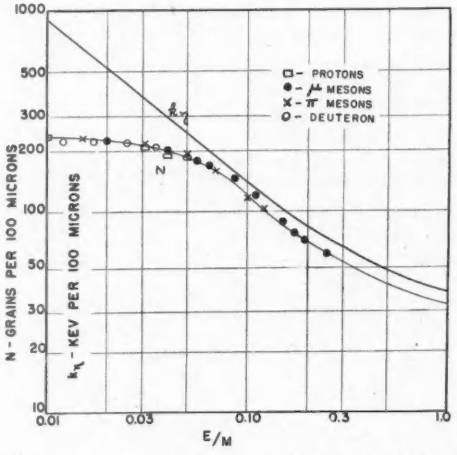

FIG. 3. *Grain-density and specific energy-loss for singly charged particles plotted versus E/M.*

specific energy-loss k_η calculated for the emulsion. It is seen that the experimental grain-densities for the various types of particles all follow the same variation with E/M, which suggests that the grain-density of an electron track will also follow this same variation with E/M. (The 12 mm. meson in Fig. 2 which left the emulsion just before the end of its range is included in Fig. 3 as a μ-meson.)

The specific energy-loss k_η shown in Fig. 3 is for energy transfers of less than 10 kev. obtained from the Bethe–Bloch formulas (7) and the composition of Ilford emulsions (3). Small energy transfers (k_η) have been considered rather than the total energy loss by ionization and collision $\left(\frac{dE}{dx}\right)$; the latter includes energy transfers to δ-rays whereas in the grain-counting results of Figs. 2 and 3 the δ-rays were ignored.

From the ratios of energy-loss and grain-density in Fig. 3 one may readily obtain the energy-loss per developed grain as a function of E/M and hence as a function of electron energy. By integrating over the electron energy one then obtains the total number of grains in the corresponding electron track. The results of this procedure for electrons with energies up to 30 kev. are shown in Table I.

TABLE I

PREDICTED RELATIONSHIP BETWEEN ELECTRON ENERGY AND TOTAL NUMBER OF GRAINS IN ELECTRON TRACK

E/M	Electron energy, kev.	k_η/N, kev. per grain	Number of grains in electron track
0.01	5	3.8	1
0.015	7.5	2.8	2
0.02	10	2.3	3
0.03	15	1.75	6
0.04	20	1.5	9
0.05	25	1.3	13
0.06	30	1.25	17

By interpolating the results of the last column in Table I we find that a δ-ray containing four developed grains is expected to require about 11 kev., and one containing 10 developed grains to require about 21 kev.

Beyond $E/M = 0.06$, the energy per developed grain remains constant at about 1.2 kev. per grain. The minimum calculated energy-loss is 38 kev. per 100 microns, which leads to an expected minimum in grain-density of 32 grains per 100 microns. It is interesting to note that the mean grain-density for 50 random "thin" tracks (assumed to be due to relativistic μ-mesons) in this batch of emulsions was found to be 33 grains per 100 microns, and for 15 electrons from μ-meson decay was found to be 37 grains per 100 microns. These latter would be expected to have rather more than minimum ionization.

Observations and Results

Fig. 4 shows the δ-ray densities for protons. The three smooth curves are those calculated for values of E'_{min} equal to 8, 10, and 12 kev. The theoretical densities have been converted from velocity to residual range dependance by means of the range-energy results of Lattes et. al. (5) and of Bradner et.al. (1). The block curve is that obtained experimentally as the mean of four protons of residual range not less than 5 mm., using the criterion that each δ-ray contains four or more developed grains. The experimental curve is seen to agree, both in absolute value and position of the peak, with an electron energy E'_{min} between 10 and 12 kev. Taking into account the normal statistical uncertainty

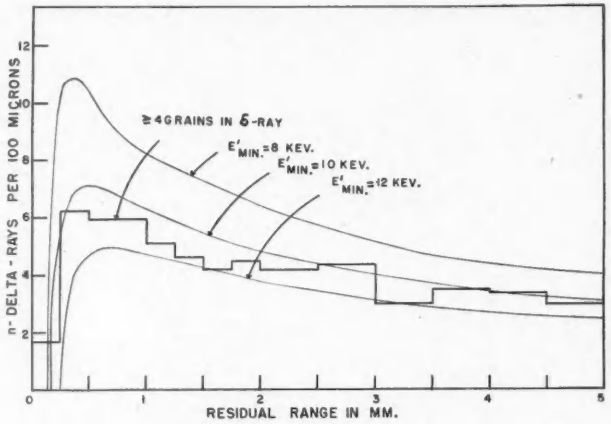

FIG. 4. *Delta-rays on protons.*

due to the finite numbers of δ-rays, and a comparable uncertainty found in reproducibility of observations, the experimental results are found to be consistent with $E'_{min} = 11 \pm 1$ kev.

The results for six μ-mesons (accompanied by decay electrons) of residual range not less than 2 mm. are shown as the block curve in Fig. 5. Here the experimental δ-ray densities indicate a value of E'_{min} between 11 and 7 kev. corresponding to four or more developed grains. Considering the uncertainties due to statistics and reproducibility of observations, the μ-meson δ-rays are found to be consistent with $E'_{min} = 9 \pm 1$ kev.

Delta-ray density measurements have been made on two long tracks of residual range 12 mm. and 1400 microns which were ejected from an interesting cosmic-ray star containing 32 prongs. These two tracks were both ejected in a backward direction with respect to the axis of a wide-angle shower containing eight charged relativistic particles.

Fig. 6 shows the observed δ-ray densities for the 12 mm. prong. This track was tentatively identified in Figs. 2 and 3 as that of a deuteron with initial energy about 85 Mev., although its identification as a 100 Mev. triton cannot be excluded on the basis of grain-counting. The three theoretical curves in

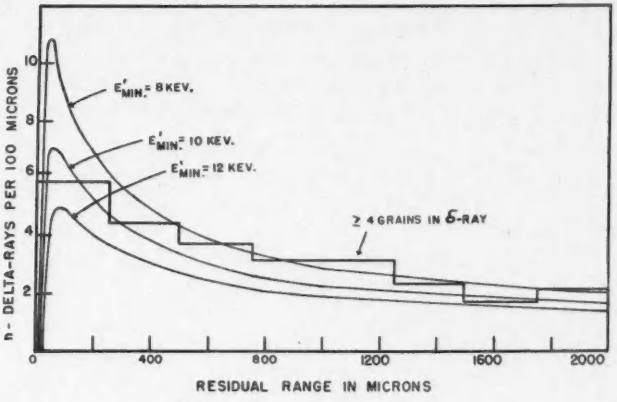

FIG. 5. *Delta-rays on μ-mesons.*

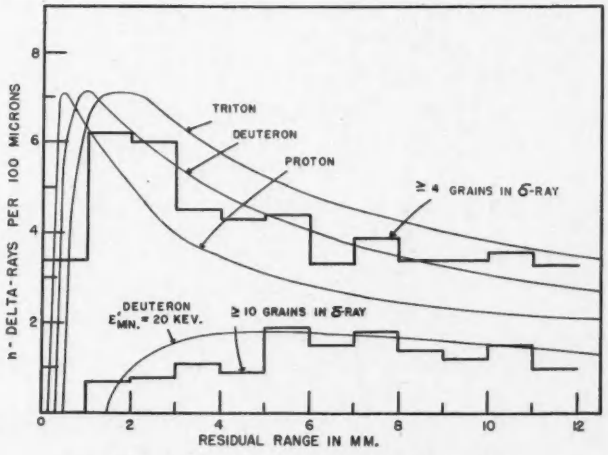

FIG. 6. *Delta-rays on a high energy deuteron.*

Fig. 6 are for a triton, deuteron, and proton based on $E'_{min} = 10$ kev., the mean energy found above for proton and μ-meson δ-rays. It is seen that the experimental curve for δ-rays having four or more developed grains on the 12 mm. track is in better agreement with the theoretical curve for a deuteron than with those for a triton or a proton. The maximum of the observed δ-ray

density curve in Fig. 6 occurs at a residual range beyond 1000 microns whereas the maximum for protons (Fig. 4) occurs near 500 microns.

The bottom curves in Fig. 6 show the observed densities for δ-rays having 10 or more developed grains on the 12 mm. track (block curve), and the theoretical curve for deuterons with $E'_{min} = 20$ kev. (smooth curve). These two curves seem to be in quite good agreement. The value $E'_{min} = 20$ kev. was chosen in computing the theoretical curve because the results of δ-ray energy determination in the preceding section indicated that an electron would require about 21 kev. to produce 10 developed grains in a δ-ray track.

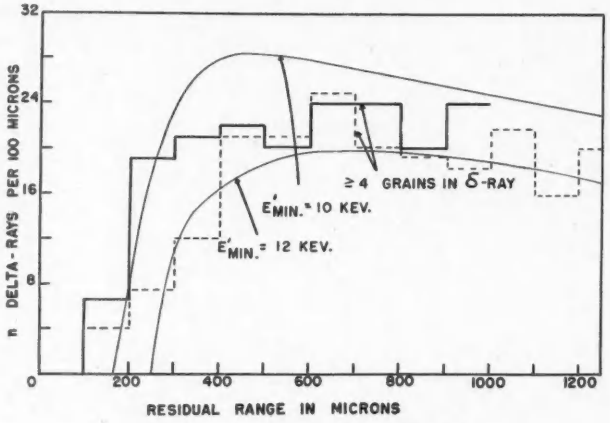

FIG. 7. *Delta-rays on alpha particles.*

The observed δ-ray densities for the 1400 micron track accompanying the 12 mm. deuteron are shown as the broken block curve in Fig. 7. The full block curve is that for a similar track found in an eight pronged star in another plate in the same batch of emulsions. These two tracks were both too dense for identification by grain-counting, indicating an atomic number greater than one. Comparison of the experimental curves in Fig. 7 with that for protons in Fig. 4 shows a ratio of nearly four in δ-ray densities for the same residual range. This is just the result to be expected from Formula (2) if the tracks were produced by α-particles. It will be seen by comparing the experimental curves for δ-rays having four or more developed grains with the theoretical curves for α-particles with E'_{min} equal to 10 kev. and 12 kev., also shown in Fig. 7, that there is agreement with $E'_{min} = 11 \pm 1$ kev.

No examples were found in the present batch of emulsions of tracks showing δ-ray densities sensibly higher than those shown in Fig. 7 for α-particles. These emulsions were flown in aircraft at an average altitude of 14,000 ft.

Discussion

In the section on energy determination of δ-rays, an electron energy of about 11 kev. was predicted for δ-rays having four developed grains. From the experimental results discussed in the preceding section it is seen that the numbers of δ-rays for all the particles studied are in agreement with theory if it is assumed that a δ-ray with four developed grains has an energy of 10 ± 2 kev. Similarly, the numbers of δ-rays having 10 or more developed grains is in agreement with theory (taking $E'_{min} = 20$ kev.) whilst the predicted energy for an electron track containing 10 grains was about 21 kev.

If we assume that the δ-ray energy determination method used here is valid then we may conclude that the theoretical formula for the production of δ-rays in photographic emulsions has been verified both in absolute value and in distribution. Thus, observations on the numbers of δ-rays and their distribution with residual range allows an absolute method for charged particle identification.

It is difficult to see how the validity of the method used here for determining δ-ray energies may be tested directly since the electron energies are so very low. For example, external electrons of 10 kev. energy would all be absorbed in the surface of the emulsion, and observations on grain counts or range under such conditions would be very poor. Although the grain counting method used here is considered to be reliable, a more direct test of the δ-ray theory may be made with higher energy electrons for which experimental range–energy data are available (6). This method would be feasible only for energetic heavy nuclei where the numbers of high energy δ-rays are much higher than is the case with the light particles available for the present study.

Acknowledgments

The author wishes to acknowledge the assistance and encouraging interest of Dr. E. Pickup during the course of this work; and to thank Mr. D. Rushton for making the photomicrographs of Fig. 1 and assistance in preparing the drawings. Grateful acknowledgement is made to Trans-Canada Airlines, who carried the emulsions on their transatlantic service.

References

1. Bradner, H., Bishop, A. S., and Barkas, W. H. Phys. Rev. 76: 587. 1949.
2. Bradt, H. L. and Peters, B. Phys. Rev. 74: 1828. 1948.
3. Feld, B. T. The photogenic mesons. Office Naval Research. Tech. Rept. No. 8. Mass. Inst. Technol. 1948.
4. Freier, P., Lofgren, E. J., Ney, E. P., and Oppenheimer, F. Phys. Rev. 74: 1818. 1948.
5. Lattes, C. M. G., Fowler, P. H., and Cuer, P. Proc. Phys. Soc. (London), 59: 883. 1947.
6. Ross, M. A. S. and Zajac, B. Nature, 162: 923. 1948.
7. Rossi, B. and Greisen, K. Rev. Modern Phys. 13: 240. 1941.
8. Sorensen, S. O. C. Phil. Mag. 40: 947. 1949.

ON THE ORIGIN OF TEN CENTIMETER RADIATION FROM THE POLAR AURORA[1]

By P. A. Forsyth[2], W. Petrie, and B. W. Currie

Abstract

Short-lived bursts of 10 cm. radiation from auroral displays have been received by radar equipment. The sources of continuous radiation from a partially ionized medium are briefly discussed. From a knowledge of the constants of the equipment used it is deduced that the power density at the receiver is at least 2×10^{-10} watts per (meter)^2, and it seems that the most likely source of this radiation is a plasma oscillation of the ionized volume associated with the auroral display. If this is so, the electron density in at least localized regions must be of the order 10^{11} per cm.^{3}

Introduction

A radar set operating at a frequency of 3000 Mc. has detected short pulses of radiation from auroral displays (6). The pulses arrive in a random manner, occuring in bursts lasting only a small fraction of a second, and are more numerous with bright displays exhibiting a definite ray structure. In view of this result it is of interest to consider the mechanisms responsible for the emission of long wave length radiation from the polar and nonpolar auroras. The following discussion is concerned with the emission of radiation at a frequency of 3000 Mc. (wave length of 10 cm.). However, the calculations can readily be modified to give the emission at other wave lengths. The emission of long wave length radiation from a partially ionized medium may result from a number of processes which we will discuss in turn.

1. Atomic and Molecular Transitions

Transitions between atomic levels and also between molecular levels produce radiation in the ultraviolet, visible, and infrared regions of the spectrum, but little or no radiation in the radio spectrum. The atoms and molecules in the earth's upper atmosphere are excited to only the lower energy levels, and transitions between these levels do not produce radiation in the wave length region in which we are interested.

2. Capture Processes

(*a*) *Electron Captures by Protons*

We have no definite information regarding the number of protons in the earth's upper atmosphere, although cosmic ray studies indicate that these particles do exist at high altitudes. A study (21) of the intensities of the Balmer lines in the auroral spectrum indicates that the capture process is not the pri-

[1] *Manuscript received October 31, 1949.*
Contribution from the Department of Physics, University of Saskatchewan, Saskatoon, Sask.
[2] *Working on a Defence Research Board grant.*

mary mechanism responsible for the production of radiation from hydrogen atoms. However, although the capture of an electron by a proton is probably an unimportant process in the upper atmosphere, the results of this capture process can be predicted quite accurately, and give us information on similar processes involving atomic and molecular ions which certainly exist in large numbers.

A number of investigations (20) indicate that the excitation temperature during an auroral display is of the order of 5000° K. The number of ions present during an auroral display is unknown, whereas the number present in the normal night sky is reasonably well determined in the E and F layers. Hence we will consider the processes which might produce long wave length radiation from the nonpolar aurora, and attempt to estimate the differences which occur during an auroral display. It should be realized that the electron temperature of the free electrons in the ionosphere is probably much less than the excitation temperature which exists during an auroral display.

Table I lists certain ionospheric data given by Grimminger (10), and Bates and Massey (2).

TABLE I

Height, km.	Temperature, Kelvin	No. particles/cm.^{3}	No. electrons/cm.^{3}
100	500	8.5×10^{13}	1×10^{4}
200	1000	1.4×10^{11}	2.5×10^{5}
300	2000	5.5×10^{9}	2.5×10^{5}
400	2000	4.7×10^{8}	1×10^{5}
500	2000	1.6×10^{8}	1×10^{5}
600	2000	6.5×10^{7}	1×10^{5}
700	2000	3.4×10^{7}	1×10^{5}

The values of temperature and electron density above 300 km. are not given by the above mentioned authors but are assumed values. The mean kinetic energy of an electron at temperatures of 500°, 1000°, 2000° K. may be found from the classical relation $1/2\ mv^2 = 3/2\ kT$. The mean kinetic energy values are 10.4×10^{-14}, 2.1×10^{-13}, 4.1×10^{-13} erg. Electrons with these energy values, when captured on the level $n = \infty$ of the hydrogen atom will emit radiation of wave lengths 191,000, 94,500, 48,400 Å. However, a number of the electrons will have less kinetic energy than the mean values, and our problem is to calculate what fraction of the electrons have velocities such that when captured on the level $n = \infty$, radiation of wave length 10^9 Å is emitted. The velocity of a free electron, which when captured on the level $n = \infty$ radiates at $\lambda = 10^9$ Å, is 2.09×10^5 cm. per sec. If we assume that the free electrons are in thermal equilibrium, then the fraction of electrons having a velocity between v and $(v + dv)$ is given by the Maxwell law,

$$f(v) = 4\pi\left(\frac{m}{2\pi kT}\right)^{3/2} v^2 e^{-\frac{mv^2}{2kT}}.$$

Substituting $v = 2.09 \times 10^5$ cm. per sec. and the three temperature values, we find that $f(v) \sim 5 \times 10^{-11}$, 1.9×10^{-11}, 0.66×10^{-11}. Hence, very few electrons will emit radiation at $\lambda = 10^9$ Å if the captures occur on level $n = \infty$. The energy radiated by an electron of velocity 2.09×10^5 cm. per sec. when captured on the level $n = \infty$ is 19.6×10^{-18} erg. Hence, the energy radiated per cubic centimeter per second at a wave length of 10^9 Å due to electron captures on the level $n = \infty$ will be the product of the figure given above for the energy release per capture, and the number of captures per cubic centimeter per second on the level $n = \infty$ of electrons with velocities of 2×10^5 cm. per sec. Actually very few captures will take place on the higher levels of the atom at the temperatures we are considering. The number of captures per cubic centimeter per second per unit velocity range may be expressed as $N_i N_e f(v) v \sigma$, where N_i is the number of ions per cubic centimeter, N_e the number of electrons per cubic centimeter, $f(v)$ the Maxwell velocity distribution law, v the velocity of the free electron before capture, and σ the target area of the ion for capture of the electron. If we substitute the value of σ as given by Menzel and Pekeris (18), the values of $f(v)$ and v which are approximately 10^{-11} and 2×10^5 cm. per sec. respectively, and assume the product $N_i N_e$ is 10^{10}, it is apparent that the number of captures on the higher levels is very small. For instance, the number of captures per cubic centimeter per second of electrons with velocities 2×10^5 cm. per sec. on the level n equals 1000, is around 10^{-15}. Hence the radiation emitted per cubic centimeter per second at 10^9 Å due to this capture process will be of the order of 10^{-32} erg or less.

(b) Electron Captures by Atomic and Molecular Ions

The positive ions which we might expect to find in the upper atmosphere in any abundance are O^+, O_2^+, N^+, N_2^+. Although the results of the capture process for these ions cannot be predicted accurately as for the case of hydrogen, captures on the high levels of these ions will still be very few, and the radiation emitted per cubic centimeter per second at a wave length of 10^9Å will probably be comparable to the value given for the hydrogen problem.

(c) Electron Captures by Neutral Hydrogen and Oxygen Atoms

The properties of the H^- ion have been carefully investigated by Chandrasekhar and Breen (3), and of the O^- ion by Bates and Massey (1). The electron affinity of H^- is around 0.7 ev. and that of O^- around 3 ev. Hence the capture of an electron by a neutral hydrogen or oxygen atom produces a continuous spectrum at much shorter wave lengths than the region in which we are interested. Bates and Massey (1) also discuss the properties of the O_2^- ion. The energy radiated when a very slow electron attaches itself to an O_2 molecule is of the order of 0.1 ev.; this energy is at shorter wave lengths than the region in which we are interested.

3. The Cascade Process After Capture

After capture, an electron cascades to lower levels and certain transitions may produce radiation in the radio spectrum. We will consider the cascade process for hydrogen and use the Bohr expression to calculate what n-values must be involved in order to give radiation at $\lambda = 10^9$Å ($\tilde{\nu} = 0.1$ cm.$^{-1}$) i.e., use $\tilde{\nu} = \frac{R}{n_1^2} - \frac{R}{n_2^2}$, and find that $n_1 = 121$, $n_2 = 120$, gives $\tilde{\nu} \sim 0.1$ cm.$^{-1}$. Transitions between other levels of large n number will also produce radiation of wave length 10^9Å. But we have pointed out that very few captures take place on a high level such as $n_1 = 121$, and then only a fraction of these electrons drop to the next lowest level $n_2 = 120$. We may calculate the number of captures on the level $n_1 = 121$, and the number of downward transitions to the level $n_2 = 120$ from the work of Menzel (17). The calculations indicate that the radiation emitted from this cascade process is negligible compared with other radiation sources which will be discussed later. We cannot make similar calculations of the cascade process for other particles, but it seems safe to say that the same arguments apply to these particles.

4. Free–Free Emission Processes

(a) *Electrons and positive ions*

Using the classical orbit theory we may consider a free electron approaching a nucleus as moving in a hyperbolic orbit, just as a bound electron moves in an elliptical orbit. A free electron may undergo a free–free transition in the field of the nucleus, and either absorb or emit energy. Free–free transitions produce continuous spectra.

This problem was first investigated quantitatively by Kramers (14) in connection with the continuous X-ray spectrum. Applying the Bohr correspondence principle, he derived an expression giving the energy radiated as the result of a transition between a free electron and a positive ion. The emission in ergs per cubic centimeter per second in the frequency range ν to $(\nu + d\nu)$ is

$$I = N_i N_e \frac{32\pi^2}{3\sqrt{3}} \frac{Z^2 e^6}{c^3 m^2} \frac{d\nu}{v},$$

where N_i = the number of ions per cubic centimeter,
N_e = the number of electrons per cubic centimeter,
Ze = the effective charge of the ion,
v = the mean velocity of the free electrons.

Eddington (5) has used this expression to calculate the emission of energy from interstellar space. Gaunt (8) has given a correction to the simple Kramer formula. Reber (24) has used the corrected expression to calculate the emission from interstellar space. We will first apply the familiar Kramer equation to compute the emission from the nonpolar aurora, and then show that a more

accurate expression yields comparable results. The positive ion density in the night sky is unknown but is not likely to be much different from the electron density. Assume the product N_iN_e in the E and F layers is 10^8 and 6.25×10^{10} respectively. Substitute these figures and temperature values of 500°, 1000°, 2000° K., and $v = \left(\frac{3kT}{m}\right)^{1/2}$. The value of I at various heights is given in Table II.

TABLE II

Height, km.	I, ergs cm.$^{-3}$ sec.$^{-1}$
100	2×10^{-30}
200	1×10^{-27}
300	7×10^{-28}
400	1×10^{-28}
500	1×10^{-28}
600	1×10^{-28}
700	1×10^{-28}

Menzel (17) has given more accurate expressions for the free–free emission based on quantum mechanics. The emission per cubic centimeter per second from a free electron moving in the field of a proton is ~

$$\frac{N_iN_ekK}{2RT^{1/2}} e^{-h\nu/kT} d\nu.$$

R is the Rydberg constant in terms of the frequency, and K a numerical constant. The frequency equivalent to $\lambda = 10$ cm. is $\nu = 3 \times 10^9$. Substitute as before $N_iN_e = 10^8$, and 6.25×10^{10}, and temperature values of 500°, 1000°, 2000° K. The values of I are given in Table III.

TABLE III

Height, km.	I, ergs cm.$^{-3}$ sec.$^{-1}$
100	3×10^{-31}
200	1.3×10^{-28}
300	9×10^{-29}
400	1×10^{-29}
500	1×10^{-29}
600	1×10^{-29}
700	1×10^{-29}

The results are close to the values obtained from the Kramer equation.

(*b*) *Electrons and atoms*

The free–free emission from an electron in the field of a neutral atom has been studied theoretically by Nedelsky (19). The radiation emitted per cubic centimeter per second from one electron encountering one atom is

$$\frac{4e^2}{3c^3} f(n)\ Va^2 \left(1 - \frac{\nu}{\nu_0}\right)^{\frac{1}{2}} \left(2 - \frac{\nu}{\nu_0}\right) \nu,$$

where $1/2\ mv^2 = 3/2\ kT = h\nu_0$, and $f(n)$ is a function of the parameters of the atomic model. This equation applies to slow electrons and may be used when

$Va^2 < 1$, where V is the energy of the incident electron in electron volts and a the radius of the screening electron shell in angstroms. a is of the order of 1Å for the case we are considering. For temperature values of 500°, 1000°, 2000° K., $Va^2 = 0.06, 0.13, 0.26$. The mean electron velocities at the above temperature values are 1.5×10^7, 2.1×10^7, 3.0×10^7 cm. per sec. Nedelsky gives values for $f(n)$ and we use the value $f(n) = 7$. If we substitute in the equation the total number of particles and electrons at the various heights, the I values are as given in Table IV.

TABLE IV

Height, km.	I, ergs cm.$^{-3}$ sec.$^{-1}$
100	1.3×10^{-25}
200	1.6×10^{-26}
300	1.8×10^{-27}
400	6.2×10^{-29}
500	2.1×10^{-29}
600	8.5×10^{-30}
700	4.5×10^{-30}

A more accurate expression for the free–free emission from an electron in the field of a neutral hydrogen atom has been given by Chandrasekhar and Breen (3). These authors have computed free–free absorption cross sections, and their values may be converted to emission transition probabilities through the use of the general relationships between emission and absorption. For discrete transitions the relations between emission and absorption are given by the well known Einstein A and B values. The relations in the case of free–free transitions have been given by Cillié (4). Chandrasekhar and Breen have pointed out that the earlier calculations of the free–free emission or absorption are inadequate, since these calculations are based on the Born approximation which does not accurately describe the motion of an electron in the field of an atom. Using the results of Chandrasekhar and Breen, and the relations between absorption and emission as given by Cillié, we find that the free–free emission values are about 10 times the values given in Table IV.

The total radiation due to free–free transitions received from the nonpolar aurora, will include radiation which originates at different heights. The element of volume of a sphere is $r^2 dr d\theta d\phi$. If we consider the radiation from a volume the surface of which subtends unit solid angle at the receiver, then $dV = r^2 dr$. The intensity of the radiation received is $\frac{Ir^2 dr d\nu}{4\pi r^2} = \frac{I dr d\nu}{4\pi}$ ergs per sec. per cm.^{2} per unit solid angle. From the previous discussion, it appears that the mechanism of free–free emission gives the greatest radiation energy at a wave length of 10^9Å. Hence if we use the results obtained from the Chandrasekhar equation, the value of the radiation intensity received from the night sky is $6.6 \times 10^{-19}\, d\nu$ ergs per sec. per cm.^{2} per unit solid angle. This is the radiation received from the E and F layers. The radiation received from the atmosphere above the F_2 layer is small compared with this figure.

These formulas for the free–free emission apply to a mixture of electrons and one type of atom or ion, and the results must be modified when we are dealing with a mixture of gases such as are present in the earth's upper atmosphere. In order to solve the problem exactly it is necessary to know the probabilities of all the possible reactions between the electrons and the ions, atoms, and molecules of the upper atmosphere. It is likely that the figures given represent the maximum free–free emission from the upper atmosphere, and the radiation from this process may actually be much less.

5. Thermal Emission

It is difficult to estimate the intensity of thermal emission from the night sky since the upper atmosphere does not radiate as a black body. The radiation density in an isothermal enclosure at long wave lengths in a wave-length interval $d\lambda$ is given by the Rayleigh–Jeans law, $\psi_\lambda d\lambda = 8\pi kT\lambda^{-4}d\lambda$. Since the total radiation per cubic centimeter is aT^4, the fraction of the total radiation at wave length $\lambda = \dfrac{8\pi kT\lambda^{-4}d\lambda}{aT^4} = 0.45\lambda^{-4}T^{-3}d\lambda$. The emission per square centimeter per second from the surface of a black body at wave length $\lambda = 0.45\sigma\lambda^{-4}Td\lambda$. The surface area of the emitting surface if it subtends unit solid angle at the receiver $= r^2$. Then the radiation per second at wave length λ from this surface received by 1 cm.^{2} of the receiver $= \dfrac{0.45\sigma\lambda^{-4}Td\lambda r^2}{4\pi r^2} = 0.204 \times 10^{-5}\lambda^{-4}Td\lambda$. In terms of frequency this expression is $6.8 \times 10^{-19}Td\nu$. Although it is difficult to estimate the value of T which should appear in the equation for thermal noise, it appears that the free–free emission and thermal noise are comparable in intensity.

Comparison of the Calculated Emission and Sensitivity of the Radar Receiver

The present investigation with radar equipment has shown that the intensity of radiation of wave length 10 cm. increases during an auroral display, and this increase is almost certainly due to the fact that the ionization density is greater in the region of the aurora. The radiation is received in bursts lasting only a small fraction of a second, and the intensity of the radiation depends upon the brightness of the aurora. A similar relationship exists between the appearance of a solar flare and an increase in the solar noise.

A simple calculation will show that the intensity of 10 cm. auroral radiation must be considerably greater than the figure given for the energy due to free–free transitions, if this radiation is to be recorded by the radar equipment presently in use. If we use the value already calculated for the free–free emission, i.e., $6.6. \times 10^{-19}\,d\nu$ ergs per sec. per cm.^{2} per unit solid angle, take the band width, cross-sectional area, and solid angle accepted by the radar receiver as $1.2. \times 10^6$ c.p.s., 10^4 cm.^{2}, and 10^{-2} steradians respectively, then the power received by the equipment is, $6.6. \times 10^{-19} \times 1.2 \times 10^6 \times 10^4 \times 10^{-2} \times 10^{-7} =$

8×10^{-18} watts. The sensitivity of the radar receiver was estimated by observing the echo received from a distant target of known range and dimensions. From the amplitude of the observed echo and the known constants of the transmitter, the detectable power density was calculated to be 2×10^{-10} watts per (meter)^2. Since the value for the target gain used in this calculation was unity, it is certain that the resulting power density represents a minimum value. The actual detectable power density is probably somewhat greater than this value. Hence, if the radiation is the result of free–free transitions, the ion density during an auroral display must be increased by a factor of 2.5×10^7 over the normal night sky values, at least in localized regions. This calculation neglects any changes in the emission due to temperature changes during an auroral display; temperature changes are of secondary importance as far as this problem is concerned. If the above figures are correct and the radiation is the result of free–free transitions, the ion density in localized regions during an auroral display must be of the order of 10^{12} per cubic centimeter. It has been suggested that the value which we used for the electron density in the *F* layer is too low. However, even if a higher density of 2×10^6 per cm.^{3} is used, the conclusions which we have reached are unchanged.

Discussion of Ion Density During an Auroral Display

Little is known regarding the ion density during an auroral display. The interpretation of the few radar studies of the aurora is not entirely clear (12, 15). Since there is evidence that during at least certain auroral displays protons or hydrogen atoms enter the earth's atmosphere, it is worthwhile showing that a diffuse stream of such particles may produce a large number of ions in the upper atmosphere.

The excitation and ionization effects of particles passing through air have been summarized in an article by Francis and Jenkins (7). Positive ion collisions have been investigated theoretically by Massey and Smith (16). The cross section for excitation and ionization of N_2 by proton collisions has been measured by Ramsauer, Kollath, and Lilienthal (23). Their results indicate that the cross section for a 10,000 ev. proton is of the order of three times the gas kinetic cross section. The gas kinetic cross section of N_2 is around 11.3×10^{-16} cm.^{2} (13, chap. 14). Hence the excitation and ionization cross section of N_2 is 34×10^{-16} cm.^{2}. If we assume that the cross section of all atmospheric particles is of the same order, the number of excitations and ionizations at the 100 km. level as a proton travels 1 cm. is $34 \times 10^{-16} \times 8.5 \times 10^{13} = 0.3$.

The ionizing power of protons in air at 1 mm. pressure has been measured by Gerthsen (9). Some of his results are given in Table V.

TABLE V

Proton energy, ev.	No. of ion pairs/cm.
19,000	19
26,000	23
35,000	26

The above figures indicate that a 10,000 ev. proton produces around 13 ion pairs per cm. Now the number of atoms per cubic centimeter at 1 mm. pressure and 0°C. = 3.56×10^{16}. Hence the number of ions per centimeter produced at different heights is given in Table VI.

TABLE VI

Height, km.	No. ions/cm.
100	0.03
200	0.5×10^{-4}
300	0.2×10^{-5}

The previous calculation indicated 0.3 excitations and ionizations per centimeter are produced in the *E* layer. If these figures are reasonably accurate it means that the majority of collisions produce excitation rather than ionization. Since the energy loss per ionization is 36 e.u. and the ionization potential of N_2 is 15.6 e.u., the energy of an electron freed from N_2 is around 20 e.u. This electron may itself produce one ionization per centimeter. Hence the total number of ions produced by incoming protons is given in Table VII.

TABLE VII

Height, km.	No. ions/cm.
100	0.06
200	10^{-4}
300	0.4×10^{-5}

These calculations are admittedly approximate but will suffice to illustrate the point we wish to make, that a low density stream of protons will produce a large number of ions in the upper atmosphere.

We have no information on the density of the solar material which reaches the earth's atmosphere. However, we may estimate what may be the density of a proton stream which will produce any given ion density per second in the earth's atmosphere. The equation relating these quantities is $n_1 v \times 0.06 = n_2$, where n_1 is the density of the incident stream, v the velocity of the incident stream, and n_2 the number of ions formed per cubic centimeter per second in the atmosphere. If v is the velocity of a 10,000 ev. proton, and n_2 is 10^{12}, then n_1 is 1.2×10^5.

This calculation indicates that the solar stream need not be very dense in order to produce a large number of ions in the upper atmosphere. Since the proton stream causes excitation as well as ionization, it is likely that a part of the radiation from excited molecules will be in the ultraviolet region of the spectrum and produce some secondary ionization.

Radiation from a Plasma Oscillation

The short duration of the bursts of radiation suggests that the electron density decreases rapidly after the passage of the ionizing particles, and that these particles arrive in discrete bundles.

The rate of expansion of a cloud of electrons is readily determined. A simple calculation indicates that if the initial electron density of the cloud is 10^{12}, the radius of the surface of the cloud expands by a very large factor in 1 μ sec. The presence of positive ions will certainly modify the expansion process, but since the electrons produced by ionization will have high velocities relative to the positive ions, the electron density may decrease rapidly owing to the diffusion of these particles through the ionized volume. It seems likely that conditions in the ionized volume are such that this volume may execute a plasma oscillation, the energy being derived from the stream of particles passing through the ionized region.

Whether or not the short duration of the bursts of radiation is due to a decrease in the electron density, and to the fact that the ionizing particles arrive in discrete bundles, we can estimate the energy radiated from a plasma oscillation by using the expression for the radiation from the classical oscillator. The theory of plasma oscillations was first investigated by Tonks and Langmuir (25). The frequency of oscillation of an electron plasma is given as $\sqrt{\frac{e^2n}{\pi m}}$, where e and m are the charge and mass of the electron, and n the electron density. If we consider that the electrons in the upper atmosphere are forced into oscillation by a proton stream, the electron density must be 1.1×10^{11} per cm.^{3} in order that the plasma oscillate with a frequency of 3×10^9.

The rate of radiation from the classical oscillator $\frac{dw}{dt}$ is $\frac{16\pi^4\nu^4q^2A^2}{3c^3}$, where q is the charge on the oscillator and A the amplitude of the oscillation. If the electron density is 1.1×10^{11} per cm.^{3}, the power radiated is $3.9 \times 10^{-6}A^2$ watts. The power collected by the receiver from a radiating volume of 1 cm.^{3} at a height of 100 km. is $\frac{3.9 \times 10^{-6} \times 10^4A^2}{4\pi \times 10^{14}} = 3.1 \times 10^{-17}A^2$ watts. A rough estimate of the amplitude of the oscillation may be obtained as follows. The electrons produced by ionization have velocities equivalent to an energy of 20 ev., i.e. 2.6×10^8 cm. per sec. If the frequency is 3×10^9 the amplitude of the oscillation will be of the order of 0.02 cm. The mean free path of a particle at the height of 100 km. is much greater than this figure, being of the order of 3 cm. Hence the power collected by the receiver will be 1.2×10^{-20} watts per cm.^{3}. Since the power must be at least 2×10^{-10} watts to be detected by the receiver, the radiating volume will have a minimum value of 10^{10} cm.^{3}. It is well to note that this is a small volume, and a much larger figure would be necessary if the same amount of power were produced as a result of free–free transitions. The oscillation of the plasma will be damped by radiation and collisions, but these

effects are small for the case we are considering. The radiation emitted during one oscillation is $\frac{16\pi^4\nu^3q^2A^2}{3c^3}$, while the total energy associated with the oscillation is $2\pi^2m\nu^2A^2$. The ratio of these factors is $\frac{8\pi^2\nu q^2}{3mc^3}$ and has the value 7.4×10^{-13}. Hence the radiation loss per cycle is small. The collisional frequency at a height of 100 km. may be as high as 2.5×10^7 if the electron density has the large value which we suggest, but this means that collisional effects are not too important when oscillations of frequency 3×10^9 are considered. This lack of appreciable damping favors the diffusion of the electrons through the ionized volume, and the consequent reduction in electron density. Collisional damping will have more effect on the emission of longer wave length radiation.

Concluding Remarks

This discussion of the likely sources of long wave length radiation from the polar and nonpolar auroras has suggested that the emission of radiation of wave length 10 cm. from the polar aurora is a result of an ionized volume executing a short-lived plasma oscillation. It does not seem that other sources of radiation of this wave length, such as free–free transitions between electrons and ions or neutron particles, can supply sufficient energy to be detected by the equipment which has been in use. The ideas presented in this summary should be examined more carefully when further data have been accumulated on the intensity of the radiation at various wave lengths. It would, perhaps, be instructive to examine the radiation for possible polarization effects. The ideas presented by Pierce (22), Haeff (11), and others should be investigated for possible application to the auroral problem.

Acknowledgment

This investigation has been supported by a grant from the Defence Research Board of Canada.

References

1. Bates, D. R. and Massey, H. S. W. Trans. Roy. Soc. (London), A, 239: 269. 1943.
2. Bates, D. R. and Massey, H. S. W. Proc. Roy. Soc. (London), A, 187: 261. 1946.
3. Chandrasekhar, S. and Breen, F. H. Astrophys. J. 104: 430. 1946.
4. Cillié, G. Monthly Notices Roy. Astron. Soc. 92: 820. 1932.
5. Eddington, A. S. Proc. Roy. Soc. (London), A, 111: 424. 1926.
6. Forsyth, P. A., Petrie, W., and Currie, B. W. Unpublished; to appear in a forthcoming issue of Nature.
7. Francis, V. J. and Jenkins, H. G. Reports on Progress in Physics, 7: 230. 1940.
8. Gaunt, H. Trans. Roy. Soc. (London), A, 229: 163. 1930.
9. Gerthsen, C. Ann. Physik, 5: 657. 1930.
10. Grimminger, G. Analysis of temperature pressure and density of the atmosphere extending to extreme altitudes. Rand Corporation, Santa Monica, California. 1948.
11. Haeff, A. V. Phys. Rev. 75: 1546. 1949.
12. Herlofson, N. Nature, 160: 867. 1947.
13. Jeans, J. H. The dynamical theory of gases, 4th ed. Cambridge University Press. 1925.
14. Kramers, H. A. Phil. Mag. 46: 836. 1923.
15. Lovell, A. C. B., Clegg, J. A., and Ellyett, C. D. Nature, 160: 372. 1947.
16. Massey, H. S. W. and Smith, R. A. Proc. Roy. Soc. (London), A, 142: 142. 1933.

17. MENZEL, D. H. Astrophys. J. 85: 330. 1937.
18. MENZEL, D. H. and PEKERIS, C. L. Monthly Notices Roy. Astron. Soc. 96: 77. 1935.
19. NEDELSKY, L. Phys. Rev. 42: 641. 1932.
20. PETRIE, W. Can. J. Research, A, 25: 293. 1947.
21. PETRIE, W. Can. J. Research, A, 26: 359. 1948.
22. PIERCE, J. R. Physics Today, 2(2): 20. 1949.
23. RAMSAUER, C., KOLLATH, R., and LILIENTHAL, D. Ann. Physik, 8: 709. 1931.
24. REBER, G. Proc. I.R.E. 28: 68. 1940.
25. TONKS, L. and LANGMUIR, I. Phys. Rev. 33: 195. 1929.

THE ANGULAR MOMENTUM OF THE ELECTRON IN CLASSICAL ELECTRODYNAMICS[1]

By F. A. Kaempffer

Abstract

It is shown that not only the rest-mass of the electron but its spin as well is carried by the surrounding electromagnetic field. The ratio of magnetic moment and angular momentum (g-factor) of the electron is determined. The law of conservation of angular momentum is checked.

It is a general belief that the angular momentum or "spin" of the electron cannot be properly described in terms of the classical theory. The use of the word "spin" indicates that one has in mind a rotating body of finite mass, whose angular momentum can be written down in terms of classical mechanics. In fact, the physicists of 1900 generally adopted the idea of H. A. Lorentz that the electron can be described as a sphere of mass m and surface charge e, having a radius $r_0 = \frac{e^2}{2mc^2}$, which is defined by the assumption that the rest-mass m of the electron is represented by the rest-energy of the surrounding electric field $\vec{E} = \frac{e}{r^3}\vec{r}$ according to the equation*

$$\frac{1}{8\pi}\int_{r_0}^{\infty} E^2 dV = mc^2. \tag{1}$$

If one tries to take into account the spin $\frac{1}{2}\frac{h}{2\pi}$ of the electron by assuming that the sphere rotates with a certain angular velocity ω, so that

$$\frac{2}{5} mr_0^2 \omega = \frac{1}{2}\frac{h}{2\pi}, \tag{2}$$

one is confronted immediately with the paradoxical consequence that the outer parts of the electron have to rotate with a velocity

$$v_{\max} = r_0\omega \approx \frac{h}{2\pi m r_0} \approx \frac{hc}{2\pi e^2} c \approx 137c \tag{3}$$

far beyond the velocity of light.

[1] *Manuscript received in original form August 26, 1949, and, as revised, November 4, 1949. Contribution from the Department of Physics, University of British Columbia, Vancouver, British Columbia.*

* *Actually one has to take into account the stress-energy which is required to hold the surface charge e together. This gives an additional factor 4/3 for the total rest-energy of the electron (see R. Becker, Elektronentheorie, Leipzig 1933, p. 353), and its radius becomes*

$$r_0 = \frac{2}{3}\frac{e^2}{mc^2}. \tag{I}$$

A more convenient way of deriving this value is to calculate the total energy of the magnetic field created by a slowly moving electron and by equating this energy to the kinetic energy of the electron, which leads to the same value (I).

It is, however, possible to take into account the angular momentum of the electron without assuming any rotational motion of the sphere. This can be done by providing the above-mentioned model with a magnetic dipole, which is located in its center and which has just the right magnetic moment $|\vec{\mu}| = \frac{eh}{4\pi mc}$ required by experimental evidence (Stern–Gerlach experiment), so that one has besides the electric field $\vec{E}$ a magnetic field $\vec{H} = 3\,(\vec{r}\vec{\mu})\,\frac{\vec{r}}{r^5} - \frac{\vec{\mu}}{r^3}$. According to classical electrodynamics this electromagnetic field carries an angular momentum

$$\vec{\Theta} = \frac{1}{4\pi c}\int_{r_0}^{\infty}[\vec{r} \times [\vec{E} \times \vec{H}]]\,dV = -\frac{1}{4\pi c}\int_{r_0}^{\infty}\frac{e}{r^6}[\vec{r} \times [\vec{r} \times \vec{\mu}]]\,dV. \quad (4)$$

If the z-axis of the co-ordinate system is put into the direction of the magnetic dipole $\vec{\mu}$, one easily calculates

$$\Theta_x = 0;\ \Theta_y = 0;\ \Theta_z = \frac{1}{4\pi c}\int_{r_0}^{\infty}\int_0^{\pi}\int_0^{2\pi}\frac{e\mu}{r^4}(1 - \cos^2\theta)\,r^2 dr \sin\theta d\theta d\phi = \frac{2e\mu}{3cr_0}. \quad (5)$$

By using the exact value (I) for r_0 one obtains the equation

$$|\vec{\mu}| = \frac{e}{mc}|\vec{\Theta}| \quad (6)$$

which shows that the model under consideration has just the right g-factor required by experiment for the electron. In other words, if one puts into (6) the experimental value $\frac{eh}{4\pi mc}$ for the magnetic moment, one gets with

$$|\vec{\Theta}| = \frac{1}{2}\frac{h}{2\pi} \quad (7)$$

just the right value for the angular momentum of the electron.

The above equation implies the statement that every dipole surrounded by an electric charge carries an angular momentum. In order to show that this is not in contradiction with the law of conservation of angular momentum, we consider a charge-element $q = \frac{e}{4\pi r^2}$, which is carried along the radius-vector $\vec{r}$ from infinity to r_0 through the magnetic field of the dipole. By moving q with the velocity $\vec{v}$ through $\vec{H}$ one has to act against the Lorentz force $\vec{K} = \frac{q}{c}[\vec{v} \times \vec{H}]$, so that at arrival at r_0 one has imposed on q the momentum

$$\vec{P} = \int_{\infty}^{r_0}\vec{K}dt = \int_{\infty}^{r_0}\frac{q}{c}\left[\frac{d\vec{r}}{dt} \times \vec{H}\right]dt = -\int_{\infty}^{r_0}\frac{q}{cr}[\vec{r} \times \vec{H}]\,dr = -\int_{r_0}^{\infty}\frac{q}{cr^4}[\vec{r} \times \vec{\mu}]\,dr. \quad (8)$$

In other words: In order to bring a charge-element q from infinity to a distance r_0 towards a magnetic dipole of moment $\vec{\mu}$ one has to put into the system an angular momentum

$$\vec{\Theta}_q = -\int_{r_0}^{\infty} \frac{q}{cr^4}[\vec{r} \times [\vec{r} \times \vec{\mu}]]\, dr. \tag{9}$$

Introduction of $q = \dfrac{e}{4\pi r^2}$ and integration over all angles θ and ϕ leads then immediately to Equation (4), q.e.d.

Thus the model has the advantage that all mechanical properties of the electron, including the spin, are represented by its surrounding electromagnetic field. It seems to have, however, on first sight the drawback that one departs from Ampère's idea that all magnetism in matter is caused by electric circuits and that, if one finds a magnetic dipole in nature, one can always find a circuit, which is the "real" cause of it. Of course if one drops the idea that velocities beyond c are impossible, one can easily show that the rotating model leads to the right magnetic moment, if the surface charge is considered as the circuit which causes the magnetic moment according to Biot–Savart's well known formula. In view of the importance of the general principles of relativity theory it seems, however, an advantage to drop the idea of Ampère and to postulate the existence of magnetic dipoles (which procedure is in fact not essentially different from the procedure by which the word "electric charge" is defined) and so to avoid contradiction with first principles of relativity theory.

Acknowledgment

The author is much indebted to the Lady Davis Foundation for grant of a Personal Fellowship. He also wishes to express his best thanks to Dr. G. M. Volkoff for a discussion on the subject of this paper.

THE DURATION OF THE 16 VOLT LEVELS OF NEON[1]

By Frank A. Grant

Abstract

Electronic apparatus has been developed to determine the rate of decay of the 16 volt levels of neon after the interruption of an electrical discharge, by measurement of the absorption of a monochromatic light beam. The half life of the $^3P_2$ metastable level has been determined as a function of pressure and discharge tube diameter. The $^3P_0$ and $^3P_1$ levels exhibit a pronounced departure from an exponential decay. The hypothesis of the imprisonment of resonance radiation is consistent with the measured duration of the $^1P_1$ and $^3P_1$ levels.

I. Introduction

The most satisfactory method of determining the population of excited atoms in a discharge tube is the measurement of the absorption of a light beam of appropriate wave length. In neon gas the spectral lines most highly absorbed by the 16 volt levels are visible, and their absorption coefficients are known. The investigation of the anomalous dispersion of excited gases by Kopfermann and Ladenburg has provided data concerning the population of these levels in a continuous neon discharge. And because of the ease with which common impurities (except argon) may be removed, neon has been used for the investigation of the duration of excited levels.

The light absorption method has been used by Dorgelo and Washington, Meissner and Graffunder, Anderson, and by Lippert to measure the half life of the $^3P_2$ metastable level of neon, but it was not possible to formulate a simple hypothesis consistent with all their results. In particular, the dependence of half life on the discharge tube diameter was not established, and in the results of Meissner and Graffunder, and of Anderson, there appeared to be a dependence on the spectral line used to measure the half life.

The use of the photomultiplier tube and cathode ray tube offers a method of obtaining experimental data much more quickly and accurately than was possible in previous investigations, and has been employed in the present research to attempt to find an explanation of these inconsistencies, and to investigate the effect of the imprisonment of resonance radiation.

II. Absorption of Light—Theory

Absorption as a Function of Number of Absorbing Atoms

If a parallel beam of monochromatic radiation traverses a uniform layer of absorbing gas, and if a (defined below) is small compared with unity, the intensity of the transmitted light is given by the following equation:—

[1] *Manuscript received December 18, 1949.*
Contribution from the McLennan Laboratory, University of Toronto, Toronto, Ont.
[2] *Holder of National Research Council Fellowships 1946–7, 1947–8. Present address: Department of Physics, University of Maryland, College Park, Md.*

$$I = I_0 \exp(-PNl), \tag{1}$$

l = length of absorbing path,

N = number of absorbing atoms per cubic centimeter,

K_0 = absorption coefficient,

$= PN$,

P = constant of proportionality,

$\alpha = \dfrac{\text{Breadth of emission line,}}{\text{Breadth of absorption line}}$,

I = Intensity of the radiation at a distance l from the origin,

I_0 = Intensity of the radiation at the origin,

= Intensity of the radiation at any l in the absence of absorbing atoms.

In the case of principal interest, N is an exponential function of time, and the half life T is defined by the equation

$$N = N_0 \exp\left(-\frac{t\ ln\ 2}{T}\right). \tag{2}$$

Combining these two equations and taking logarithms twice, a linear function of time is obtained:—

$$C - \frac{t \log 2}{T} = \log \log\left(\frac{I_0}{I}\right)$$

$$= \log \log\left(\frac{1}{1-A}\right). \tag{3}$$

Equation (3) is represented by the broken lines of Fig. 1. The slope is inversely proportional to the half life T. The absorption A is defined by Equation (6).

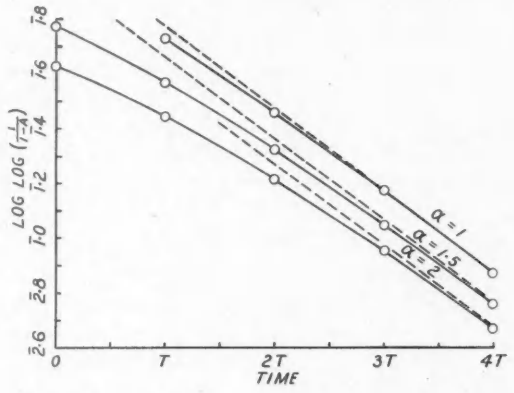

FIG. 1. *log log* $\left(\dfrac{1}{1-A}\right)$ *plotted as a function of time. Absorption calculated from Equation (8). Exponential decay of N assumed.*

If the quantity a is not small compared with unity, then the absorption is given by the following expression:—

$$A_a = \frac{\int_{-\infty}^{\infty} \left(\exp\left[-\left(\frac{\omega}{a}\right)^2\right]\right)\left(1 - \exp\left[-k_0 l \exp\left(-\omega^2\right)\right]\right) d\omega}{\int_{-\infty}^{\infty} \exp\left[-\left(\frac{\omega}{a}\right)^2\right] d\omega} \tag{4}$$

ω is a parameter depending upon the breadth of the absorption line. Using the data of Mitchell and Zemansky (10), the corresponding curves for $a = 1$, 1.5, and 2, have been plotted in Fig. 1. The departure of these curves from linearity is not great.

Light Beam of Finite Cross Section, Nonuniform Medium

The absorption A is defined in terms of light flux, so that it represents an average absorption across the light beam.

$$A \equiv 1 - \frac{\phi}{\phi_0} \tag{5}$$

$$= 1 - \frac{\int_{\text{across beam}} I dS}{\int_{\text{across beam}} I_0 dS}. \tag{6}$$

To study the effect of a nonuniform layer of absorbing gas, it is convenient to express Equation (4) in the following forms:—

$$A_a = \frac{(k_0 l)}{(1 + a^2)^{\frac{1}{2}}} - \frac{(k_0 l)^2}{2!(1 + 2a^2)^{\frac{1}{2}}} + \frac{(k_0 l)^2}{3!(1 + 3a^2)^{\frac{1}{2}}} - \ldots \tag{7}$$

$$A_1 = \frac{(PN_0 l)}{2^{\frac{1}{2}}} \exp\left(-\frac{t \ln 2}{T}\right) - \frac{(PN_0 l)^2}{2! 3^{\frac{1}{2}}} \exp\left(-\frac{t \ln 2}{\frac{T}{2}}\right) + \ldots \tag{8}$$

If $PN_0 l$ varies with radius of the discharge tube, but is small, all terms except the first may be neglected, and no error is introduced when the absorption is averaged across the light beam. When higher terms cannot be neglected, however, integration with respect to the radius results in an expression which is not a simple function of the half life T. Moreover, any attempt to calculate T by the foregoing method results in a value that depends on the spectral line used, and on the orientation of the light beam with respect to the axis of the absorption tube (9).

Since it is assumed that $N = 0$ at the wall, it is important to eliminate the effect of the light reflected from the wall of the discharge tube. The light beam must be restricted to the interior, where the variation of N with radius is assumed to be negligible.

III. The Decay of Excited Levels After the Cessation of the Excitation–Theory

Transitions between the Triplet Levels

Two of the triplet levels of neon are metastable (Fig. 2). Under the conditions of the present research, the probability that an atom will leave a metastable level in a collision is much greater than the probability of a radiative transition.

The $^3P_0$ and $^3P_2$ levels are separated by an energy difference of 0.09 v., and kT at 300°K is 0.026 v. Consequently the probability of a transition from a metastable level to the $^3P_1$ level in a collision with a normal atom is not negligible. The behavior of the $^3P_1$ level is important in determining the rate of decay at the metastable levels.

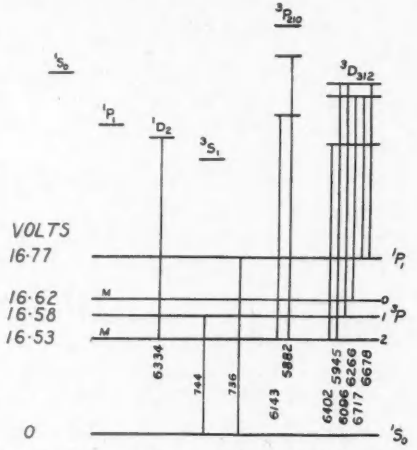

FIG. 2. *Energy diagram of the 16 volt levels of neon.*

The Imprisonment of Radiation

Meissner and Graffunder (9) measured the duration of the nonmetastable $^3P_1$ level. At a pressure of 2.15 mm. of mercury they obtained an apparent half life of 0.2 milliseconds. In the absence of imprisonment of resonance radiation the "natural" lifetime of this level is of the order of 10^{-7} sec. In their work on the anomalous dispersion of excited gases (6) Kopfermann and Ladenburg found it necessary to assume the imprisonment of radiation to account for the concentration of the $^3P_1$ level.

Shortley (7) has calculated that the probability of the transition from the $^1P_1$ level to the ground level is about 13 times that from the $^3P_1$ level. To be consistent with the hypothesis of the imprisonment of resonance radiation a considerable increase in the lifetime of the singlet level is also to be expected.

The Decay of the Triplet Levels

In early studies of metastable levels, attention was directed to the mech-

anism by which a metastable atom could revert to the ground level. It was assumed that at pressures below 1 mm. of mercury the principal loss of the energy of excitation resulted from collisions of metastable atoms with the walls. At pressures greater than 2 mm. transitions to the $^3P_1$ level became increasingly important. Following this transition, resonance radiation was emitted, and reversion to the ground level took place.

If imprisonment of resonance radiation takes place, however, the emitted photon will be absorbed and re-emitted many times, until it

(*a*) is absorbed by the wall,

(*b*) is absorbed by a neon atom which is in collision with a foreign atom,

or (*c*) is absorbed by a neon atom whose co-ordinates and momenta with respect to a neighboring atom are such that a transition to another level (most probably $^3P_2$) takes place (4).

The metastable $^3P_2$ atom in turn may

(*d*) impart its energy directly to the wall,

(*e*) be transferred to another level (most probably $^3P_1$) by collision with a normal neon atom,

(*f*) be ionized by collision with another excited atom,

or (*g*) excite or ionize a suitable foreign atom (Penning effect).

Process (*f*) would cause a hyperbolic decay of the $^3P_2$ level. Since no evidence has been obtained for a decay of this type, the process will be ignored. In pure neon processes (*a*), (*c*), (*d*), and (*e*) determine the rate at which the energy of excitation diffuses and is imparted to the wall of the vessel.

During the excitation process the relative concentrations of the triplet levels are determined by the electron temperature (7), and are approximately the same as the statistical weights of the levels. After the excitation is interrupted, this distribution is altered by the collision processes listed.

The probability of a transition from one triplet level to another of greater energy is dependent on the fact that in only a fraction of the collisions is the kinetic energy of the colliding partners sufficiently great. No such restriction is effective in the case of the reverse transition. It is therefore reasonable to expect a period in which the number of atoms transferred from the $^3P_0$ and $^3P_1$ levels to the $^3P_2$ level will greatly exceed the number transferred in the reverse direction. After this initial period the rates of decay of the three triplet levels should tend to the same value—the half life of the $^3P_2$ level.

The Dependence of T on Pressure

Zemansky (11) derived an expression for the half life of the $^3P_2$ level of the form:

$$\frac{1}{T} = \frac{B}{P} + CP \tag{9}$$

The constant B was expressed as a function of the atomic weight, temperature,

dimensions of the vessel, and σ^2 the cross section of the atom for the diffusion process. The CP term represented process (e). If imprisonment of radiation takes place, the effect of this process is reduced by process (c), which was neglected in the derivation of Equation (9).

Equation (9) will be used empirically until it is found to be inconsistent with experimental results.

Dependence of B and C on Discharge Tube Diameter

In the investigations of Meissner and Graffunder (9), Anderson (2), and Lippert (8), and in preliminary experiments of the present research, Fig. 16, the maximum half life at 300°K. was reached at a pressure between 1 and 2 mm. of mercury, regardless of the discharge tube diameter. This seemed to indicate that the constant C varied with diameter in the same way as the constant B. The contrary indication of the present research will be discussed in a later section.

Theoretical treatments of the subject were made by Meissner and Graffunder (9), Anderson (1), and Zemansky (11). The constant B was found to be dependent on the tube geometry through the factor

$$\left(\frac{23.2}{\text{Diam.}^2}+\frac{\pi^2}{\text{Length}^2}\right).$$

In a long discharge tube the derived relation indicated that at sufficiently low pressures T should be proportional to the square of the discharge tube diameter.

The experimental results of previous research showed wide disagreement in the values of Ba^2 (Table IV). Much of the present research was undertaken to determine whether this disagreement was the result of the inaccuracy of the experimental data or of neglect of the imprisonment of resonance radiation.

IV. The Technique of Measurement

It has been shown that the absorption of monochromatic radiation is a function of a and N [Equation (8)]. If the quantity a is small or known, N (in

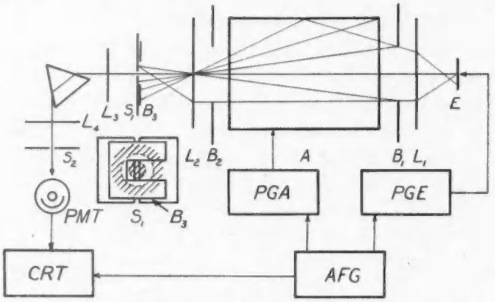

FIG. 3. *Diagram illustrating the apparatus used in the determination of the absorption of light as a function of time.*

arbitrary units) can be determined from the absorption of a beam of light of the appropriate wave length.

The emission and absorption discharge tubes, E and A, Fig. 3, both contain neon gas. After traversing A, the light from E is focused at the slit of the monochromator S. Monochromatic light is incident on the photomultiplier tube PMT and the voltage output displayed on the cathode ray tube CRT. After interruption of the excitation in A, the absorption is measured as a function of time, and used to determine the number of excited atoms present in A.

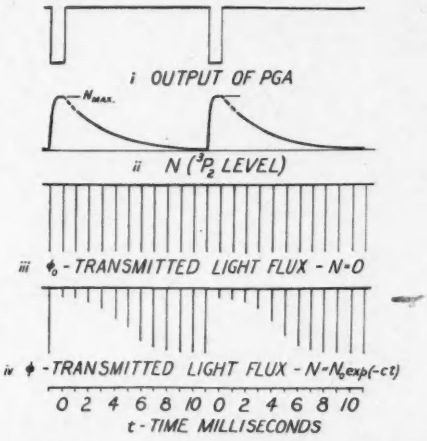

FIG. 4. *Diagram illustrating the pulse technique used in the determination of the absorption of light as a function of time.*

1. The first requirement of such a system is a voltage pulse (Fig. 4i) with a rapid decay, to excite the atoms in A. N can then be determined during the interval between pulses, when the excitation is interrupted. If the duration of the pulse is sufficiently great, an equilibrium is established between the electrons and excited atoms (7), and conditions in the tube are independent of the pulse repetition frequency. For accuracy of measurement, however, it is desirable to make the time interval between these pulses sufficiently great for the absorption to reach a negligible value. In this way a zero reference is obtained.

Kopfermann and Ladenburg (6) have shown that the excitation curve N vs. current density exhibits a maximum. If the optimum current density is exceeded, the effect of the "vernichtenden Elektronenstössen" causes a reduction of N. To obtain the maximum concentration of excited atoms regardless of the discharge tube diameter or of the pressure, the amplitude of these voltage pulses must be adjustable.

2. The second requirement is a minimum disturbance of the gas in A by the light from E. Hence light pulses are used of duration short compared with the interval between them (Fig. 4iii). The light flux incident on the photomultiplier

tube must produce an output voltage large compared with the "noise" output. To enable this requirement to be met with the use of a source of low intensity, the design of the monochromator is important. Hence the need of a wide slit and prisms of high dispersion.

3. The emission line should exhibit negligible self-reversal.

4. All forms of broadening of the emission and absorption lines should be kept to a minimum. In particular, the value of a should not be large compared with unity. The use of pulse excitation reduces the temperature rise in both discharge tubes to a negligible value.

V. Apparatus

PGA

Pulse Generator *A* (Fig. 5) was designed to produce an output voltage of up to 2500 v., of duration 0.5 to 1.0 milliseconds, and pulse repetition frequency 50 to 200 c.p.s. To reduce the effect of stray capacitance, the standard practice of using low values of load resistance was followed.

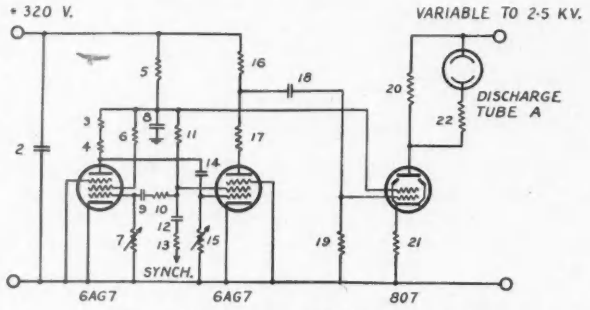

FIG. 5. *Circuit diagram of Pulse Generator A.*

TABLE I

COMPONENTS OF FIG. 5

1. 500 picofarads	9. 0.05 microfarads	17. 2 kilohms
2. 8 microfarads	10. 4.7 kilohms	18. 0.05 microfarads
3. 1 kilohm	11. 5.6 "	19. 470 kilohms
4. 1.3 "	12. 0.1 microfarads	20. 10 "
5. 2. "	13. 22 kilohms	21. 100 ohms
6. 5.6 "	14. 1000 picofarads	22. 10 kilohms
7. 500 "	15. 800 kilohms	
8. 8 microfarads	16. 2. "	

PGE

Pulse Generator *E* (Fig. 6) was designed to produce an output voltage up to 1500 v., of duration 0.02 milliseconds, and a pulse repetition frequency 1000 c.p.s.

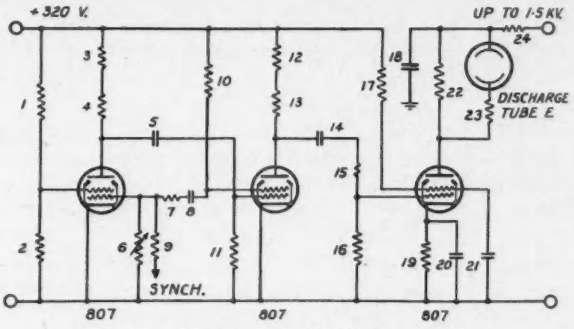

FIG. 6. *Circuit diagram of Pulse Generator E.*

TABLE II

COMPONENTS OF FIG. 6

1. 35 kilohms	9. 15 kilohms	17. 5 kilohms
2. 2.2 "	10. 4 "	18. 2 microfarads
3. 2.5 "	11. 100 "	19. 1 kilohm
4. 2.5 "	12. two 10 k in	20. 0.25 microfarads
5. 100 picofarads	13. parallel	21. 8 "
6. 240 kilohms	14. 0.1 microfarads	22. 10 kilohms
7. 2.5 "	15. 100 ohms	23. 7 "
8. 3000 picofarads	16. 470 kilohms	

Discharge Tube A

The absorption discharge tube *A* (Fig. 7) was circular in cross section with optically plane Pyrex windows at both ends. The electrodes were circular and made of 20 mil tungsten wire concentric with the walls of the discharge tube.

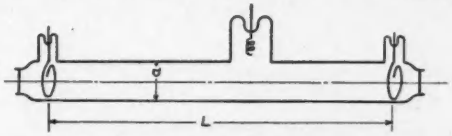

FIG. 7. *The absorption discharge tube A.*

Three tubes, of 30 mm., 46 mm., and 81 mm. inside diameter were used. The power dissipated in the tubes was so small that no increase in temperature could be detected by the hand.

Discharge Tube E

The light was emitted from a capillary tube 4 mm. in diameter and 4 cm. in length. The discharge tube was filled with neon at a pressure of 3 mm. The power dissipated in the emission tube was less than 0.5 w.

Photomultiplier Tube

A 931-A photomultiplier tube with accelerating voltages of 105 v. was used. The load resistor was 19,000 ohms.

Cathode Ray Tube

This was a Dumont Type 208-B with a blue trace.

Monochromator

To enable a wide slit to be used, three carbon disulphide prisms were used in the monochromator. In this way a satisfactory signal–noise ratio in the output of the photomultiplier tube was obtained with the lowest possible intensity of the light source.

Baffles

Paper baffles, B_1 and B_2 (Fig. 3), were attached to both ends of the absorption tube. Circular apertures 25 mm. in diameter concentric with the axis of the tube determined the beam diameter. To eliminate the effect of light reflected from the wall of the absorption tube, an image of the first aperture was focused at the slit of the monochromator, and a third baffle was inserted to allow only the light forming this image to enter the slit.

Gaseous Purity

The neon was purified first by a discharge in a potassium pool discharge tube permanently connected to the absorption tube, and, second, by the heating to incandescence of the tungsten electrodes in A for several hours. The second method appeared to be the more effective in removing hydrogen, but the potassium was very effective in the removal of mercury vapor. The gas was found to contain a trace of argon, which of course was not removed by these methods.

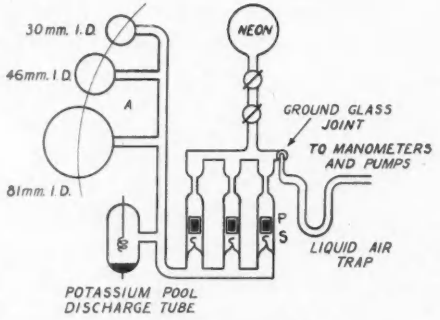

FIG. 8. *Vacuum system.*

Since stopcocks caused a serious deterioration of the purity, all purification was accomplished with the system sealed off. To change the pressure, the discharge tube A was connected to the manometers and pump by breaking a glass seal S (Fig. 8). By the use of a magnet, it was possible to raise the steel pellet P and allow it to fall, breaking the seal S. To avoid contamination of the neon, the pellet was enclosed in glass.

Manometers

The pressure was measured with a McLeod gauge and an oil manometer, using Octoil–S.

Synchronism

For convenience of time measurement, both pulse generators and cathode ray tube were synchronized with an audio frequency generator *AFG*, Fig. 3. In all cases the pulse repetition frequency of *PGE* was about 1000 c.p.s. so that the time interval between pulses was about 1.0 millisecond. In some cases both generators were synchronized with a 2000 c.p.s. voltage from *AFG*. The period of *PGE* was adjusted to be an even multiple (two) of 0.5 millisecond, and the period of *PGA* to an odd multiple, making a cathode ray tube pattern with an apparent interval between successive *PGE* pulses of 0.5 millisecond.

Photography

The noise level of the system was sufficiently high to make direct measurement of the cathode ray tube trace impracticable. This effect was eliminated by making a 30 sec. exposure when photographing the trace.

The effect on the curvature of the cathode ray tube screen was reduced by limiting the amplitude of the image to $2\frac{1}{2}$ in. (one half the screen diameter), and by placing the reference line (zero absorption) within an inch of the center of the screen. In addition to this, absorption of less than 5% was ignored when making measurements.

VI. Summary of the Phenomena Investigated

Imprisonment of Radiation.—Because of the relatively small absorption, a long discharge tube (90 cm. long, 46 mm. inside diam.) was used to investigate the duration of the $^1P_1$ and $^3P_1$ levels.

The Decay of the Triplet Levels.—Because of the convenient path length (90 cm.), the investigation of the decay of the ^3P levels was made with the same discharge tube. Reproducibility was checked by making two independent observations of the decay of the $^3P_0$ and $^3P_1$ levels; the results of these investigations are plotted in Figs. 12, 13, and 14.

The $^3P_2$ Level–Various Spectral Lines.—The dependence of the half life of the $^3P_2$ level on the spectral line used was investigated at the same pressure and using the same discharge tube as in the foregoing investigations. The results are plotted in Fig. 15.

$^3P_2$ Level–The Constants B and C.—The dependence of the constants B and C of Equation (9) on the discharge tube diameter was determined using tubes of inside diameter 30, 46, and 81 mm., all 70 cm. in length. Two sets of observations were made, and are plotted in Figs. 17 to 20.

In all cases the interval between *PGE* pulses was 1 millisecond.

VII. The Treatment of Experimental Data

In order to determine the half life of the $^3P_2$ metastable level, it is necessary to make an assumption of the value of α (see Fig. 1). Because of the negligible temperature rise in both tubes, the Doppler breadth of both emission and absorption lines was assumed to be the same, and α taken as unity. The difference between the slopes of the curves $\alpha = 0$ and $\alpha = 1$, between the ordinates $\bar{1}.6$ and $\bar{1}.0$ is 6%. Whenever possible the portion of the curve lying between these limits (Fig. 9 and Fig. 10) was used for the determination of the slope, and the value of the half life so obtained was reduced by 6%.

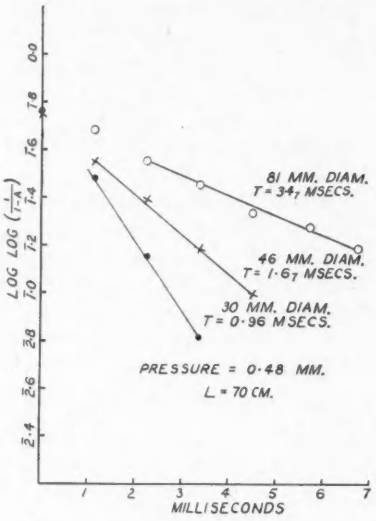

FIG. 9. *The decay of the quantity log log* $\left(\frac{1}{1-A}\right)$ *as a function of time. Wave length 5945Å. $^3P_2$ level.*

It was then attempted to represent the half life of the $^3P_2$ level by the empirical relation:—

$$\frac{1}{T} = \frac{B}{P} + CP. \tag{9}$$

Using the method of Mitchell and Zemansky (10), the quantity $\frac{P}{T}$ was plotted against P^2 in Figs. 17 and 18. The value of B is the intercept made by the straight line on the vertical axis, and the value of C is equal to the slope. The curves of Figs. 19 and 20 are plotted using the values of B and C obtained from Figs. 17 and 18.

Measurements of the absorption were made from the photographs of the cathode ray tube screen by placing the photographic plate on a piece of squared

paper. In these photographs, of which Fig. 11 is an example, zero absorption corresponds to the asymptote of the envelope of the figure as time increases without limit.

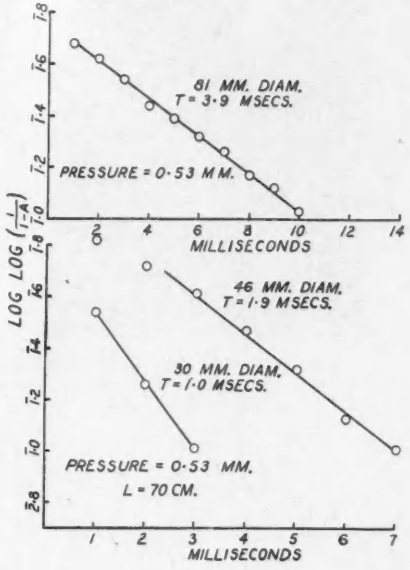

FIG. 10. *The decay of the quantity log log* $\left(\frac{1}{1-A}\right)$ *as a function of time. Wave length 5945Å.* $^3P_2$ *level.*

VIII. Experimental Results and Discussion

Imprisonment of Radiation

To investigate the effect of imprisonment of resonance radiation in lengthening the life of the $^3P_2$ level, measurements of the duration of the $^1P_1$ and $^3P_1$ were made. The half life of the $^1P_1$ level was found to be 0.8 milliseconds (Fig. 11). The decay of the $^3P_1$ level is not exponential (Fig. 12), but the absorption does not decrease to 10% until 3 milliseconds after the interruption of the excitation.

Both these measurements are consistent with the hypothesis of imprisonment of resonance radiation.

The Decay of the Triplet Levels

In Figs 12 and 13, the first three milliseconds constitutes the period of transition discussed previously. A pronounced departure from an exponential decay is exhibited by the $^3P_0$ and $^3P_1$ levels. For comparison, the rate of decay of the $^3P_2$ level is represented by the broken line. Measurements of the rate of decay of the $^3P_0$ and $^3P_1$ levels were made by Dorgelo (3) and by Meissner and

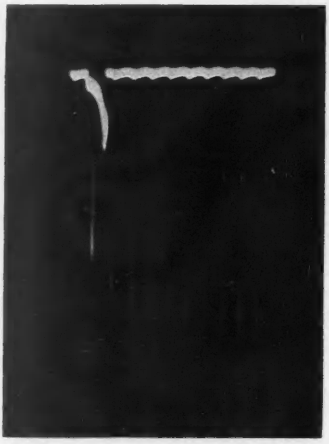

FIG. 11. $^1P_1$ *level. Photograph of the oscillogram showing the absorption as a function of time. Spectral lines 6678 and 6717 Å. Discharge tube diameter, 46 mm.; length, 90 cm. Pressure, 1.3 mm. Intervals, 1/2.06 millisecond.*

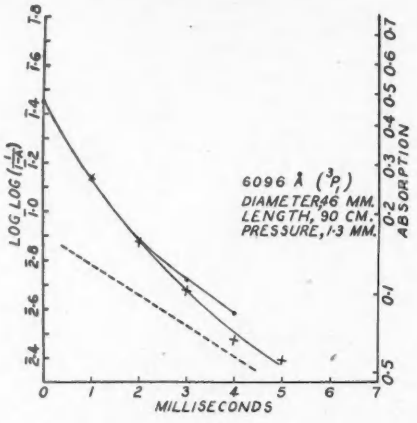

FIG. 12. *The decay of the quantity* $\log \log \left(\frac{1}{1-A}\right)$ *as a function of time. Wave length, 6096 Å. $^3P_1$ level.*

Graffunder (9). The accuracy of measurement, however, was insufficient to indicate a departure from an exponential decay.

In the decay of the $^3P_2$ level, the period of transition is less evident (Fig. 14).

The $^3P_2$ Level–Various Spectral Lines

The results of Meissner and Graffunder (9) and of Anderson (2) indicated that the apparent half life of the $^3P_2$ level depended on the spectral line used.

A possible cause of this effect is the variation of the quantity PNl with radius [equation (8)]. A similar effect would be produced if stray light from the emission tube were allowed to enter the photomultiplier tube. Precautions were

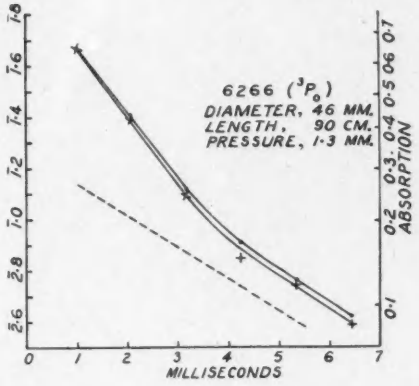

FIG. 13. *The decay of the quantity* $\log \log \left(\frac{1}{1-A}\right)$ *as a function of time. Wave length, 6266Å.* $^3P_0$ *level.*

taken to eliminate these effects by the introduction of baffles and by reducing to a negligible intensity the stray light entering the photomultiplier tube. In spite of these precautions, there still remained the following effect to be explained.

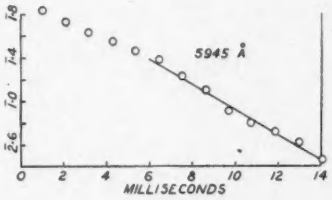

FIG. 14. *The decay of the quantity* $\log \log \left(\frac{1}{1-A}\right)$ *as a function of time. Wave length 5945Å.* $^3P_2$ *level.*

In Fig. 15 the quantity $\log \log \left(\frac{1}{1-A}\right)$ is plotted as a function of time for the wave lengths 6402, 5945, 6143, 6334, and 5882Å. The absorption of all these spectral lines is dependent on the $^3P_2$ level. The plotted curves have been calculated in the same manner as those of Fig. 1. In every case a half life of 2.35 milliseconds has been assumed. The origins of the time scales have been chosen to give the best fit to the experimental points. If the same half life is assumed for all curves, a good fit can only be obtained by assuming different values of a.

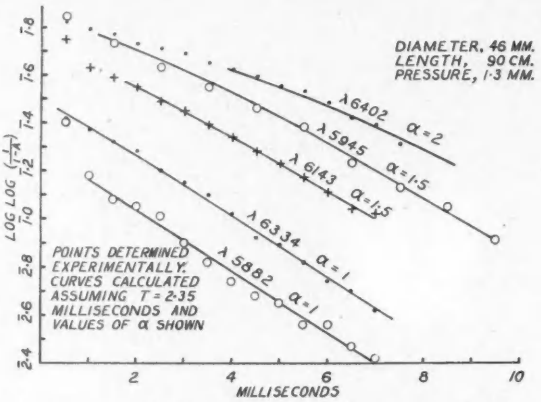

FIG. 15. $^3P_2$ *level. Curves calculated as explained in the text.*

The $^3P_2$ Level—The Constant C

No satisfactory interpretation of the constant C has been made (5). Since the neon used in the present research was found to contain a trace of argon, it is possible that this impurity is responsible for the CP term. The slope of -1 (Fig. 16) indicates that the effect is proportional to the first power of the pressure.

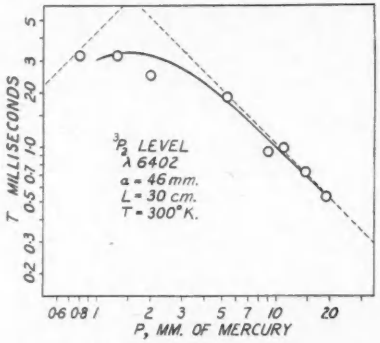

FIG. 16. $^3P_2$ *level. log T plotted as a function of log P, illustrating the predominance of the CP term of Equation (9) at higher pressures.*

It was stated in a foregoing section that the results of previous investigations seemed to indicate that the maximum half life occurred at a pressure between 1 and 2 mm. of mercury regardless of the diameter of the discharge tube. To investigate this point, it was important that discharge tubes of different diameters, containing identical gas, should be used. Consequently, the three tubes used in this research were permanently connected by 15 mm. tubing, and mounted so that one tube could be removed and replaced by another without disturbing the remainder of the system.

In Figs 17–20, the three readings corresponding to any given pressure were obtained within an interval of three minutes. The readings were taken in the sequence 81-46-30, 30-46-81, 81-46-30, etc.

There is no close agreement between the values of C (Table V) obtained. However, the maxima of these curves are reached at different pressures, and the conclusion is reached that B and C do not vary with diameter in the same way.

Dependence of B on Diameter

Figs. 17 and 18 illustrate the manner in which the constant B was determined from the experimental data. It is assumed that the end effect is negligible in a discharge tube 70 cm. long. To determine if B is inversely proportional to the square of the discharge tube diameter in a long tube, values of Ba^2 are tabulated in Table III.

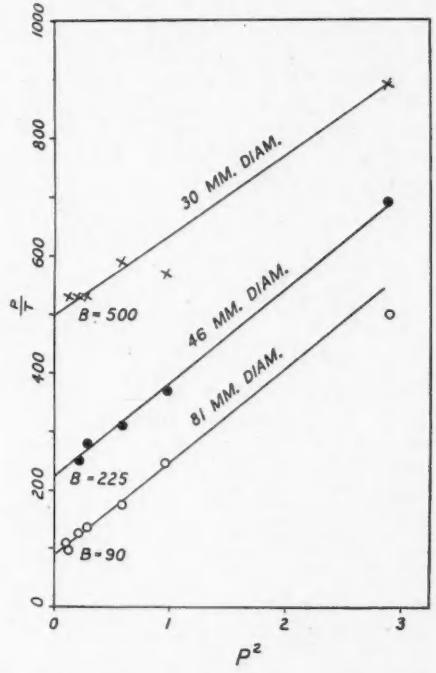

FIG. 17. $^3P_2$ *level. The determination of the constants B and C of Equation (9).*

TABLE III

EXPERIMENTAL VALUES OF CONSTANT B OF EQUATION (9)

$^3P_2$ Level

Wave length 5945Å

L = 70 cm.

Inside diameter, a, mm.	B	$Ba^2 \times 10^{-4}$	Probable error, $\times 10^{-4}$
30	500	45	2
30	460	41	2
46	225	48	2
46	240	51	3
81	90	59	10
81	75	49	10

These results indicate a slight increase of Ba^2 with increase in the discharge tube diameter.

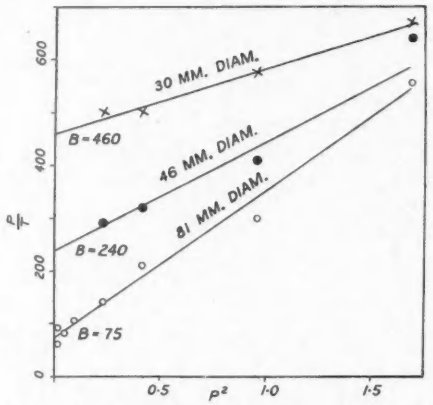

FIG. 18. $^3P_2$ *level. The determination of the constants B and C of Equation (9).*

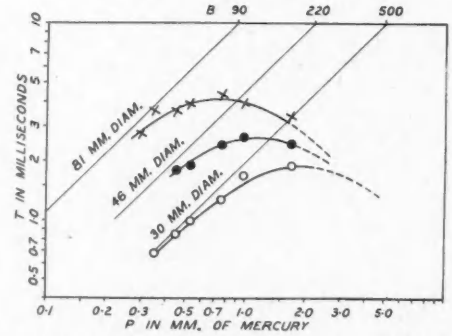

FIG. 19. $^3P_2$ *level. log T plotted as a function of log P. Curves calculated using Equation (9) and the values of B and C obtained from Fig. 17. L = 70 cm.*

TABLE IV

EXPERIMENTAL VALUES OF CONSTANT B

	Inside diameter, a, mm.	B	$Ba^2 \times 10^{-4}$
Meissner and Graffunder	36	2000	260
Anderson	10	1200	12
Preliminary measurement, present research	46	230	49

TABLE V

EXPERIMENTAL VALUES OF CONSTANT C OF EQUATION (9)

$^3P_2$ Level

Wave length 5945Å

L = 70 cm.

Inside diameter	C
30	137
30	120
46	160
46	204
81	160
81	280

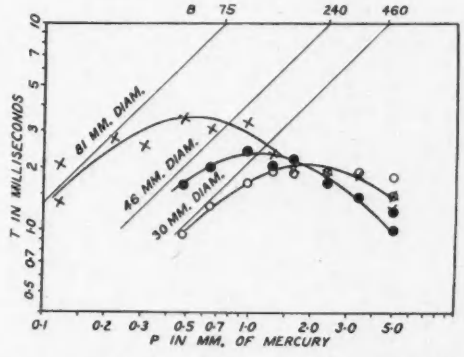

FIG. 20. $^3P_2$ *level. log T plotted as a function of log P. Curves calculated using Equation (9) and the values of B and C obtained from Fig. 18. L = 70 cm.*

Acknowledgments

The author wishes to express his thanks to Dr. J. M. Anderson and Dr. R. W. McKay, who supervised the work, for their encouragement and constructive criticism.

References

1. ANDERSON, J. M. Can. J. Research, 2: 13. 1930.
2. ANDERSON, J. M. Can. J. Research, 7: 443. 1932.
3. DORGELO, H. B. and WASHINGTON, T. P. K. Akad. Wetensch. Proc. Amsterdam, 30: 33. 1937.
4. DE GROOT, W. and PENNING, F. M. Handbuch der Physik, XXIII. Verlag von Julius Springer, Berlin. 1933.
5. HOLSTEIN, T. Phys. Rev. 72: 1212. 1947.
6. KOPFERMANN, H. and LADENBURG, R. Z. Physik, 48: 15. 1928.
7. LADENBURG, R. Revs. Modern Phys. 5: 243. 1933.
8. LIPPERT, W. Ann. Physik, 30: 136. 1937.
9. MEISSNER, K. W. and GRAFFUNDER, W. Ann. Physik, 84: 1009. 1927.
10. MITCHELL, ALLAN, C. G. and ZEMANSKY, MARK W. Resonance radiation and excited atoms. Cambridge: The University Press. 1934.
11. ZEMANSKY, M. W. Phys. Rev. 34: 213. 1929.

CANADIAN JOURNAL OF RESEARCH

Notes on the Preparation of Copy

GENERAL:—Manuscripts should be typewritten, double spaced, and the **original and one extra copy** submitted. Style, arrangement, spelling, and abbreviations should conform to the usage of this Journal. Names of all simple compounds, rather than their formulae, should be used in the text. Greek letters or unusual signs should be written plainly or explained by marginal notes. Superscripts and subscripts must be legible and carefully placed. Manuscripts should be carefully checked before being submitted, to reduce the need for changes after the type has been set. If authors require changes to be made after the type is set, they will be charged for changes that are considered to be excessive. **All pages, whether text, figures, or tables, should be numbered.**

ABSTRACT:—**An abstract of not more than about 200 words, indicating the scope of the work and the principal findings, is required.**

ILLUSTRATIONS:

(i) *Line Drawings:*—All lines should be of sufficient thickness to reproduce well. Drawings should be carefully made with India ink on white drawing paper, blue tracing linen, or co-ordinate paper **ruled in blue only**; any co-ordinate lines that are to appear in the reproduction should be ruled in black ink. Paper ruled in **green, yellow, or red should not be used** unless it is desired to have all the co-ordinate lines show. Lettering and numerals should be neatly done in India ink preferably with a stencil (**do not use typewriting**) and be of such size that they will be legible and not less than one millimeter in height when reproduced in a cut three inches wide. All experimental points should be carefully drawn with instruments. Illustrations need not be more than two or three times the size of the desired reproduction, but the ratio of height to width should conform with that of the type page. **The original drawings and one set of small but clear photographic copies are to be submitted.**

(ii) *Photographs:*—Prints should be made on glossy paper, with strong contrasts; they should be trimmed to remove all extraneous material so that essential features only are shown. Photographs should be submitted **in duplicate;** if they are to be reproduced in groups, one set should be so arranged and mounted on cardboard with rubber cement; the duplicate set should be unmounted.

(iii) *General:*—**The author's name, title of paper, and figure number should be written in the lower left hand corner (outside the illustration proper) of the sheets on which the illustrations appear.** Captions should not be written on the illustrations, but typed on a separate page of the manuscript. All figures (including each figure of the plates) should be numbered consecutively from 1 up (arabic numerals). **Each figure should be referred to in the text.** If authors desire to alter a cut, they will be charged for the new cut.

TABLES:—Titles should be given for all tables, which should be numbered in Roman numerals. Column heads should be brief and textual matter in tables confined to a minimum. **Each table should be referred to in the text.**

REFERENCES:—**These should be listed alphabetically by authors' names, numbered in that order, and placed at the end of the paper.** The form of literature citation should be that used in the respective sections of this Journal. **Titles of papers should not be given in references listed in Sections A, B, E, and F, but must be given in references listed in Sections C and D.** The first page only of the references cited in papers appearing in Sections A, B, and E should be given. **All citations should be checked with the original articles.** Each citation should be referred to in the text by means of the key number; in Sections C and D the author's name and the date of publication may be included with the key number if desired.

The *Canadian Journal of Research* conforms in general with the practice outlined in the *Canadian Government Editorial Style Manual*, published by the Department of Public Printing and Stationery, Ottawa.

Reprints

Fifty reprints of each paper without covers are supplied free. Additional reprints, if required, will be supplied according to a prescribed schedule of charges. On request, covers can be furnished at cost.